

Utah State University

DigitalCommons@USU

All Graduate Theses and Dissertations

Graduate Studies

12-2021

Characteristic of the Dynamics of Disorder in Crystalline and Amorphous Materials

Amir Behbahanian
Utah State University

Follow this and additional works at: <https://digitalcommons.usu.edu/etd>

 Part of the [Mechanical Engineering Commons](#)

Recommended Citation

Behbahanian, Amir, "Characteristic of the Dynamics of Disorder in Crystalline and Amorphous Materials" (2021). *All Graduate Theses and Dissertations*. 8364.
<https://digitalcommons.usu.edu/etd/8364>

This Dissertation is brought to you for free and open access by the Graduate Studies at DigitalCommons@USU. It has been accepted for inclusion in All Graduate Theses and Dissertations by an authorized administrator of DigitalCommons@USU. For more information, please contact digitalcommons@usu.edu.



CHARACTERISTIC OF THE DYNAMICS OF DISORDER IN CRYSTALLINE AND
AMORPHOUS MATERIALS

by

Amir Behbahanian

A dissertation submitted in partial fulfillment
of the requirements for the degree

of

DOCTOR OF PHILOSOPHY

in

Mechanical Engineering

Approved:

Nicholas Roberts, Ph.D.
Major Professor

Barton Smith, Ph.D.
Committee Member

Geordie Richards, Ph.D.
Committee Member

Mark Riffe, Ph.D.
Committee Member

Todd Moon, Ph.D.
Committee Member

D. Richard Cutler, Ph.D.
Interim Vice Provost of Graduate Studies

UTAH STATE UNIVERSITY
Logan, Utah

2021

Copyright © Amir Behbahanian 2021

All Rights Reserved

ABSTRACT

Characteristic of the Dynamics of Disorder in Crystalline and Amorphous Materials

by

Amir Behbahanian, Doctor of Philosophy

Utah State University, 2021

Major Professor: Nicholas Roberts, Ph.D.

Department: Mechanical and Aerospace Engineering

In this dissertation I address the effect of randomness on the dynamics of crystalline and amorphous materials. I developed a wavepacket-based methods to capture the energy of a frequency band and simulated the time evolution of that wavepacket with its defined energy without the presence of other modes. This method provided minimal decay of that frequency band although the wavepacket has activated the modes beyond their anharmonic character. In addition, I used the method to evaluate Molecular Dynamics (MD) simulations in the context of missing quantum effects and found that even at low temperatures the MD simulations are reliable up to frequencies as high as 1 THz. As a result of the decay analysis in the first part, I hypothesised the importance of the existence of other frequency modes in the dynamics of vibrations in crystalline materials. To evaluate the hypothesis I checked the thermal conductivity as a measure of the character of vibrations under conventional and Langevin dynamics. The result of this section provided evidence for the random character of vibrations at high temperatures that makes the dynamics of vibrations in crystalline materials comparable to the dynamics of vibration of amorphous materials. At the end of this dissertation, I evaluated the source of high thermal conductivity in amorphous silicon and found computational evidence for sub-micron vibrational modes in this material. In the last piece of my analysis I utilized a notion called “Dynamical Structure Factor” to get

the lifetime of lattice vibrations that provided the chance to evaluate the property under the effect of full anharmonicity. This advantage makes picture of the physics provided by this dissertation more reliable compared to the other worked using methods such as “Static Structure Factor” that fails to capture the full anharmonic picture of vibrations. The result of this work will provide the evidence for further research of the application of random matrix theory to model crystalline materials at high temperatures. This method has been used to model amorphous materials and showed capabilities to model systems beyond the capabilities of conventional MD simulation.

(114 pages)

PUBLIC ABSTRACT

Characteristic of the Dynamics of Disorder in Crystalline and Amorphous Materials

Amir Behbahanian

This work provides the evidence to apply simulation methods that are applicable to systems with structural randomness to simulate crystalline materials at high temperatures. My work not only open the avenue to expand the simulation capability of materials but also provides insight to the physics of vibrations of atoms under different temperature and for different types of materials. I have also evaluated the reliability of Molecular Dynamics simulations at the frequency level and found that theses types of simulations, despite the previous belief, are reliable at low temperatures but up to a measurable frequency. In addition, the result of my work explains the reason for high thermal conductivity of amorphous silicon by showing computational evidence for the presence of high wavelength modes in this material and this work is the first computational work reaching reported low-frequency modes.

To my parents, my beloved wife, and my brother. I couldn't have done it without your support.

ACKNOWLEDGMENTS

I wouldn't be at this point writing my dissertation without the constant support of my advisor Dr. Nicholas Roberts. I owe becoming a Ph.D. student to his trust in me, and he always supported me during the hard times of developing the idea of this work. He mentored me to create a clear picture of my idea and supported putting the puzzle pieces together to create a cohesive scholarly work. I should also mention that I owe my knowledge and interest in nano-scale heat transfer to his guidance and mentorship.

I thank Dr. Barton Smith for introducing me to Dr. Roberst, and I learned so much from him during his classes and my conversations with him while developing this work. I thank Dr. Mark Riffe for the great discussions we had about the concept of Lattice Dynamics and the Dynamics of Vibrations, and I owe so much of my understanding in this area to the great conversations I had with him. I thank Dr. Todd Moon and Dr. Geordie Richards for their fantastic courses, in which I learned so much about mathematics. Their classes changed and formed my understanding of mathematics. Last but not least, I would like to thank Dr. Yanqing Su for her support, and without her contribution, I couldn't defend my dissertation during this semester.

I also would like to appreciate Dr. Jason Larkin's guidance during the last two years of my Ph.D. My dissertation would not have a solid conclusion without his generous help. I want to show my gratitude to the following individuals who help me during my Ph.D. education: Christine Spall, Joan Rudd, Tanner Yorgason, Arden Barnes, and James Moughamian.

Amir Behbahanian

CONTENTS

| | Page |
|--|------|
| ABSTRACT | iii |
| PUBLIC ABSTRACT | v |
| ACKNOWLEDGMENTS | vii |
| LIST OF TABLES | x |
| LIST OF FIGURES | xi |
| ACRONYMS | xiv |
| 1 INTRODUCTION | 1 |
| 1.1 Crystal Structures | 4 |
| 1.2 Thermal Conductivity | 5 |
| 1.2.1 Phonon Dispersion Relation (PDR) | 6 |
| 1.2.2 Experimental studies of Thermal Conductivity | 14 |
| 1.2.3 Computational studies of Thermal Conductivity | 16 |
| 1.3 Dynamics of vibration in amorphous materials | 22 |
| 2 PHONON WAVEPACKET SIMULATIONS USING THE QUANTIZED DEFINITION OF ANERGY AND TEMPERATURE-DEPENDENT PDR AND DOS | 25 |
| 2.1 Introduction | 25 |
| 2.2 Methods | 28 |
| 2.2.1 Phonon Dispersion Relation (PDR) and Density of States (DOS) | 28 |
| 2.2.2 Simulation Conditions | 31 |
| 2.2.3 Wavepacket Generation and Energy Calculation | 32 |
| 2.3 Results and Discussion | 36 |
| 2.3.1 Importance of the Temperature and Energy dependent definition of a Wavepacket | 36 |
| 2.3.2 Frequency Based Validation of MD Simulations | 41 |
| 2.4 Conclusion | 42 |
| 3 TEMPERATURE INDUCED RANDOMNESS IN CRYSTALLINE DIELECTRICS | 44 |
| 3.1 Introduction | 44 |
| 3.2 Methods | 46 |
| 3.2.1 Simulation Conditions | 47 |
| 3.2.2 Thermal Conductivity | 49 |
| 3.2.3 Vibrational Characterization | 52 |
| 3.3 Results and Discussion | 53 |
| 3.4 Conclusion | 62 |

| | | |
|-------|--|----|
| 4 | ATOMISTIC MODELING OF THE MICRON-SCALE PROPAGATION LENGTHS IN AMORPHOUS SILICON | 63 |
| 4.1 | Introduction | 63 |
| 4.2 | Methods | 65 |
| 4.2.1 | Structural Analysis and MD simulations procedure | 65 |
| 4.2.2 | Post-Processing | 66 |
| 4.3 | Results and Discussion | 68 |
| 4.4 | Conclusion | 81 |
| 5 | Summary and Conclusion | 82 |
| | REFERENCES | 84 |
| | CURRICULUM VITAE | 98 |

LIST OF TABLES

| Table | Page |
|---|------|
| 2.1 Lattice Constant Values from computational work $a_{comp.}$ and comparison with the experimental $a_{exp.}$ values. | 38 |

LIST OF FIGURES

| Figure | Page |
|--|------|
| 1.1 (a) single atom basis (b) primitive cell made by translation vectors (PTV (c) face centered unit cell made by the choice of PTV (d) a crystal | 3 |
| 1.2 (a) crystal structure made by putting primitive cells on lattice points (b) crystal structure formed by propagating atoms along the translation vectors (computational purposes) | 5 |
| 1.3 Dispersion relation (Left) and the Density of States (Right) of Argon in different crystallographic diffraction directions at $0K$. The curve is obtained by the GULP package with a Lattice Dynamics (LD) calculation. | 7 |
| 1.4 (a) face centered cubic (FCC) unitcell, (b) FCC primitive structure. In both a and b the primitive vectors are indicated as, a_1, a_2 and a_3 | 8 |
| 1.5 Thermal conductivity comparison between amorphous and crystalline Silicon Dioxide, data extracted from the experimental work by Cahil and Pohl [1] | 23 |
| 2.1 (a) primitive structure conducive to the spatial Fourier analysis (b) validation system (c) volumetric mesh in k -space | 28 |
| 2.2 (a) representation of a displacement wave (b) the displacement wave with interatomic distance marked on it | 33 |
| 2.3 PDR curve and the DOS of the argon crystal at four different temperatures. For comparison the PDR computed, using lattice dynamics (LD), is also included | 34 |
| 2.4 (a) Uncertainty in frequency analysis, inset showing a zoomed area of the graph for more visibility (b) NVT results showing slight difference in frequencies at high frequencies, the NVT results at 50 K and 30 K are not presented for the clarity of the graph (c) The comparison between the PDR resulted from a Green's function approach and experimental work [2] at 10 K The red circles are experimental and the black triangles are computational data, respectively | 37 |
| 2.5 Spatial Fourier validation of of the perturbation (left) and the temporal Fourier validation (right) for four different frequencies at (a) 10 K (b) 30 K (c) 50 K (d) 70 K. The arrows are the 0 K frequencies that are commonly used in the interpretation of the wavepacket simulations. The arrows are color coded with the colors used for each temperature | 39 |

| | | |
|-----|--|----|
| 2.6 | Energy oscillation of the simulation (the shaded area) compared to the energy calculated for each temperature calculated based on the quantum particle picture of the problem (black hexagons) at (a) 10 K (b) 30 K (c) 50 K (d) 70 K | 40 |
| 3.1 | DSF of systems at temperatures 10 K-70 K under the conventional and the CR potential. | 47 |
| 3.2 | Autocorrelation decay calculated using NMD method for a system under presence of a single frequency mode and thermostated at a temperature close to zero | 53 |
| 3.3 | A comparison between thermal conductivity values calculated with NMD and GK, under conventional and CR potential, and the experimental values[Thermal conductivity of solid argon] at four different temperatures 10 K, 30 K, 50 K, and 70 K. The x-axis values are shifted by 1K for every temperature for better visibility | 54 |
| 3.4 | Uncertainty analysis of the Green-Kubo method using 3000 data points derived from ten different ensembles and 100 different trajectories, k_x , k_y , and k_z are considered equal due to the isotropy of the thermal conductivity in argon[20] | 55 |
| 3.5 | Lifetime of modes travelling in the [100] direction. The top row is showing results under the conventional potential and at four different temperature (left to right 10k,30k,50k,70k), The bottom row is showing the results for the same temperatures but for a CR system. The solid black line is the Ioffe-Regel limit of frequency and lifetime. | 57 |
| 3.6 | Spectral Free Path comparison of cases under conventional and CR potential at temperature from 10 K-70 K, the dashed line is indicating the equilibrium lattice constant at the indicated temperature. The calculation is based on $\Lambda_\omega = \tau_\omega v_\omega$, in which the mode velocity (v_ω) is calculated as the derivative of the polynomial fitted to the dispersion relation curve. The graphs are (a), (b), (c), and (d) related to temperatures 10-70 K, respectively. | 58 |
| 3.7 | Spatial coherence calculations for two temperatures 10 K and 70 K. The dotted line is indicating the lattice constant of the argon crystal. | 60 |
| 3.8 | Spatial coherence calculations for two temperatures 70 K and 700 K. The dotted line is indicating the lattice constant of the argon crystal. | 61 |
| 4.1 | The Dispersion resulted from the dynamical Structure factor analysis on both Tersoff (left) and the Stillinger-Weber (right) potentials | 68 |

| | | |
|------|---|----|
| 4.2 | Radial Distribution function 100k WWW system compared with two other experimental, and computational results [3, 4]. The Laaziri experimental results and the computational results of the Larkin work are extracted from the graphs. | 68 |
| 4.3 | top: lifetime of a-Si for both Stillinger-Weber and Tersoff potential. An spline fit is used to fit the data of each branch (Transverse and Longitudinal) for the purpose of eye guide. Bottom: The comparison of density of states for both SW and Tersoff potentials, obtained from lattice dynamics analysis. . | 69 |
| 4.4 | (a) comparison of diffusivities for both SW and Tersoff potentials (top) and the resting group velocities (bottom) the circles are the interpolations required to map the frequency based diffusivities to the wavevector based ones (b) comparison between different values of the broadening factor in the computation of the diffusion for both the SW (top), and the Tersoff potential. . | 73 |
| 4.5 | Group Velocity as a combination of the derivative of the dispersion relation and the AF velocity (top), and the dispersion relation resulted from the peaks of the dynamical structure factor | 74 |
| 4.6 | Spectral Free path of modes calculated using both SW and Tersoff potential, in comparison with other experimental and computational data, and the predicted profile by Minnich | 75 |
| 4.7 | lifetimes of doped samples with Hydrogen, Germanium, and Si-29 (right column) and the corresponding spectral free paths with a constant group velocity approximation (left column) | 77 |
| 4.8 | lifetimes of doped samples with Hydrogen, Germanium, and Si-29 (right column) and the corresponding spectral free paths with a sine interpretation of the dispersion relation and defining group velocity as its derivative (left column) | 78 |
| 4.9 | Green-Kubo calculation of thermal conductivity of three different system sizes. 100k, 4096, and 1000 atom systems | 79 |
| 4.10 | Lifetimes of a 4096 atom sample tiled three (down) and six (up) times. . . . | 80 |

ACRONYMS

| | |
|---------|---|
| FCC | face centered cubic |
| PDR | Phonon Dispersion Relation |
| LD | Lattice Dynamics |
| TDTR | Time-domain thermoreflectance |
| TTG | Transient Thermal Grating |
| AFM | Atomic Force Microscope |
| MD | Molecular Dynamics |
| BTE | Boltzmann Transport Equation |
| DM | Diffuse Mismatch |
| DOS | Density Of States |
| NVT | Canonical Ensemble |
| NVE | Microcanonical Ensemble |
| NPT | isothermal-isobaric Ensemble |
| GULP | General Utility Lattice Program |
| LAMMPS | Large-scale Atomic/Molecular Massively Parallel Simulator |
| CR | conventional plus randomness |
| NMD | Normal Mode Decomposition |
| GK | Greewood-Kubo |
| DSF | Dynamical Structure Factor |
| SSF | Static Structure Factor |
| MFP | Mean Free Path |
| BB-FDTR | Broadband Frequency Domain Thermo Reflectance |
| NEMD | Non-Equilibrium Molecular Dynamics |
| AF | Allen-Feldman |
| SW | Stillinger-Weber |
| RDF | Radial Distribution Function |
| FA | First-Avalanche |

CHAPTER 1

INTRODUCTION

Material characterization has always been the building block of research and development processes in multiple industries. The characterization process targets the discovery of parameters defining the behavior of a material. As a result, any system that deals with the flow of heat as a problem or as an energy source requires better understanding of thermal transport properties. The most frequent applications of fundamental and nanoscale thermal transport properties characterization are thermoelectric devices, thermal interface materials and coupled mechanical resonators. In all of these applications the performance of the devices is dependent upon the thermal properties of materials used in the device.

Thermoelectric devices work based on the thermoelectric effect, which states that applying a voltage difference across a multi-material interface will result in a temperature difference (Peltier effect) and the temperature difference across a multi-material interface will produce voltage difference (Seebeck effect). The effect has applications in waste heat recovery and ultrafast thermal management (heating-cooling) devices [5]. All of these applications initiated multiple research efforts to increase the efficiency of these devices [6–11]. Despite the benefits of the thermoelectric devices, the efficiency of them has not yet met the needs of the industry [5], as a result increasing their efficiency is an active area of research. The efficiency in thermo-electrical systems is defined in the context of the figure of merit equation, the equation defines the efficiency of the system in terms of Seebeck coefficient (S), electrical conductivity (σ), temperature (T), and the thermal conductivity (k), respectively, the thermal and electrical transport properties have always been the knob for a better efficiency,

$$ZT = \frac{\sigma S^2 T}{k}. \quad (1.1)$$

The increasing demand for smaller yet more efficient electronics has pushed the industry towards the limitation induced by the increased volumetric heat generation. This obstacle initiated research efforts to reduce the thermal interface resistance either by thermal interface materials at the macro level [12,13] or manufacture material joints with better coupled properties [14,15]. The high computational and storage power provided by manipulating the boundary conductance of an interface has motivated researchers to inspect these properties and try to explore the potential enhancement opportunities of these properties [16].

Advances in sensing technologies have always demanded precise detection of vibrations. Better sensing in advanced microscopy techniques [17,18] and more precise mass sensing in gravimetric sensors [19,20] are examples of technologies that can take advantage of higher sensing resolution, as a result of better coupled mechanical resonators, which is based on maximum vibrational energy transportation between two resonator and minimum decay across an interface in a coupled resonator. The advantages offered by the better sensing technologies has provided the motivation for research efforts targeting a more coupled contact between dissimilar materials [21].

The classical definition (Fourier's law of Heat Transfer) of thermal conductivity (k) defines it as the constant of the linear relationship between heat flow across a temperature gradient. Fourier's law describes a system at steady state. The need for a fundamental understanding of the thermal conductivity that accounts for the temperature dependency of the property and employs the importance of fundamental material characteristics in the definition, resulted in a more convoluted definition of the property. The definition appreciates the frequency (ω), Density of states ($D(\omega)$), equilibrium particle distribution function (f_0) of vibrations, the temperature (T) dependence of these parameter and the heat capacity $c(\omega, T)$. It defines the thermal conductivity in terms of the heat capacity, phonon (Collective vibration of atoms) group velocity (v), and the frequency dependent

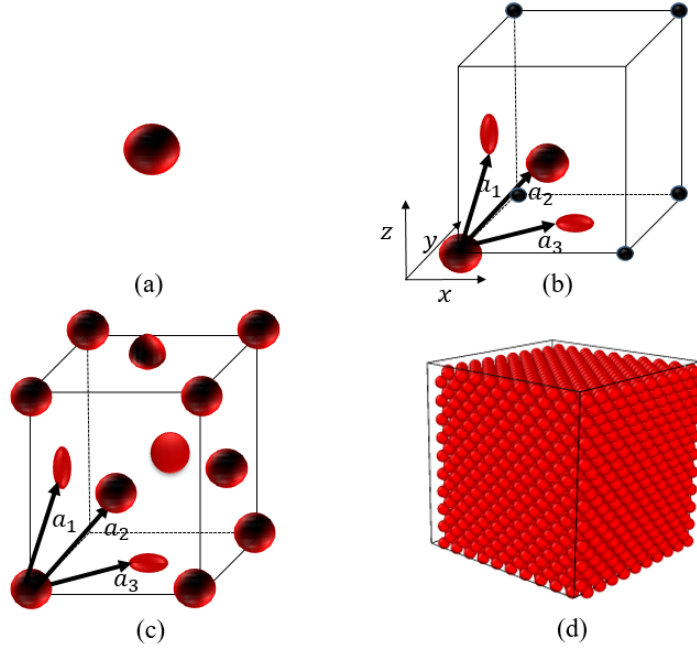


Fig. 1.1: (a) single atom basis (b) primitive cell made by translation vectors (PTV) (c) face centered unit cell made by the choice of PTV (d) a crystal

phonon lifetime ($\tau(\omega)$),

$$c(\omega, T) = \hbar\omega \frac{df_0}{dT} D(\omega),$$

$$k = \frac{1}{3} \int_0^{\omega_{max}} \tau(\omega) v^2(\omega) c(\omega, T) d\omega. \quad (1.2)$$

As the equation presents, manipulation of thermal conductivity is possible with having a better understanding of the frequency behavior of both heat capacity and phonon-lifetime. The aforementioned research areas, to support ongoing technology advances, are dependent on the frequency-based analysis of energy storage and transport in materials. Considering the two types of energy carriers, electrons and lattice vibrations (Phonon), we will limit ourselves to the prominent energy carries in non metals (Phonon). The importance of phonons in a crystal structure became more prominent with the consideration of their role in the definition of thermal conductivity.

Amorphous and crystalline materials are both used in the aforementioned applications. In this dissertation I am searching for resemblance between the dynamics of vibrations in these two types of structures. The resemblance will shed light on the dynamics of crystalline materials at high temperatures and I will use the developed tools to address the low frequency scaling of lifetimes and mean free paths in amorphous silicon. The mentioned two aims will prove the possibility of using methods used to model amorphous materials for crystalline materials at high temperatures, and will provide evidence for high thermal conductivity of amorphous silicon compared to other materials, respectively. I will expand more upon the problem in the methods section. Before I explain the research procedure and my methods I will setup the basis with explaining the concept playing an important role in setting up the line logic in this proposal. The concepts are the notion of crystal, the computational and theoretical background to calculate the thermal conductivity, and a brief description of the dynamics of amorphous materials.

1.1 Crystal Structures

Any material in the solid state that has its atoms in an ordered orientation is called a crystal. The building block of a crystal is a primitive cell, which is the three dimensional translation of basis atoms with three vectors (a_1, a_2, a_3) . These vectors are called primitive translation vectors. They propagate the atoms in a way that the view of the primitive cell formed by the translation operation is the same from any two points r and r' . The points are the result of the following translation equation [22],

$$r' = r + c_1 a_1 + c_2 a_2 + c_3 a_3. \quad (1.3)$$

In the hierarchy of structural complexity we start with a basis (in this case a single atom is the basis Fig.1.1.a) then we form a primitive cell (Fig.1.1.b) and by putting primitive cells on the lattice points (black points in the Fig.1.1.b), we form a crystal structure (Fig.1.1.d). The choice of different primitive translational vectors will provide different unit cell structures such as face centered cubic (FCC) (Fig.1.1.d). The structure used for com-

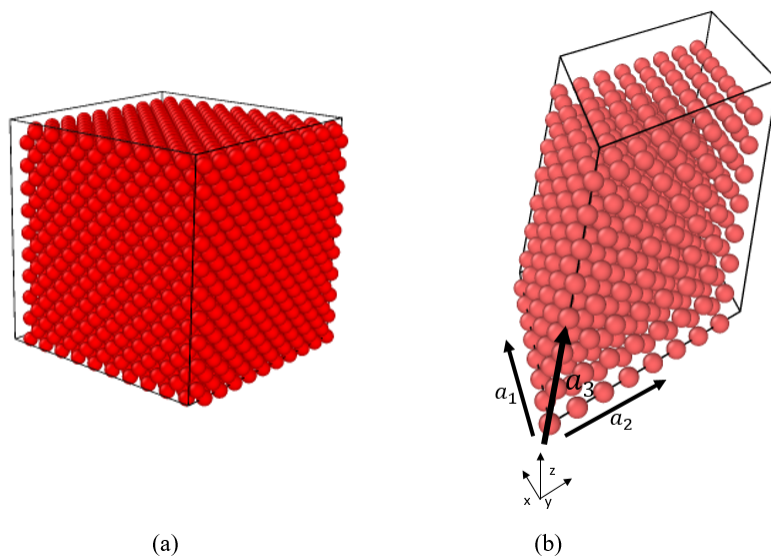


Fig. 1.2: (a) crystal structure made by putting primitive cells on lattice points (b) crystal structure formed by propagating atoms along the translation vectors (computational purposes)

computational purposes is formed with expanding the crystal along the translational vectors, I call this structure a primitive structure. All the computational applications that require symmetry with respect to the primitive cell use the primitive structure for their analysis (Fig.1.2.b).

Crystal structures with a basis that have more than one basis atom are more common in nature. Silicon, sodium chloride and magnesium silicide are examples of crystal structures with more than one atom in their basis. In many crystallographic analyses the behavior of the whole crystal is averaged for all basis atoms in the structure, and mapped onto the frequency space by a spatial Fourier transform. As a result the number of atoms in the chosen basis play an important role in the precise presentation of the crystal behavior.

1.2 Thermal Conductivity

The thermal conductivity is classically defined as a material's thermal transport property that is defined in the state of equilibrium. The simplest definition of thermal conductivity k is a constant of linear relationship between the temperature difference ΔT across

a sample with known thickness Δx and passing known amount of heat rate q . The linear relation is well-known as Fourier's law of heat transfer,

$$q'' = -k \frac{\Delta T}{\Delta x}. \quad (1.4)$$

The definition is able to define the property in the linear region of the behavior but fails to provide a reasonable definition of thermal conductivity as a function of temperature with a single measurement. It also doesn't consider the material structure role in the definition of the property. To address both problems the bulk thermal conductivity can be defined in terms of the nanoscale contribution of phonons, which is a temperature dependent phenomenon Eq. 1.2. The equation provides a more detailed definition of thermal conductivity, which will leverage the possibility of designing thermal system with optimum efficiencies.

In the following section I will explain the Phonon Dispersion Relation (PDR) that is the frequency-wavevector characterization of atomic vibrations in a material. The notion is the most fundamental approach analysis that provides the information required to characterize the transport properties. PDR can be developed computationally and experimentally, I will explain the theoretical and computational approaches to develop PDR due to the computational nature of this proposal.

1.2.1 Phonon Dispersion Relation (PDR)

The Phonon dispersion relation is the relationship between a material frequencies and wavelengths, which is a one-to-one correspondence for crystalline materials at low temperatures and the correspondence becomes a surjective map for amorphous materials. The slope of the graph in a bijective map presents the phonon group velocities. This relationship characterizes the frequency dependent dynamics of a system of particles (Fig. 1.3).

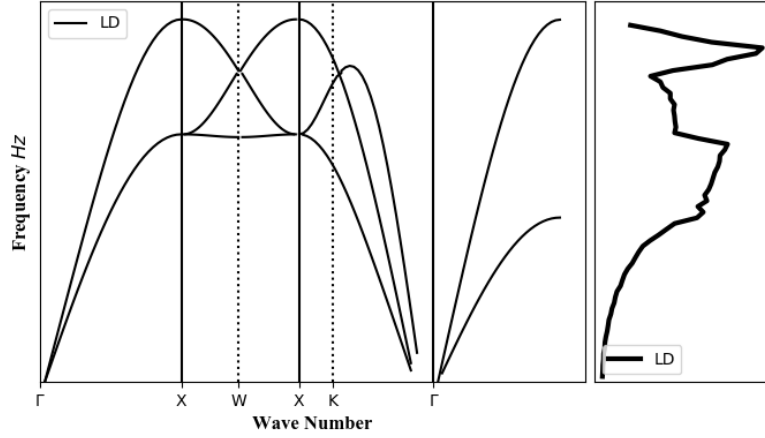


Fig. 1.3: Dispersion relation (Left) and the Density of States (Right) of Argon in different crystallographic diffraction directions at $0K$. The curve is obtained by the GULP package with a Lattice Dynamics (LD) calculation.

Phonon Dispersion Relation (PDR) Theoretical Understanding

The phonon dispersion relation is traditionally developed based on small perturbation of the canonical coordinates q , which define the state of a system at each microstate

$$q_i = q_{i0} + \eta_i \quad (i : \text{particle number} | 1, 2, \dots, n).$$

Based on the small perturbations we can define the Lagrangian of the system as the difference between the kinetic T and potential V energy, where m is the particle mass and ν_{ij} is the diatomic potential change with respect to two coordinates $\nu_{ij} = \frac{\partial^2 V}{\partial q_i \partial q_j}$

$$L = T - V = \frac{1}{2} \sum_i \sum_j (m_{ij} \dot{\eta}_i \dot{\eta}_j - \nu_{ij} \eta_i \eta_j). \quad (1.5)$$

Now we can take advantage of Lagrange's equation and define the equation of motion for all the particles, in a system with n degrees of freedom (number of particles) limited by

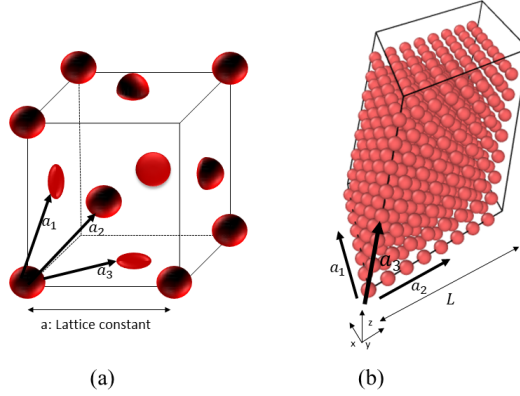


Fig. 1.4: (a) face centered cubic (FCC) unitcell, (b) FCC primitive structure. In both a and b the primitive vectors are indicated as, a_1, a_2 and a_3 .

c number of constraints

$$\frac{d}{dt} \frac{\partial L}{\partial \dot{\eta}_i} - \frac{\partial L}{\partial \eta_i} = 0$$

$$\sum_{j=1}^{n-c} (m_{ij} \ddot{\eta}_j + \nu_{ij} \dot{\eta}_j) = 0 \quad , \quad j = 1, \dots, n. \quad (1.6)$$

The path to a solution considering the wave-vectors ($k|k_0 = 0, k_1 = \frac{2\pi}{aL}, \dots, k_m = \frac{2\pi}{a}$, the resolution of the wave-vector steps is dependent on the symmetric system size (L) and the lattice constant (a) Fig. 1.4), and the frequencies goes through the definition of a solution format and defining our system of particles in the context of basis atoms ($a, b|1, 2, \dots$, No. of atoms per basis). Considering,

$$\eta_j^b(t) = \frac{1}{\sqrt{m_i m_j}} P_k e^{ik \cdot q_b} e^{-i\omega_k t} \quad (1.7)$$

in which, P is the wave-vector dependent constant (Eigenvector) and ω is the wave-vector dependent frequency, we can solve the ordinary differential equation (Equation of motion),

$$\omega_k^2 P_k = \frac{1}{\sqrt{m_a m_b}} \sum_a \sum_b \left[\sum_l \nu_{ab} e^{ik \cdot q_{a,b}} \right] P_k. \quad (1.8)$$

The value in the brackets is considered to be the spatial Fourier transform of the inter-atomic potential $\tilde{\nu}_{ij}$ with respect to the canonical coordinate q , and the summation is over the same basis atoms in different basis groups l . It is also important to mention that the subscripts a, b are defining the relative generalized coordinate of atoms a and b in the basis, but the origin of the basis containing atom a can be taken as zero to define all the generalized coordinates from the origin.

The value in the brackets, combined with the mass terms, is called the dynamical matrix $D(k)$. As the spatial Fourier transform maps the average behavior of the basis atoms onto the Fourier Space, the number of basis atoms determines the number of vibrational branches (each curve in the PDR) in the dispersion relation. To avoid folded branches (braches caused by interaction between repetitive atoms) all the calculations including a spatial Fourier transform require a primitive system, which is the result of basis atom propagation,

$$D_{ab}(k) = \frac{1}{\sqrt{m_a m_b}} \tilde{\nu}_{ab}. \quad (1.9)$$

and finally the dispersion relation is the solution to the following eigen problem,

$$\omega_k^2 P_k = \sum_a \sum_b D_{ab}(k) P_k. \quad (1.10)$$

In the context of theoretical mechanics [23], there is a modal based solution that states the atomic displacements in terms of single vibrational modes. To achieve such a solution modal matrix (M), which is composed of all the available eigenvectors, is formed,

$$M = \begin{bmatrix} P_0^0 & P_0^{k_1} & \dots & P_1^{k_m} \\ \vdots & \vdots & \ddots & \vdots \\ P_{k_m}^0 & P_{k_m}^{k_1} & \dots & P_{k_m}^{k_m} \end{bmatrix}. \quad (1.11)$$

On the basis of this new matrix a new displacement variable can be defined, that is called generalized coordinates $\zeta(t)$. And a linear proportionality equation is considered

between the displacement $\eta(t)$ and the generalized coordinate $\zeta(t)$,

$$\eta(t) = M\zeta(t) \quad (1.12)$$

because of the matrix nature of M the relation takes the following format, by multiplying both sides by $M^T m_{kk}$,

$$M^T m \eta(t) = \zeta(t). \quad (1.13)$$

By rewriting the Lagrangian equation using the new variable,

$$L = \frac{1}{2} \sum_k (\dot{\zeta}_k^2 - \omega_k^2 \zeta_k^2)$$

we can offer a solution to the Lagrange's equation,

$$\zeta = A_k e^{ikq_i} e^{-iw_k t}$$

and using the Eq. 1.12, we can define the displacements in modal format at each instant.

$$\eta_k(t) = \sum_i A_k P_k e^{ikq_i} e^{-iw_k t} \quad (1.14)$$

The summation is over all the atoms in the system, for every isolated wave-vector k and frequency ω_k . This equation was used by Henry and Chen [24] in their phonon lifetime analysis, with the consideration of removing the time dependence of the equation to find the instantaneous amplitude A_k . They calculated the autocorrelation function of the amplitude over time to track the decay of the amplitudes (phonon lifetime).

PDR Computational Methods of development

In this section I will explain the computational methods to develop temperature dependent PDR and the DOS. Except the Lattice Dynamics methods that are based on the theoretical explanation of PDR with no time evolution of the dynamics and can't capture the temperature dependency of PDR, I found two methods that are both based on the

temperature dependent dynamics of the system.

Before I explain the development of temperature dependent PDR I will expand more on the Lattice Dynamics methods that was briefly mentioned in the previous paragraph, explaining two of the algorithms used for the calculation. The first algorithm is based on the theoretical background of the dispersion relation. The computational algorithm moves the atoms, grouped in smaller chunks of atoms called super-cells, in different directions and develops the dynamical matrices [25, 26]. This method is based on the density functional perturbation theory and is also called frozen-phonon method. The theoretical derivation that is provided in this document can be used for both frozen phonon method and the next algorithm. The second method uses the equation of motion and finds the derivative of potential for a diatomic or multi-atomic potential and mathematically solves the equation of motion to obtain the frequencies for different wave-vectors [27].

Both of the provided methods calculate the dispersion relation, but at zero Kelvin. For most of the applications the required understanding of the system behavior is at temperatures above the zero kelvin. Two computational methods provide the dispersion relation at any target temperature. The first method uses molecular dynamics simulations and outputs the atom velocities and forms the velocity autocorrelation functions for different polarizations p and wave-vectors k ,

$$v^\alpha(k, t) = \sum_i v_i^\alpha(t, r) e^{-ikr_i} \quad (1.15)$$

$$A^\alpha(k, t) = \frac{\langle v^\alpha(k, t) \cdot v^\alpha(k, 0) \rangle}{\langle v^\alpha(k, 0) \cdot v^\alpha(k, 0) \rangle}$$

$$A^\alpha(k, \omega) = \sum_{T_{sim}} A^\alpha(k, t) e^{-i\omega t} \quad (1.16)$$

In which, the velocities are transformed to the spatial Fourier transform of the instantaneous velocities (Eq. 1.15). The dispersion relation is the result of the Fourier transform analysis of the obtained data set for every wave-vector. Heino claimed that the accuracy of the model is limited to the accuracy of the interatomic potential [28].

The last molecular dynamics-based method that I will also use as part our methodology is the method developed by Ling Ti Kong [29, 30]. He defined the dynamical matrices ($D_{iq}(k)$) as a function of force constant matrices ($\phi_{iq}(k)$), and the force constant matrices as a function of instantaneous atom position (\tilde{R}_{iq}), which is the spatial Fourier transform of atom positions of the primitive cell locations (r_l), for any favorable canonical coordinates q like the atom positions. Please also consider that the indices i and j are to indicate atoms in a primitive cell (unless otherwise is stated).

$$\tilde{R}_{iq} = \frac{1}{\sqrt{N}} \sum_l R_{i,q} e^{-iqr_l} \quad (1.17)$$

Kong used the Green function $G_{ij} = \frac{1}{k_b T} \langle u_i u_j \rangle$, to correlate the interatomic interactions to the second moment of atomic displacements u with temperature T and the Boltzmann constant k_b as the constants of correlation. He transformed the equality to one that is related to the instantaneous positions for easier calculations,

$$\tilde{G}_{ij} = \langle \tilde{R}_{iq} \tilde{R}_{jq} \rangle - \langle \tilde{R}_{jq} \rangle \langle \tilde{R}_{iq} \rangle. \quad (1.18)$$

Using the definition of force constants $\phi_{iq}(k)$ we can define it as follows,

$$\phi_{iq}(k) = k_b T G^{-1}. \quad (1.19)$$

As a result of the definition the dynamical matrices are defined,

$$D_{iq}(k) = \frac{1}{\sqrt{m_i m_j}} \phi_{iq}(k). \quad (1.20)$$

The above definition provides the frequencies for every wave-vector as the eigenvalues of the eigenequation (Eq.1.8). Lets work out an example to provide a better understanding of the indices. Assuming a system with n particles and symmetric with respect to the primitive cells, we also limit the motions of the atoms in three translational dimensions (x, y, z). Considering our hypothetical system of particles having two atoms in the primitive cell like

a system of particles in a diamond structure, we will get two 3×3 dynamical matrices for every wave-vector and each atom in the primitive cell. Each of the dynamical matrices will provide both the optical and acoustic eigenvalues corresponding to the respective branches of vibration on a dispersion curve.

The recent method provides an easy to apply method for the development of phonon dispersion relation at all required temperatures. It also provides the dynamical matrices that have a substantial role in the analytical and computational thermal transport properties characterization methods provided in the computational sections (sec.1.2.3).

1.2.2 Experimental studies of Thermal Conductivity

The experimental studies of thermal conductivity of materials in the solid state can be divided into two main subcategories, bulk and nanoscale thermal conductivity analysis. The bulk measurement methods provide the thermal conductivity of samples in millimeter scale up to large samples. But knowing the thermal conductivity of materials at the nanoscale requires special setups. In the following paragraphs I will provide a concise definition of bulk thermal conductivity measurement techniques and will add the main techniques to measure nanoscale thermal conductivity to our discussion.

The bulk thermal conductivity measurement methods are typically based on the Fourier's law of heat transfer. The main idea is to apply a temperature difference across a sample and let it equilibrate around the required temperature. The heat flow in the sample is measured by measuring the heat flow in the side clamps, holding the sample, and averaging the values to get an estimate of the heat flow in the sample. The thermal conductivity is then calculated knowing the temperature difference across the sample, heat flow in the sample and the geometry of the sample [31].

The thermal conductivity measurement at the nanoscale enables the analysis of manufactured and existing systems in the scale. The three main methods to obtain nanoscale understanding of material properties are, Time-domain thermoreflectance (TDTR), scanning thermal microscopy, and nanometer-scale thermal analysis/manufacturing [32]. The 3ω method and the suspended-islands nanofabricated devices also provide the thermal transport properties at the nanoscale, but both methods are limited compared to the other three mentioned methods. We will provide an overview of these methods in the following paragraphs.

In 1986 Maris and Eesley separately provided the characterization of thermal transport properties of material with the aid of thermoreflectance analysis. The method has remained almost untouched over the years. The approach is to deposit a transducer layer on top of the sample then a pump laser beam is applied to that layer and the change of the reflectivity of the sample due to the temperature change is measured by a differentiated and lagged

piece of the main beam, called the probe beam (Probe beam). The collected data is then fitted to the analytical models of a system subjected to an oscillatory heat source, to obtain the unknowns of the model [33].

Scanning thermal microscopy is another technique that takes advantage of fitting the analytical solution to the experimental data. The approach facilitates the thermal conductivity measurement of metal thin films. A metal thin film is deposited on a dielectric substrate with a shape that provides a bottle neck for the flow of electrons, which creates an expansion region due to Joule heating plus a temperature gradient. The Scanning Probe Microscope with a thermal measurement tip can sense the gradient at different heating frequencies, which completes the measurement setup [34].

The two previous setups are dependent on an external source of heat generation. Techniques that take advantage of the Atomic Force Microscopy (AFM) are able to use the AFM tip to create the hot spot on the sample by the tip of the microscope and measure the temperature at the same time. An understanding of the heat flow between the tip and the substrate provides the means to measure the thermal properties of the sample [35]. Although not related to the thermal characterization, one of the interesting uses of the setup is that the setup with an injection capability at the tip can facilitate the lithography on a substrate, which provides tremendous resolution and spatial resolution for manufacturing in that scale [36].

The two other mentioned methods provide valuable information about the effective thermal conductivity of the sample-system [32]. The 3ω method uses a sinusoidal voltage source to create an oscillating heat source on the sample. The heat source oscillates with twice the frequency of the voltage source and creates a temperature oscillation with the same frequency, which leads to a temperature dependent resistance oscillation, with three times the voltage source frequency. Finally the third harmonic resistance oscillation creates the third harmonic temperature oscillation that is carrying the material properties information [37]. The suspended-island method is one of the suitable methods for the measurement of transport properties of the nanostructures. The method has two islands, one creating

the Joule heating and thus a temperature difference across the sample placed between the islands. The result of the temperature measurements and an understanding of the thermal conductance between the nanostructure and the islands provides the required information for the thermal conductivity measurement of the sample [38].

1.2.3 Computational studies of Thermal Conductivity

Computational studies of thermal conductivity can be performed using a powerful simulation tool called molecular dynamics. Molecular dynamics (MD), in general refers to any coded package that simulates the inter-atomic interactions and solves the equations of motion for all the entities in the simulation box to provide the time evolution of the system. The package produces important information about the dynamics of the system at each time-step, which are used to characterize the system of study.

Thermal characterization methods based on MD simulations are categorized in two main groups, equilibrium and nonequilibrium. The nonequilibrium method uses Fourier's law of heat transfer and simulates a system with a heat source and a heat sink. The heat sink removes the same amount of heat that is supplied by the heat source. The process is based on interchanging the velocity of the hottest atom in the hot region with the velocity of the coldest atom in the cold region [39]. With MD packages like LAMMPS the addition and subtraction of heat are two separate processes. After equilibrating the system and having the temperature gradient, the sample thickness, area, and the heat flux the thermal conductivity of the sample will be calculated using Fourier's law of heat transfer (Eq.1.4). The method is used extensively, because of the simplicity in setup and post-processing, in different thermal analysis simulations as Nanoparticle effect on thermal conductivity and etc. [40].

The equilibrium MD approaches are based on the fluctuation dissipation theorem and regarding the theorem one can find the material properties based on the information obtained from the MD simulations. The following two sections will explore one non-MD based and the most common MD-based methods for calculating the thermal conductivity. These methods are explained due to their extensive use in the past ten years.

Thermal Conductivity based the solution of the Boltzmann Transport Equation (BTE)

The classical attempts to provide a descriptive definition of transport in materials, included a cumulative contribution of frequency in their analysis [41–44]. Callaway solved the Boltzmann Transport Equation (BTE) based on the gray assumption, with which the a single relaxation time is assumed for all the polarization directions and frequencies [42].

$$k = \frac{k_b}{2\pi^2 |\nu_g|} \left(\frac{k_b T}{\hbar}\right)^3 \int_0^{\theta_D/T} \tau(x) \frac{x^4 e^x}{(e^x - 1)^2} dx \quad (1.21)$$

where k_b is the Boltzmann Constant, v_g is the phonon group velocity, T is the temperature, \hbar is the reduced Plank constant, θ_D is the Debye temperature, $\tau(x)$ is the cumulative phonon lifetime, and x is defined as $\frac{\hbar\omega}{k_b T}$.

Callaway's work was extended by Holland, who added the frequency dependency of the phonon lifetime to Callaway's work, using the Debye approximation of the phonon dispersion, and assumed a dispersion relation with a constant slope (Constant group velocity). The result of his work was a polarized thermal conductivity definition, distinguishing between the Longitudinal and Transverse polarization directions.

$$k = k_{Longitudinal} + k_{Transverse}$$

$$k_L = \frac{1}{3} \int_0^{\theta_D/T} C_L T^3 \tau_L(x) \frac{x^4 e^x}{(e^x - 1)^2} dx$$

$$k_T = \frac{2}{3} \int_0^{\theta_D/T} C_T T^3 \tau_T(x) \frac{x^4 e^x}{(e^x - 1)^2} dx \quad (1.22)$$

$$C_{L,T} = \frac{k_b}{2\pi^2 |\nu_g|_{L,T}} \left(\frac{k_b}{\hbar}\right)^3$$

Regarding the assumptions made by Holland and Callaway, the bulk thermal conductivity calculations made by these approaches over-estimate the conductivity [45]. The fact can be justified by the lower group velocity of phonons (v_g) at high frequencies compared to the sound velocity at lower frequencies.

A wide range of applications introduced the need for a better understanding of transport properties with incorporation of nonlinear dispersion relation. As a result, Majumdar and Mazumder introduced the first comprehensive algorithm to solve BTE with nonlinear dispersion relation and considering various polarizations [46]. Their approach was based on the Monte Carlo solution technique, they created six independent stochastic spaces and defined the phonon vectors and positions with the random numbers and the scattering process was also defined based on the scattering time scale and the time step in the simulation. Despite the convoluted procedure they didn't define the effect of optical branches in their analysis. Mittal and Mazumder solved the problem and added the contribution of optical phonons in thermal conductivity of silicon [47]. They found the importance of optical phonons in temperatures above 200 K, also defined the three phonon interactions with the definition provided by Kelemns [48], and defined new scattering regimes provided by Narumanchi [49]. The BTE technique has also been used in the thermal boundary conductance analysis [50], which is a vast research discipline and will be addressed in a separate section.

Statistical Mechanics based Analysis (Based on MD)

Statistical mechanics is the other approach to model and characterize physical systems. The approach can provide a remarkable amount of information from the transport properties in a material to the statistical evolution of a system over time.

Ryogo Kubo used this approach and modeled a hypothetical many-particle system with the aid of linear response theory, which correlates an observable in the system with a set of other observables (or a single observable) in a linear relationship. The transport properties of the system in any context (Electrical/Mechanical) is the constant of this relationship. Considering a heat problem, the linear relation is the equation for the heat current J and the temperature gradient ∇T , and the thermal conductivity is the constant of the linear relationship [51, 52],

$$J = -k\nabla T. \tag{1.23}$$

Kubo used statistical mechanics to define the constant of the relationship. As a function of Boltzmann-constant (k_b), temperature (T), volume (V), and heat current (j) Autocorrelation within the time window-length of t_w ,

$$k = \frac{1}{Vk_bT^2} \int_0^{t_w} \frac{\langle j(0)j(t) \rangle}{3} dt. \quad (1.24)$$

The most adopted version of the heat current by the heat transfer research community is the time derivative of the sum over all particles energy (E_i) and position (r_i),

$$j = \frac{d}{dt} \sum_i r_i E_i. \quad (1.25)$$

The heat current for a pair potential is defined, knowing the inter particle distance (r_{ij}), inter atomic force (F_{ij}), and particle velocities (v_i). The summation is over all the particles in the system, neglecting self interaction ($i \neq j$),

$$j = \sum_i E_i v_i + \sum_{ij} r_{ij} (v_i \cdot F_{ij}) \quad (i \neq j). \quad (1.26)$$

With the improvement of the computational power, research attempts led to computational analysis of frequency-based phonon lifetime including a full-dispersion curve. Volz calculated the thermal conductivity of silicon and achieved reliable thermal conductivities at high temperatures [53, 54], at which the long wavelength phonons contribute less to the thermal conductivity. He attributed the low frequency errors in his calculations to two main problems, 1) the limitation of simulation size and the removal of wavelengths bigger than the simulation cell size and 2), the dependency of heat flux vector on the spatial Fourier transform of the local heat vectors.

McGaughey and Kaviany followed the same approach to calculate the thermal conductivity. They provided an additional piece of information and characterized the cumulative (averaged for all frequencies) lifetime of phonons with a two-stage behavior and attributed the fast decay to the nearest neighbor interactions, and the second decay time to the long

range interactions [55]. The time-decays were defined based on the heat flux-autocorrelation normalized by its initial value,

$$\frac{\langle j(0) \cdot j(t) \rangle}{\langle j(0) \cdot j(0) \rangle}. \quad (1.27)$$

McGaughey and Kaviany expanded their next work and defined the preferred path of travel for the energy in SiO_4 with an energy autocorrelation [56]. They also characterized the behavior of atom-atom bond in the process of energy transport, using the same autocorrelation results. The last piece of their trilogy was to make the connection between the BTE solution approach and the Kubo analysis. The analysis was to find the decay of normal modes, considering the energy autocorrelation function decay and using a fit for the calculated decay times. They used the fitted value for decay as the lifetime for BTE-based thermal conductivity calculation, also reported acceptable match between the result of two approaches [57].

In continuation of these valuable works, Henry and Chen defined their frequency-based phonon lifetime on the basis of the normal coordinate-based atom vibration amplitudes time-decay [24],

$$A(k, p, t) = \sum_j (r_j - r_{j0}) P_j(k, p) \exp(i.k.r_{j0}). \quad (1.28)$$

The above equation define the vibrational amplitudes as a function of polarization (p), wave-vector (q), time (t), atom displacement over time ($r_j - r_{j0}$), and dynamical matrix eigenvectors $P(q, p)$. They monitored the decay time with the aid of initial and instantaneous amplitudes autocorrelation for each wavevector,

$$\frac{\langle A(0) \cdot A(t) \rangle}{\langle A(0) \cdot A(0) \rangle}. \quad (1.29)$$

The Henry and Chen's work is based on the dispersion relation, which is a very important relationship between the allowable frequencies, wavelengths and the phonon group velocities (The velocity of a wave in its direction of travel) at each temperature (Sec.1.2.1).

The motioned techniques are to provide the thermal conductivity of a single material in both nanoscale and bulk scales for a single material, but most of the industrial applications

put two same or different material in contact with each other that defines a new transport property called thermal boundary (interface) conductance. The property is the subject of multiple research efforts and will be briefly reviewed in the following section.

Thermal Boundary Conductance

Even a perfect perfect contact between two materials will inherit a resistance called thermal interface resistance. The definition of thermal interface resistance or in its reciprocal format thermal interface conductance was first based on the Acoustic Mismatch (AM) model, that defines the transmission across an interface in terms of the acoustic impedance ($Z = \rho c$) of two materials [58]. The definition will fail to define the transmission across two materials with the same crystal structures as they have the same impedance. The mentioned limitation led to the definition of a new analysis method called the Diffuse Mismatch (DM) model, the model predicts the transmission of phonons based on a perfect crystal phonon dispersion relation. The probability of a phonon passing an interface or the scattering events are dependent on the frequency-based homogeneity of two sides of the interface. A more involved description on the model defines the transition with the aid of Fermi's Golden Rule, which defines the transition between energy states in a continuum of states by applying the perturbation theory to the system.

Both aforementioned approaches are unable to define the interface-geometry contribution to the interface resistance [59]. Schelling introduced the phonon dynamics simulation for a better definition of the interface transmission [60]. The method is based on creation of waves with a Gaussian envelope, known wave-vector, and polarization in an MD simulation. The wave will interact with the interface and by monitoring the characteristic of the wave and the passed wave the transmission is defined for the well defined wave packet.

The other method that can differentiate between different frequencies and polarizations is the Green's function method. The method uses the coupled greens functions of a sample sandwiched between two contacts to define the solution of the dynamical equation of the coupled system. The definition provides the transmission function in terms of the Green's function and the connection matrices defined within the dynamics definition of the

system. [61]. Although the method provides a detailed frequency-based analysis, the calculation becomes cumbersome for complicated geometries. As a result the calculation is limited to simple nanostructures like nanowires [62].

Barrat used the Green-Kubo formulation to define the boundary conductance but they were missing the frequency decomposition of the analysis as with other Green-Kubo based analysis [63]. The method is based on the spatial average of the power (P) on both sides of the interface, and defines the boundary conductance (G) in regards.

$$G = \frac{1}{Ak_bT^2} \int_0^{\omega_{max}} \langle P(0).P(t) \rangle dt \quad (1.30)$$

The Green Kubo formulation also helped other researcher to develop methodologies defining the frequency-frequency contribution in boundary conductance [64].

The understanding developed in the preceding sections are all defined in the context of crystalline materials, although most of them can be used for amorphous materials with some modifications. As growing a crystal in many cases is expensive, a great piece of literature is based on amorphous materials and understanding their odd thermal conductivity behavior versus temperature [1]. In the following section I will explain the details of the dynamics of vibrations in amorphous materials as the last piece in the introduction section.

1.3 Dynamics of vibration in amorphous materials

The difference in the temperature dependency of thermal conductivity in crystalline and amorphous materials (Fig. 1.5) has initiated research efforts to understand this phenomenon [65, 66]. These efforts resulted in a diverse taxonomy in defining vibrational behavior and scattering events of amorphous materials. The three main modes of vibrations defined for amorphous materials are Propagons (P)(propagating modes), Diffusons (D), i.e., vibrational modes with no defined wave vector but having energy transport capabilities, and Locons (L) that are local modes with high local magnitudes and low contribution to thermal conductivity [67]. As a result, the frequency transition limits from one regime to the other are defined as Ioffe-Regel and the mobility edge. The former is the frequency

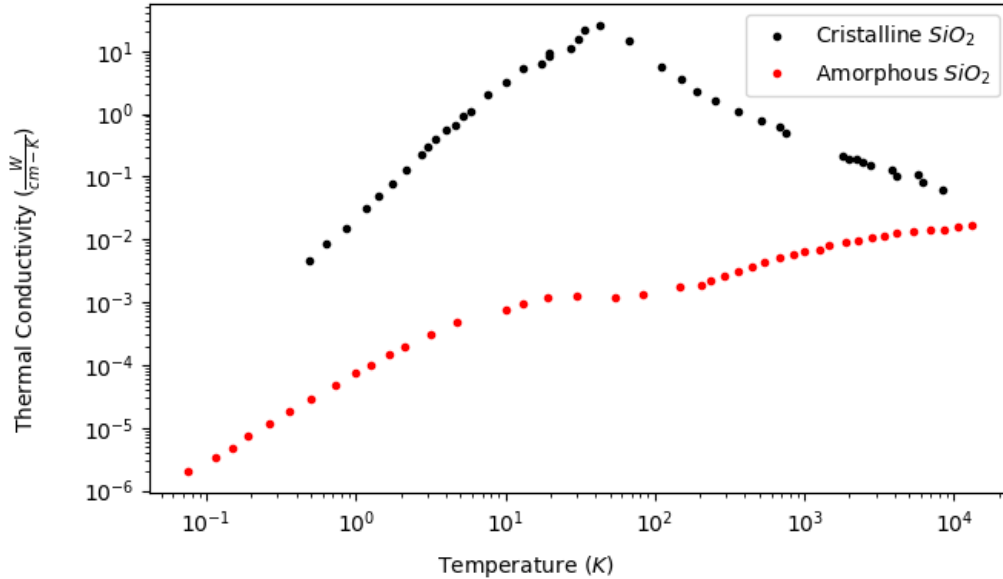


Fig. 1.5: Thermal conductivity comparison between amorphous and crystalline Silicone Dioxide, data extracted from the experimental work by Cahil and Pohl [1]

border between P-D and the later is the border between D-L [67] and has its roots in the concept of electron localization [68]. Although the need for such terminology was disputed by some authors experimentally [69], the terminology resulted in the definition of thermal properties based on the classification [70], and some authors mandated the definition to explain their results [71]. Less commonly used modes are floppy modes that are temporally and spatially trapped modes [67] and Resonant modes that are spatially non-exponentially decaying modes [70].

Along with the classifications of types of vibrations, defining types of scattering with respect to frequency is another approach, in parallel with the previous one, to find explanation for the odd temperature behavior of the thermal conductivity in amorphous materials. Kittel scattering defines the frequency independence of scattering on a scale that the mean free path is lower than the atomic distance [65]. Klemens scattering defines the scattering resulting from transverse and longitudinal modes' interactions through the anharmonic terms of the interatomic potentials or interaction with local modes [66]. Moreover, the most historically used scattering classification [72] is a Mean Free Path or lifetime vs. frequency

classification. For example ω^{-2}, ω^{-1} are the behaviors defining the lifetime vs. frequency data in the low frequencies regime, and ω^{-4} (Rayleigh Scattering), ω^{-3} [73] explains the scattering events in the mid-range frequencies interval. These regimes were observed in both experimental [69,74] and computational [67] works.

On the one hand, the science associated with this terminology has opened the avenue to phonon engineering [75], and it creates the motivation to seek its application for homogeneous materials. This motivation is legit, neglecting its possible physical relevance for homogeneous materials. On the other hand, the effect of the statistical character of heat source on thermal properties [76], the anisotropy of heat current related to the homogeneous molecules [77], and the possible break down of phonon gas model at high temperatures [78] provide the evidence of possible deviation of homogeneous systems from a wave-particle picture. The claim is due to the system's constraints by temperature-dependent statistics of vibrations, interactions of vibrations, and anharmonicity effects, or all the mentioned effects.

As a result, I will first develop a methodology that removes the temperature effect from a system yet can still capture temperature-dependent frequency behavior. The method will remove any possible random behavior due to temperature. I will use the phonon lifetime as a measure for comparison to monitor the effect of the absence of temperature induced randomness. Next, I will use the thermal conductivity as a measure of comparison. Correspondingly, I will induce more randomness to a system under a temperature constraint to observe the effect of extra randomness added to the system on its thermal conductivity and use the amorphous material terminology to analyze the resulting data. The extra randomness is achieved through Langevin dynamics. Finally, I will use the developed codes for the analysis above to analyze a long-standing question about the lifetimes' frequency-scaling in amorphous silicon and its possibility of diverging the thermal conductivity at low frequencies.

CHAPTER 2
PHONON WAVEPACKET SIMULATIONS USING THE QUANTIZED DEFINITION
OF ANERGY AND TEMPERATURE-DEPENDENT PDR AND DOS

2.1 Introduction

Material selection and material engineering has shown to be the promising approaches to overcome design bottlenecks in multiple engineering disciplines dealing with thermal or lattice vibration related problems. The target properties are achieved through either designing new materials that doesn't exist in the nature [79] or through a better understanding of the physics of the existing materials. Increasing the thermal conductivity at an interface for the sake of controlling the temperature below the maximum operational temperature of electronics, decreasing the thermal conductivity to increase the figure of merit in thermoelectric systems, and finally increasing the coupling in mechanical resonators to approach better sensing capabilities are the most common applications that will benefit from a better understanding of thermal transport properties in materials [32, 45, 80]. Analytical and computational modeling are considered effective tools to characterize the physics of the existing materials.

Both computational and analytical approaches are categorized into two main streams, (1) equilibrium analysis, and (2) non-equilibrium analysis. The Boltzmann Transport Equation (BTE) based simulations, and Green-Kubo simulations are the main equilibrium approaches to provide the frequency-based behavior of a material. Fisher et al. used the BTE approach to calculate the relaxation time and, as a result, the conductance across the Si/Ge interface [81], and LV et al. proposed a Kubo-based approach for the exploration of mode-mode contribution to thermal conductivity and performed a case study on amorphous and crystalline silicon [82]. Analytical approaches in the category of equilibrium analysis are the Green's function analysis and n-phonon interaction analysis based on the radiative

heat flux analysis approach [83,84]. These are techniques that have been proven to provide detailed results in the frequency space. One other method that is not as ubiquitous as the methods mentioned above is the frequency-based transmission analysis performed by Volz and Chalopin. This analysis provides comprehensive frequency-based transmission across the Si/Ge interface in the specular regime [85].

In addition, the wavepacket creation method is a non-equilibrium method used to study the interface transport and can look at the dynamics of a frequency band in a system of particles. This technique of creating wavepackets is called “phonon dynamics” [32] and the method was proposed by Schelling [60]. It is based on the creation of a sinusoidal wave, which is in a Gaussian envelope. The created wave travels in the defined system, and monitoring the dynamics of the motion can provide characteristics such as phonon transport properties and phonon boundary transmission. Schelling and other researchers used the method to calculate the transmission across twist grain boundaries [86,87] and to explore the heat transfer mechanisms of graphene along the in-plane direction [88]. The method was proven to provide reliable and accurate results for transmission across an interface, time-dependent energy distribution, scattering, and phonon lifetime calculations [89,90]. Other authors have also used the results for validation [91]. The phonon dynamics has always been used assuming an arbitrary constant for the amplitude of a wavepacket as a result, the direct effect of the wavepacket amplitude on the amount of energy it carries has been neglected.

A phonon counting process is an essential part of most of the mentioned analysis. As a result, correct definition of the phonon density of states (DOS) is correlated to any subsequent analysis. The use of DOS in thermal conductivity calculations started with Callaway’s linear consideration of the DOS and was reused by other researchers [41,92]. The full-Brillion Zone consideration of the DOS provided results that matched the experiment better [93]. Yet still, a nonlinear (frequency dependent phonon group velocity) full-zone consideration of the DOS provided a more realistic model of materials. Aksamija and Kenzevic considered a nonlinear and full zone DOS and were able to capture the dependency

of graphene nanoribbons thermal conductivity on the chiral angle of the ribbons. They also performed the same analysis on silicon-on-insulator nanomembranes and observed the anisotropy of thermal conductivity in these materials. Despite the possibility, the temperature dependence of the DOS was never addressed in computational thermal property calculations, although the decrease of the range of lattice-vibration frequencies with increasing temperature is an accepted and experimentally observed phenomenon in physics research [94, 95]. This phenomenon was attributed to the coupling of optical and acoustic phonons [96] or the electron-phonon interactions [97]. Typically, the temperature dependency of the calculation is solely based on the temperature dependence of the Bose-Einstein distribution [98, 99], although the importance of the temperature dependent DOS and PDR was recently addressed by Gerboth and Walker in the context of size-dependent softening of nanoribbons [100].

The phonon dynamics has always utilized the 0 K DOS and PDR, and in the its definition the selection of the displacement amplitude is arbitrary. The introduction of the energy to the definition of a wavepacket is addressed in this work through the consideration of the temperature dependent DOS and PDR. We used a Green's function based definition of the temperature dependent DOS and the PDR [30] in order to get the energy of a frequency band. The frequency space of the wave packet created using the mentioned approach was tested using a Fourier analysis based method to provide the difference between considering the temperature dependence and ignoring it. In addition, the knowledge of the energy of a wavepacket based on the quantum definition of phonons provided the chance to quantitatively check the extent of validity of MD simulations in frequency space and at different temperatures.

To present the details of the work, we first elucidate the details of the computational approaches for the calculation of the PDR and the DOS ($g(\omega)$) followed by the methodology to capture the correct kinetic energy of a wavepacket. The Methods section defines the system, which is the test specimen to simulate and validate the proposed methodology. In the end, we present our results and discuss the uncertainty of the numerical calculations.

2.2 Methods

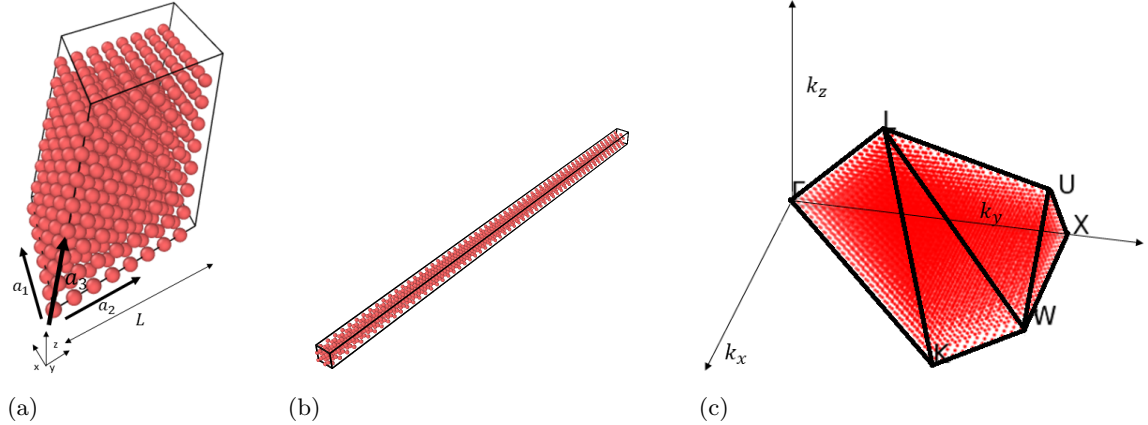


Fig. 2.1: (a) primitive structure conducive to the spatial Fourier analysis (b) validation system (c) volumetric mesh in k -space

We designed an extension to the phonon dynamics method that captures the correct kinetic energy of a frequency band in a wavepacket, which results in a wavepacket carrying the same amount of energy at a specific temperature in the frequency band flowing in a specific Cartesian direction. The definition of the energy is based on the quantum definition of energy for the range of frequencies within a frequency band in a Gaussian envelope. For the temperature dependent definition of the energy in any system we require the temperature dependent definition of the PDR and the DOS. In this section we start with the definition of the PDR and the DOS then we define the methodology to structure a wavepacket considering the temperature dependent definition of the PDR and the DOS.

2.2.1 Phonon Dispersion Relation (PDR) and Density of States (DOS)

We encountered two computational methods that can capture the temperature dependency of the PDR and is able to capture the full anharmonic picture of the dynamics. The first approach was proposed by Heino [28], which is based on mapping the velocity field to the k -space ($k = \frac{2\pi}{\lambda}$) and getting the spatial Fourier transform of the velocity field $v^\alpha(t, r)$. α indicates the direction in the coordinate system for each particle indexed with

i. The calculation is followed by the computation of the autocorrelation function $A^\alpha(k, t)$ of the k -space velocity vectors. As a result, the PDR is the output of the temporal Fourier transform over the total simulation time T_{sim} of $A(k, t)$, which provides the autocorrelation function as a function of angular frequency ω and k vectors ($A(k, \omega)$).

$$\begin{aligned} v^\alpha(k, t) &= \sum_i v_i^\alpha(t, r) e^{-ikr_i} \\ A^\alpha(k, t) &= \frac{\langle v^\alpha(k, t) \cdot v^\alpha(k, 0) \rangle}{\langle v^\alpha(k, 0) \cdot v^\alpha(k, 0) \rangle} \\ A^\alpha(k, \omega) &= \sum^{T_{sim}} A^\alpha(k, t) e^{-i\omega t} \end{aligned} \quad (2.1)$$

The second method is a particle tracking model and defines the dynamical matrices $D(k, \omega)$ in the context of atom positions over time [29, 30]. This method first maps all the α -component of the atom positions at each time (t), $R_{i\alpha}(x, t)$, in the k -space by a spatial Fourier transform. The sum is over the location of each primitive cell (Fig. 2.1-a) in the primitive structure, but it reduces to a summation over atoms i as we have one atom per unit cell, due to the distribution of atoms along the primitive lattice vectors,

$$R_{i\alpha}(k, t) = \frac{1}{\sqrt{N}} \sum_i R_{i\alpha}(x, t) e^{-ikr_i}. \quad (2.2)$$

The force constants matrix elements ($\phi_{i\alpha, j\beta}(k)$) are defined with respect to the positions in k -space ($R_{i\alpha}(k, t)$). The definition is based on defining the Green's function in terms of the time dependent, α and β component of the position of atoms i and j . k_b and T are the Boltzmann constant, and the simulation temperature, respectively. Besides, the $*$ sign denotes the complex conjugate of a complex vector.

$$\begin{aligned} G_{i\alpha, j\beta}(k) &= \langle R_{i\alpha}(k, t) \cdot R_{j\beta}^*(k, t) \rangle \\ &\quad - \langle R_{j\beta}(k, t) \rangle \cdot \langle R_{j\beta}^*(k, t) \rangle \\ \phi_{i\alpha, j\beta}(k) &= k_b T G_{i\alpha, j\beta}^{-1}(k) \end{aligned} \quad (2.3)$$

As a result, we defined the dynamical matrices with the aid of force constant matrices, and the square of angular frequencies are the eigenvalues of the proper eigenproblem (Eq. 2.4). This method up to the generation of dynamical matrices is available as `fix-phonon` in the LAMMPS molecular dynamics package [101].

$$D_{i\alpha,j\beta}(k) = \frac{1}{\sqrt{m_i m_j}} \phi_{i\alpha,j\beta}(k)$$

$$| D_{i\alpha,j\beta}(k) - \delta_{\alpha\beta} \delta_{ij} \omega^2(k) | = 0 \quad (2.4)$$

The DOS ($g(\omega)$) is the count of frequencies within a frequency bin centered at ω . The width of the frequency bins were chosen to be equal to 0.01 THz. It is also essential to perform the DOS normalization precisely by considering all of the three polarizations p (Eq. 2.5), that results an integration over all frequencies of the DOS(ω) being equal to three,

$$\int_0^{\omega_{\max}} g(\omega) d\omega = \sum_p 1 = 3. \quad (2.5)$$

The temperature dependency of PDR and DOS is a phenomenon addressed by other researchers as phonon softening [94]. The frequency shift due to temperature change is also an observable phenomenon in Raman spectroscopy experimental measurements [102]. The change in the frequency behavior of the PDR and softening of the frequencies was attributed to the change of the lattice constant due to thermal expansion [103]. Although the work by Yun et. al. is on UO₂ their observation is relevant to this work on argon as the thermal conductivity of UO₂ is lattice dominated up to high temperatures (1400K) [104], which is well above the temperatures understudy in the work by Yun et. al. [103]. We confirmed this behavior in our system by first running ten different simulations at 50 K with 10 different random velocity seeds to capture the numerical oscillation of the results, and monitoring the frequency-space of the system at the same four different temperatures under the canonical ensemble (NVT), the analysis will ensure the change being beyond the statistical variations.

2.2.2 Simulation Conditions

Two distinguished systems of particles were defined, (1) for the characterization of the Lennard Jones Argon, and (2) to compare the expected characteristics of a wavepacket with the ones used in the literature neglecting the temperature effects. To achieve a high k -space resolution, in the analysis system, we chose a $40 \times 40 \times 40$ unit cell system in the format of a primitive structure. We modeled the interatomic interactions with the 6-12 Lennard-Jones potential. The constants of the potential ϵ and σ are 1.69×10^{-21} J and 3.4×10^{-10} m, respectively [55], as a result, we calculated the lattice constant at 0 K is 5.2411 Å [105]. The run process, of the analysis section, is a combination of a 5×10^5 timesteps of equilibration followed by 9.5×10^6 timesteps of calculation for every temperature, and, each timestep is 2 fs. Both equilibration and calculations steps are in an NPT ensemble, which allows for expansion of the system under the thermal stresses. The validation system (Fig. 2.1-b) dimensions are $2 \times 60 \times 2$ unit cells in the format of a cubic structure (not unit cell), and the potential constants are the same as the analysis system. Simulations in the validation system are performed for each wavenumber (5×10^5 timesteps, timestep temporal length of 1 fs) and were all in a microcanonical ensemble (NVE). The temperature dependency was observed in the validation system by applying an expanded lattice constant for every temperature under analysis. The approach helped us run the system at 0 K and still be able to observe the temperature-dependent PDR. The possibility of observing the frequency space temperature dependence at 0 K provided us the chance to isolate any other possible reason resulting in a temperature dependent behavior and validate lattice expansion as the reason for this type of behavior in dielectrics.

To get the averaged lattice constant at each temperature, we ran the validation system with no extra wavepackets under NPT and the temperature conditions for 5×10^6 timesteps and calculated the average lattice constant after the convergence of macrostates. The calculation of the lattice constant was through the calculation of the average of the atom-atom distances over the time of simulations.

2.2.3 Wavepacket Generation and Energy Calculation

We defined the wavepacket as a sinusoidal function in a Gaussian envelope (Fig. 2.2-a). The Gaussian envelope ensures the smooth decay of the oscillation to avoid unwanted vibrations as a result of abrupt spatial changes in atom displacement. We chose the standard deviation, s of the Gaussian to be ten times the temperature-dependent lattice constant of argon to get a full-wave for wave numbers as low as $\frac{0.1\pi}{a}$, and the Gaussian is centered at the center of the validation system by the definition of μ . The oscillatory part of the displacement function is a simple cosine (Eq. 2.6). The exponential definition of oscillation introduces an imaginary part that defines the phase of a hypothetical wave, which is immaterial in the definition of an initial condition,

$$z(y) = A \exp\left(\frac{(y - \mu)^2}{2s^2}\right) \cos(yk). \quad (2.6)$$

We applied the displacement to all the atoms in the validation system as a function of the atoms positions y , which is the direction containing 60 unit cells.

To calculate the amplitude of the displacement signal, we first need to define the energy of the wavepacket. We calculated the wavepacket energy using the frequency-based kinetic energy (Ke) equation. The equation defines the contribution of each angular frequency ω to the energy as the product of the reduced Planck's constant and angular frequency, $\hbar\omega$. Then the energy in a frequency band (integration between two frequencies) or the total energy (integration over the whole spectrum of frequencies) of the system is the summation of energies considering both the DOS and the Bose-Einstein distribution,

$$Ke = \int_0^{\omega_{\max}} g(\omega) \frac{\hbar\omega}{1 - \exp(\frac{\hbar\omega}{k_b T})} d\omega. \quad (2.7)$$

Before we apply Eq. 2.7 to the wavepacket energy calculation, we should notice the effect of a Gaussian envelope in real space on the wave, in frequency space. The standard deviation (s) in real space translates to $1/s$ in frequency space, which requires the consid-

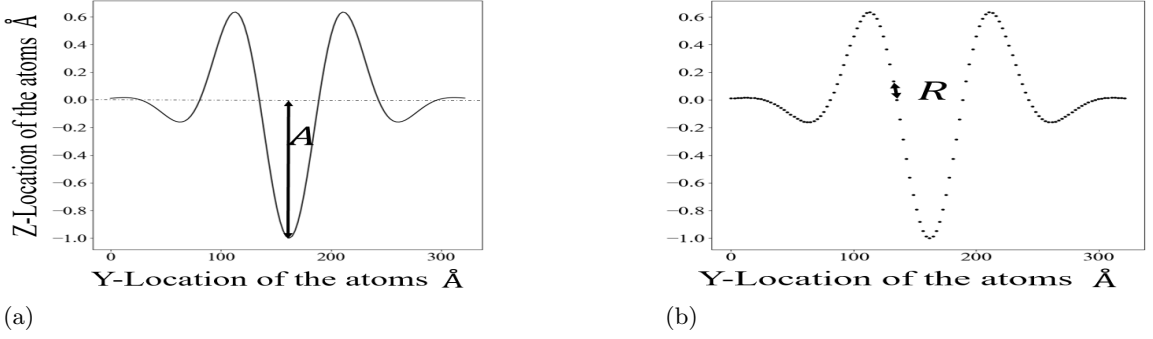


Fig. 2.2: (a) representation of a displacement wave (b) the displacement wave with inter-atomic distance marked on it

eration of the effect of the Gaussian envelope in the calculation of the kinetic energy of a wavepacket. The phenomenon becomes more evident by considering the following,

$$\frac{1}{\sqrt{2\pi s^2}} \int_{-\infty}^{\infty} e^{-\frac{x^2}{2s^2}} e^{i2\pi kx} dk = e^{-2\pi^2 s^2 k^2}. \quad (2.8)$$

The Gaussian distribution in the frequency space (Eq. 2.8) requires us to multiply the energy of the frequency bins, activated by creating a wavepacket, by the Gaussian value of the corresponding frequency. The Gaussian in the frequency space is a function of wavenumber $k(\omega)$ and is centered at $k'(\omega)$. As a result, the kinetic energy of the entire system between two frequencies ω_1 and ω_2 , $Ke_{\omega_1 \leq \omega' \leq \omega_2}$ is defined,

$$Ke_{\omega_1 \leq \omega' \leq \omega_2} = \int_{\omega_1}^{\omega_2} \left(\frac{e^{s^2(k(\omega) - k'(\omega'))^2}}{\sqrt{2\pi s^2}} \right) \times \left(g(\omega) \frac{\hbar\omega}{1 - \exp(\frac{\hbar\omega}{k_b T})} \right) d\omega. \quad (2.9)$$

The calculated kinetic energy is the kinetic energy of a frequency band flowing in all traveling directions and polarizations. We are interested in the energy of a wavepacket traveling in a specific direction. Eigenvectors of the dynamical matrices are usually used to define the flow direction of energy, but the eigenvectors are not continuous in the frequency space and we can't use them in an integration process. As a result, we defined the directional dependency of the energy flow considering the main crystallographic directions. This

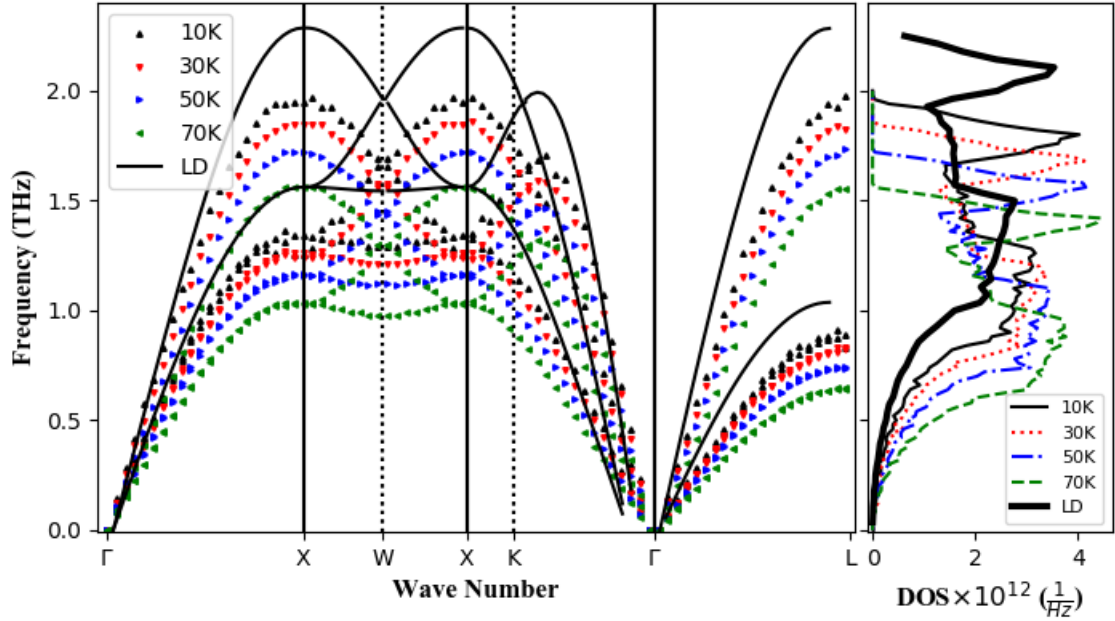


Fig. 2.3: PDR curve and the DOS of the argon crystal at four different temperatures. For comparison the PDR computed, using lattice dynamics (LD), is also included

consideration is supported by the Raman spectroscopy data [106]. Correspondingly, we divide the calculated energy into three sections for each of the three main crystallographic directions in the FCC argon lattice, weighted by the linear atomic density (LD) in the structure. We calculated the share of the energy to be 0.47, 0.33, and 0.2 in directions [110], [100], and [111], respectively.

The polarization affects the calculation based on our observation that the creation of a wave by transverse displacement results in the generation of longitudinal modes. We attributed this fact to the creation of a compression field in the crystal in front of a propagating transverse wave. The longitudinal wave has the longitudinal frequency of the same wavenumber. The observation suggests the need for the addition of the longitudinal energy modes to our energy calculation. As a result, a wavepacket carries both the energy of the transverse bandwidth plus the energy of the longitudinal contribution. To calculate the energy of each branch contributing to the energy carried by a wavepacket, we are required to divide the energy of a frequency bin, calculated by the Eq. 2.9 by three, if the frequency is less than the maximum frequency of the transverse branch. The same approach

has been used with the analytical calculation of thermal conductivity and the contribution of different polarizations [107]. Considering the energy of the frequency band between ω_1 and ω_2 , the directional linear atom density LD_D , the division of energy based on polarization, and the contribution of different polarization, we can define the total energy of a wavepacket $Ke_{(Tot,D)}$. The definition is for two cases, one that with frequencies below the maximum transverse frequency $\omega_{T,max}$ and with the frequencies above the maximum transverse frequency,

$$\begin{aligned}
Ke_{(Tot,D)} &= LD_D \left(\frac{1}{3}Ke(\omega'_T) + \frac{1}{3}Ke(\omega'_L) \right), \\
&\quad \{\omega'_L(k') \mid 0 \leq \omega'_L(k') \leq \omega_{T,max}\} \\
Ke_{(Tot,D)} &= LD_D \left(\frac{1}{3}Ke(\omega'_T) + Ke(\omega'_L) \right), \\
&\quad \{\omega'_L(k') \mid \omega_{T,max} \leq \omega'_L(k') \leq \omega_{L,max}\}.
\end{aligned} \tag{2.10}$$

To enforce the kinetic energy on the wavepacket, we calculated the interatomic distance R (Fig. 2.2-b) based on the Lennard-Jones potential by equating the potential equation to the value of the potential (P_{max}) at the bottom of the potential well minus the calculated kinetic energy (Eq. 2.9). The difference between the two positive roots is the displacement magnitude of the atoms from their equilibrium positions. This protocol provides the energy-based definition of amplitude instead of choosing it as an arbitrary parameter,

$$\begin{aligned}
P_{max} + Ke_{(Tot,D)} &= 4\epsilon \left[\left(\frac{\sigma}{r} \right)^{12} - \left(\frac{\sigma}{r} \right)^6 \right], \\
\{r \mid r \geq 0 \wedge \text{Im}(r) \equiv 0\}, \quad R &= |r_1 - r_2|.
\end{aligned} \tag{2.11}$$

Then we use an algorithm that increases the amplitude of the wave in small steps to get an average of the interatomic distance r equal to the calculated value from Eq. 2.11. As the perturbation is applied to the z -direction only, there is no change in the interatomic distance except for the transverse and longitudinal directions along each string of the atoms. As a result, we have no displacement in the x -direction.

2.3 Results and Discussion

We used the method developed by Kong [29,30] to generate the wavevector-frequency structure of the argon crystal (Fig. 2.3). For comparison and validation, we calculated and added the lattice dynamics based dispersion, the data is created using the GULP package [108]. We have also compared our result for one temperature with the experimental data [2] to confirm the data calculated by Kong’s method (Fig. 2.1-c). The comparison show acceptable match within the statistical limit, which will be discussed below.

The numerical oscillations showed a maximum of ~ 7.7 percent change in the results (Fig. 2.4-a), which is significantly smaller than the pronounced temperature dependence of frequency under the NPT ensemble. The NVT results also provided intact frequencies for most of the frequency interval and under all four temperature conditions (Fig. 2.4-b). We observed slight changes beyond the statistical oscillation in the PDR at high frequencies, which are not lattice constant related and contradictory to our assumption of lattice constant-dependency of the PDR. Ocelli et al. showed the dependency of phonon frequencies on many-body terms in potential functions for argon [109], the many-body terms are absent in the Lennard-Jones potential used in this work, thus the effect on frequencies (Fig. 2.4-b). The statistical variations observed at NVT provided the evidence that the decreasing trend observed in the frequencies as a function of temperature is not the artifact of statistical variations.

2.3.1 Importance of the Temperature and Energy dependent definition of a Wavepacket

Based on the presented data we have confidence in the observed temperature dependence in our simulations and its reason being the lattice expansion as suggested by the existing experimental data [103]. Using the PDR and DOS data we can create wavepackets and compare the frequency space of the system considering the temperature dependence and ignoring it. To structure our validation system with the required temperature induced lattice constant, we captured the lattice constants after the expansion by relaxing our vali-

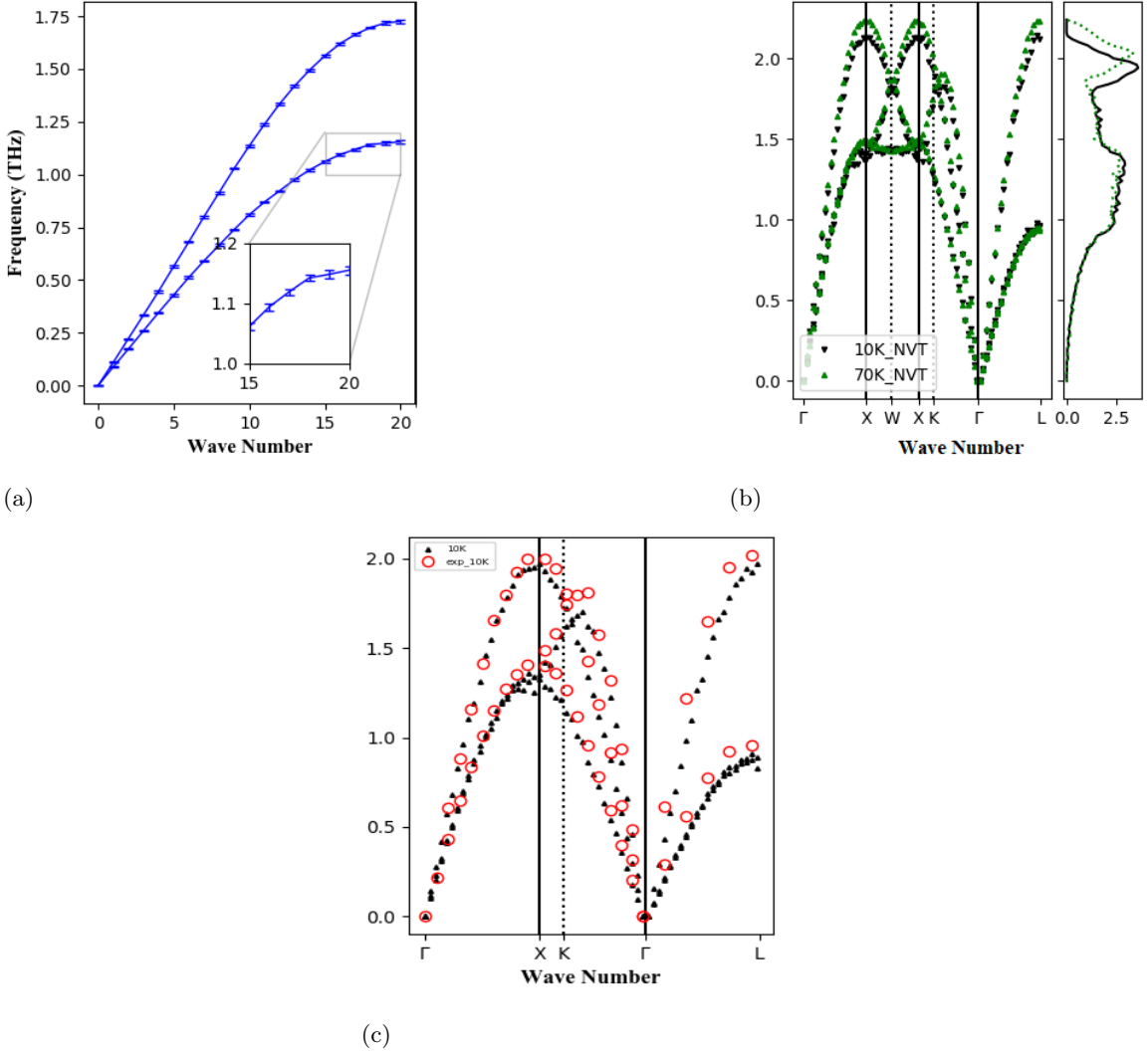


Fig. 2.4: (a) Uncertainty in frequency analysis, inset showing a zoomed area of the graph for more visibility (b) NVT results showing slight difference in frequencies at high frequencies, the NVT results at 50 K and 30 K are not presented for the clarity of the graph (c) The comparison between the PDR resulted from a Green's function approach and experimental work [2] at 10 K The red circles are experimental and the black triangles are computational data, respectively

dation system at each temperature. The resulting lattice constants are listed in Table 2.1, where we have also compared the results with the experimental values [110]. The computed lattice constants are in good agreement with the experimental work. We see deviations at higher temperature, which we attribute to the absence of many body terms in the potential [109], as the terms provide more constraint to the atom motions thus limiting the lattice

constant at high temperatures.

The wavepacket validation process is performed in the validation system and under the explained conditions in the Methods section. The simulation results provided the importance of the consideration of the temperature dependence of the PDR and DOS in defining a wavepacket. Neglecting this dependence result in frequencies that are not the correct frequencies in the system (Fig. 2.5, compare the arrows with the dotted lines). The 0 K frequencies for the same wavevectors are shown on the figure 2.5 the 0 K frequencies are commonly used in interpreting the results of phonon dynamics simulations. The arrows are coded with the colors assigned to each temperature. As a result of comparing the location of the arrows with the targeted frequencies (dashed vertical lines), we notice the increase in the gap between them with increasing temperature. The observation emphasizes the importance of the temperature dependence at higher temperatures. We also compare the expected frequencies from the PDR analysis with what we observed in our wavepacket simulations. At 10 K the wavenumber (right side of each plot) and the frequencies (left side of each plot) match the expected values (solid Gaussian for the wavenumbers and dashed line for frequencies) (Fig. 2.5-a). The matching trend continues for both 30 K and 50 K except for minimal deviations at the expected frequencies, which we attribute to the uncertainty in the first method used in this work (Fig. 2.5-b,2.5-c). The 70 K data does not show deviations, but we observed low peaks at the target frequencies due to large peaks at low frequencies, which are due to decay to low frequencies. We couldn't avoid the decay as the FFT resolution is dependent on the length of the data set, hence the decay was inevitable (Fig. 2.5-d). At 70 K we observed nonzero spacial frequency values, two to three

Table 2.1: Lattice Constant Values from computational work $a_{comp.}$ and comparison with the experimental $a_{exp.}$ values.

| Temperature | Lattice Constant (Å) | $\frac{a_{comp.} - a_{exp.}}{a_{exp.}} \times 100$ [110] |
|-------------|----------------------|--|
| 0 K | 5.24 | |
| 10 K | 5.29 | 0.2% |
| 30 K | 5.33 | 0.2% |
| 50 K | 5.39 | 0.75% |
| 70 K | 5.46 | 0.92% |

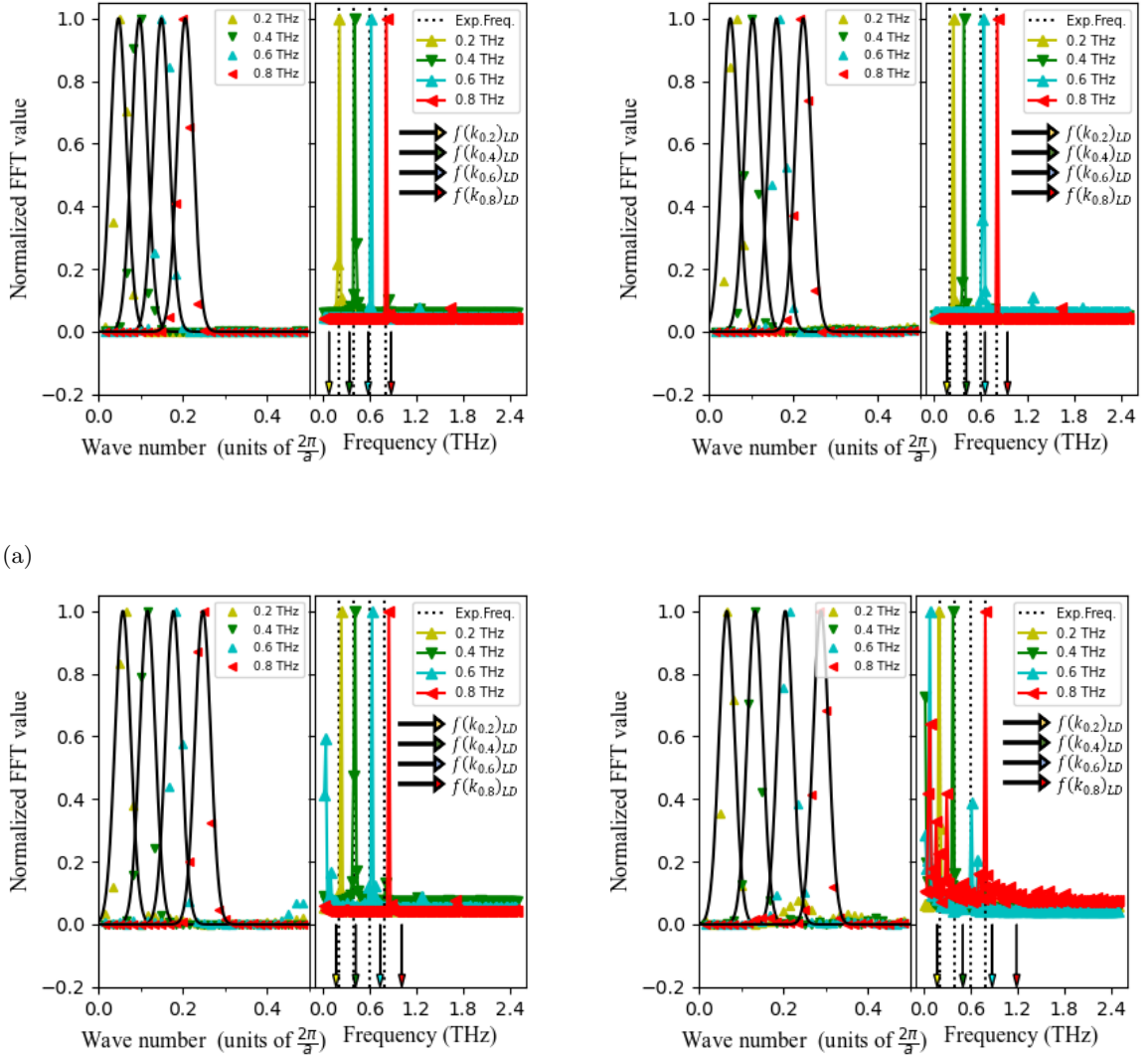


Fig. 2.5: Spatial Fourier validation of the perturbation (left) and the temporal Fourier validation (right) for four different frequencies at (a) 10 K (b) 30 K (c) 50 K (d) 70 K. The arrows are the 0 K frequencies that are commonly used in the interpretation of the wavepacket simulations. The arrows are color coded with the colors used for each temperature

sigmas away from the expected maximum, which we attribute to the low frequency-space resolution in the spatial Fourier analysis. The low number of atoms (60) along the y-axis is the reason for low spatial frequency resolution and can be solved by choosing a more computationally extensive system. Nevertheless, we were able to target a frequency with a specific wavevector and show the importance of the temperature dependent definition of a

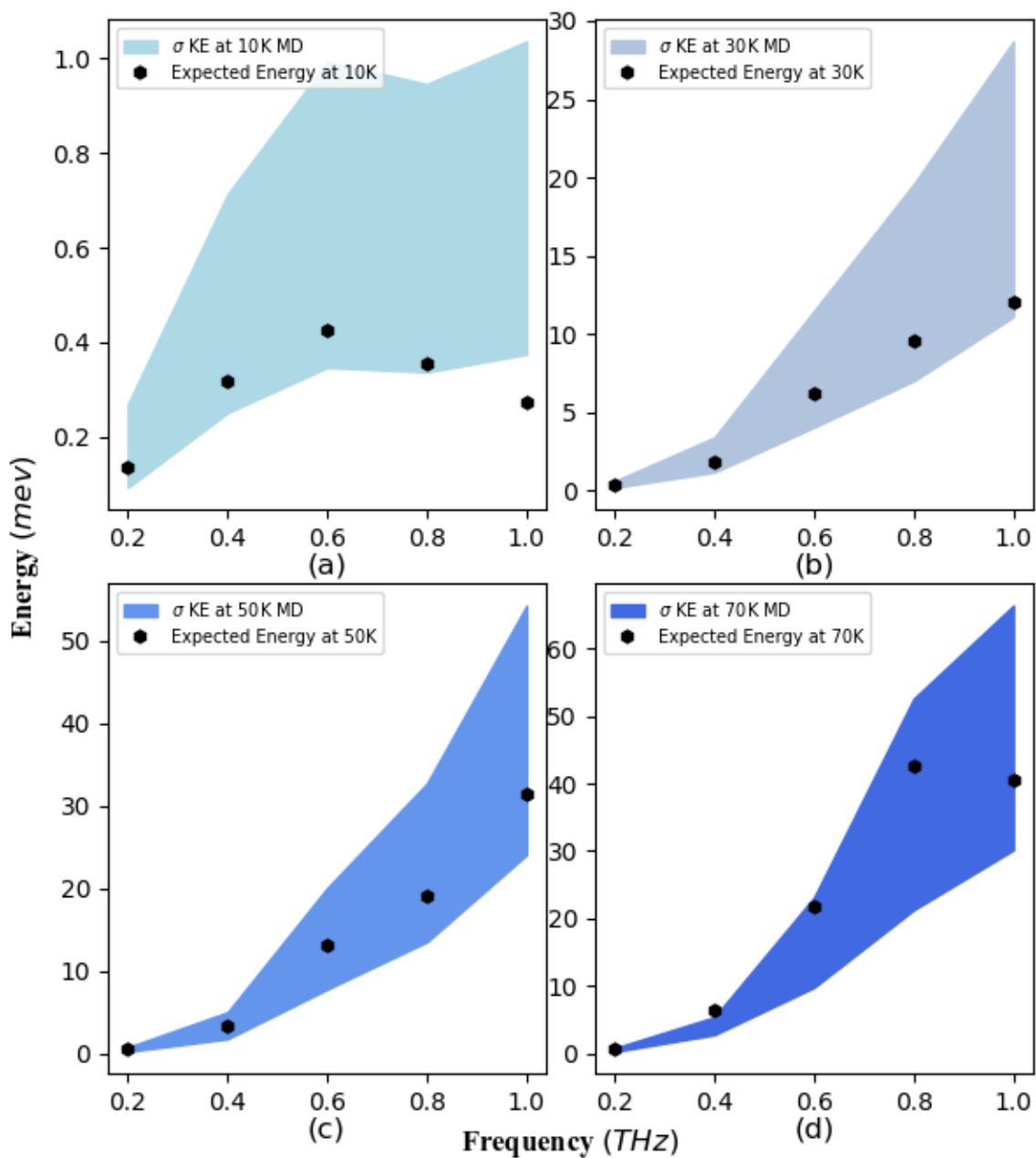


Fig. 2.6: Energy oscillation of the simulation (the shaded area) compared to the energy calculated for each temperature calculated based on the quantum particle picture of the problem (black hexagons) at (a) 10 K (b) 30 K (c) 50 K (d) 70 K

wavepacket.

2.3.2 Frequency Based Validation of MD Simulations

MD simulations do not represent the quantum particle character of phonons due to their classic nature and the miss representation is pronounced more at temperatures well below the Debye temperature, where the quantum effects dominate [111, 112] and the classical MD can over predict the frequency contribution to the specific heat. The quantum effects specifically for an argon crystal of particles are mentioned heuristically to be important in a range between one tenth [111] to a quarter of the Debye temperature [113]. The wavepacket method as a frequency specified method and with the additional energy details provided us the chance to do a frequency-based assessment of MD simulations and develop a frequency-based measure to evaluate the reliability of MD simulations with respect to temperature. As a result, we monitored the oscillation of the total kinetic energy (shaded region in Fig. 2.6) in the simulation and compared the results with the calculated (expected) energy (Eq. 2.9-2.10) for all four frequencies and all four temperature data points (Fig. 2.6). At 10 K, we observed the first four frequencies (0.2, 0.4, 0.6, and 0.8 THz) lie within the trend of oscillations of the MD-calculated kinetic energy (Fig. 2.6(a)). The last data point falls out of the MD oscillation band due to the over prediction of the contribution of the frequency at 10 K (Fig. 2.3). The data shows that the kinetic energy calculated by the MD code is reliable at temperatures as low as one eighth of the Debye temperature of solid argon [110, 114], and up to the frequency of 1 THz. This observation is a more exact reliability limit for MD simulations in comparison with the previous ones [111, 113]. At 30 K, 50 K, and 70 K we observed that the expected data points follow the trend of the MD oscillations. The decline in the 1 THz point for 70 K does not refute the energy definition of MD at 70 K, yet still illustrates the importance of the DOS in the definition of the the kinetic energy, which is an important concern at low temperatures.

The quantum definition of the energy used in this work can not be represented with MD simulations. Consequently, we find the expected value of the energy on the bottom of the energy oscillation at high frequencies of low temperatures and the fact is due to the consideration of the density of states in the calculations. The observation matches

the calculation much better at high temperatures, where the calculated energy is near the maximum of oscillations. We expected the midpoint of the oscillation to match the quantum particle-based energy calculation, as the calculated energy was added to the system with an algorithm setting the average of atomic displacement to the calculated value. As a result, the MD simulations can be a close estimate of a dielectric material even at low temperatures for low frequencies and at high frequencies of high temperature where the DOS has a rapid decrease behavior the MD energy loses the quantum energy trend but its oscillation still enfolds the quantum value.

It is also necessary to address the current concerns about the acoustic wave picture of phonons. Henry and Seyf proposed a new definition, as an extension to the concept defined by Allan and Feldman [115], of lattice vibration with the existence of impurities in materials and raised concerns about the limit of the acoustic wave assumptions of phonon behavior [116]. Although the phonon dynamics provides valuable results, the concern brings questions about the limits, in which this method can provide reliable results. Considering the nature of this work, which is evaluating the dynamics of phonons within a pure crystalline material, this method distances itself from this criticism.

2.4 Conclusion

In this work we introduced an extension to the phonon dynamics method. The method has always been used disregarding the temperature dependent PDR and DOS, under which the wavepacket is evolving and the amount of energy a wavepacket carries. We utilized a Green function based approach to capture the temperature dependency of the PDR and the DOS and compared wavepackets in two cases, one that neglects the temperature dependency and uses the Lattice Dynamics (0 K) results and cases in which the temperature dependency is considered. The difference in the frequency space of a system considering the temperature dependence and the one using 0 K results was shown and we discovered that its importance increases at higher temperatures, making the consideration more important. Consideration of the temperature dependent PDR and DOS enabled the definition of the wavepacket amplitude as a parameter that specifies the amount of energy a wavepacket carries. As

a result, we improved the phonon dynamics method that considers the amplitude of the wave as an arbitrary parameter with considering the amplitude as a tuning knob of the energy. Finally, we were able to use the method to improve a heuristic rule for the validity of MD simulations considering their classical nature and provide a quantitative measure in frequency space for the matter. The result of the last piece of our work on one hand provided that at high temperatures although the MD simulations under a thermostated and equilibrated condition are able to reproduce the correct DOS, are unable to do so with a frequency band in an expanded system to the lattice constant of high temperatures, as a result the lost of the energy trend at high frequencies at high temperatures. On the other hand, despite the common belief that at low temperatures the MD simulations are not able to provide acceptable results in comparison with the quantum picture of vibrations, it still provides reliable results at temperatures as low as the one eighth of the Debye temperature and up to 1 THz in the argon case.

CHAPTER 3

TEMPERATURE INDUCED RANDOMNESS IN CRYSTALLINE DIELECTRICS

3.1 Introduction

The difference in the temperature dependence of thermal conductivity in crystalline and amorphous materials has initiated research efforts to understand this phenomenon [65, 66]. These efforts resulted in a diverse taxonomy in defining vibrational behavior and scattering events of amorphous materials. The three main modes of vibrations defined for amorphous materials are Propagons (P)(propagating modes), Diffusons (D), i.e., vibrational modes with no defined wave vector but having energy transport capabilities, and Locons (L) that are local modes with high local magnitudes and low contribution to thermal conductivity [67]. The frequency transition limits from one regime to the other are defined as Ioffe-Regel and the mobility edge. The former is the frequency border between P-D and the later is the border between D-L [67] and has its roots in the concept of electron localization [68]. Although the need for such classification of modes was disputed by some authors experimentally [69], the classification resulted in the definition of thermal properties for each class of vibrations and resulted in an improved estimate of the thermal conductivity for amorphous silicon [70, 71]. Less commonly used modes are floppy modes that are temporally and spatially trapped modes [67] and Resonant modes that are spatially non-exponentially decaying modes [70] These modes are mainly used to define and explain computational results that are a subject of size effects.

Along with the classifications of types of vibrations, defining types of scattering with respect to frequency is another approach to find explanation for the odd temperature behavior of the thermal conductivity in amorphous materials. Kittel scattering defines the frequency independence of scattering on a scale that the mean free path is lower than the atomic distance [65]. Klemens scattering defines the scattering resulting from transverse

and longitudinal modes' interactions through the anharmonic terms of the interatomic potentials or interaction with local modes [66]. Moreover, the most historically used scattering classification [117] is a Mean Free Path or lifetime vs. frequency classification. For example ω^{-2}, ω^{-1} are the behaviors defining the lifetime vs. frequency data in the low frequency regime, and ω^{-4} (Rayleigh Scattering), ω^{-3} explains the scattering events in the mid-range frequency interval [73]. These regimes were observed in both experimental [69, 74] and computational [67] works.

On the one hand, the science associated with this terminology has opened the avenue to phonon engineering [75] and it creates the motivation to seek its application for crystalline materials. On the other hand, approaches such as random matrix theory has been used to model amorphous materials and they provided the chance to model amorphous materials beyond the capabilities of Molecular Dynamics [118]. If resemblance between the dynamics of amorphous material and crystalline is found under specific conditions the random matrix theory provides the path to achieve larger simulations for crystalline materials. In addition, the affect of the statistical character of heat source on thermal conductivity and the property being a heat source dependent property [76], and the possible break down of phonon gas model at high temperatures [78] provide the evidence for temperature dependent character of the dynamics of vibrations and possible deviation of crystalline systems from a wave-particle picture, respectively. The mentioned behaviors are due to constraints enforced on the system by temperature dependent statistics of vibrations, interactions of vibrations, and anharmonicity effects, or all the mentioned effects. As a result, I borrow tools and the terminology from the analysis of thermal properties in amorphous material to analyze the possibility of their use to characterize the behavior of crystalline materials at high temperatures.

To set up our line of logic, I first used the method I developed in our previous work to eliminate the effect of other modes in a system and study the decay of a bandwidth of frequencies in a system under their anharmonic nature of vibrations [119]. This allows us to explore the absence of any additional parameters in the decay of modes and study the

vibrations in a simpler setup. Next, I explore the effect of random perturbations on the interatomic forces on crystalline materials at different temperatures. This approach will model the spatial randomness in amorphous materials with an added random term to the potential modeling the interatomic interactions for a crystalline material. The approach allows the comparison of a crystalline material's thermal conductivity, as a measure of comparison between the dynamics of the two system one, under conventional and conventional with randomness (CR). It is also the opposite of what I explore first with removing the effect of any possible randomness caused by other modes. Using the mentioned approach, I target exploring the physics of vibrations in crystalline dielectrics by studying the two extremes in terms of having random motions in a system of particles and comparing them with each other and with a system under conventional potential. Then I expand our analysis and explore the possibility of observing amorphous materials' vibrational features in systems under conventional and a system under a potential, having a deeper potential well, at different temperatures. As a result, I first explain the methods to support this line of logic; then, I discuss our results to find a connection between the dynamics of amorphous materials and crystalline materials at high temperatures.

3.2 Methods

This section explains the methods used and the logic for choosing these methods. For our analysis, an argon system is simulated under a Lennard-Jones two-body potential interaction. The effect of adding random perturbation to the interatomic potential on our system of particles' thermal conductivity is explored. In other words, I will run simulations using conventional potential and a conventional potential with randomness (CR). The thermal conductivity is measured using two well-established methods, Greenwood-Kubo [51, 52, 120, 121] and Normal Mode Decomposition (NMD) [122]. This analysis will inspect the possibility of having spatially localized modes in a crystalline system of particles at different temperatures. I also examine the possibility of observing vibrational features in amorphous materials in a crystalline system using the dynamical structure factor (DSF) (Fig. 3.1). The DSF (Spatial Energy Density [123, 124]) is a powerful tool to examine the existence of

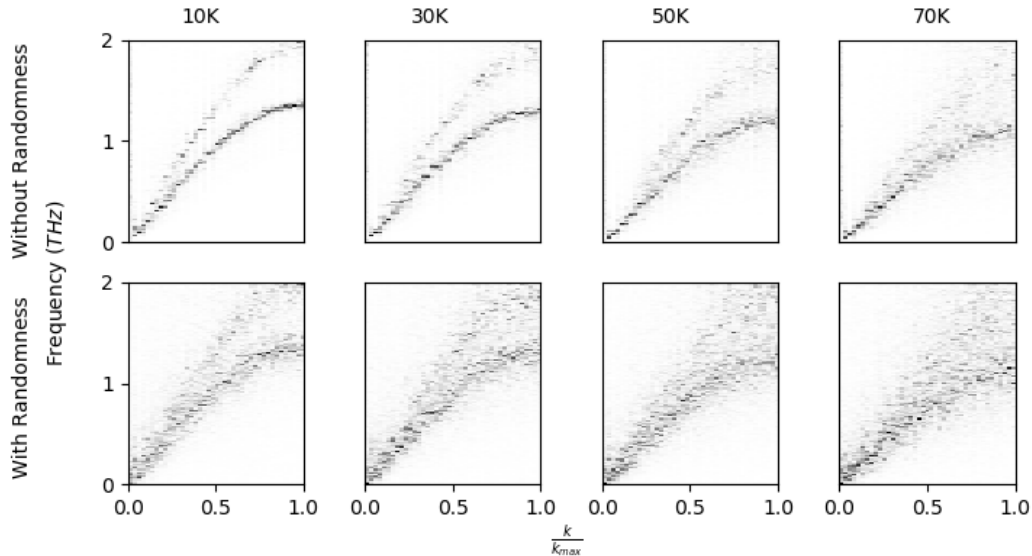


Fig. 3.1: DSF of systems at temperatures 10 K-70 K under the conventional and the CR potential.

Diffusons [125] that are localized modes contributing to the thermal conductivity of the material unlike Locons. The DSF also measures the spatial coherence of vibrations [123]. The spatial coherence of a vibrational mode is a measure of spatial extent of a vibration and is a measure of having localized modes (Diffusons and Locons) in the system.

3.2.1 Simulation Conditions

I performed our simulations using LAMMPS [101], which is a Molecular Dynamics package. Our simulations were on a system of argon with 64000 atoms in a tetrahedral box that was propagated along the primitive vectors of the argon FCC unit cell. The structure of the box and propagation of atoms makes the calculation of DSF and normal modes easier because of having one atom per unit cell with this structure. I performed two sets of simulations at each temperature. One, to get the temperature dependent eigenvectors of the equations of motion, using a method developed by Kong [29, 30]. The other set of simulations generate the trajectory data required for the calculation of thermal conductivity and the vibrational characterization as a post-processing step.

I performed the first set of simulations for 10^7 timesteps with the timestep length of 2 fs. To gather the data and calculate the dynamical matrices, I equilibrated the system for 5×10^5 timesteps and calculated the averaged dynamical matrices every 5×10^4 timesteps up to the end of the simulations. The calculation of the dynamical matrix is performed using the `fix-phonon` command. The second set of simulations were performed for 5×10^6 timesteps for the conventional potential and 6×10^6 timesteps for cases with the CR potential; all simulations in the second set used the 1 fs timestep length. Simulations in the second set under the conventional potential were equilibrated for 3×10^6 timesteps under isothermal-isobaric (NPT) ensemble followed by 2×10^6 timesteps under canonical ensemble (NVT). I added an extra equilibration section under the microcanonical ensemble (NVE) to the CR potential cases, with the length 1×10^6 steps. The data collection for NMD and DSF analysis was done every 10 fs, for 6×10^4 timesteps, and the Green Kubo (GK) analysis data collections were every 50 fs, and 6×10^6 timesteps. All data collections were executed under the microcanonical ensemble (NVE).

The interatomic potential used in all simulations was the Lennard-Jones with parameters [55] $\epsilon = 1.69 \times 10^{-21}$ J and $\sigma = 3.4 \times 10^{-10}$ m. The cutoff distance was set to 2.6σ . I used the `fix-Langevin` command to apply the Brownian Dynamics to the potential with random numbers drawn from a uniform distribution to thermostat the temperature [126]. This command simulates the system as if a solvent was present in the system, and the atoms were scattered at every interaction with the solvent atoms. The nature of the system under Brownian Dynamics makes it a proper candidate to observe the effect of random dynamics in a system. The application of Langevin Dynamics in LAMMPS doesn't provide the chance to tune the amount of randomness added to the dynamics as it is implemented as a thermostat and targets the set temperature, this option is enabled through methods such as random matrix theory [118] but one must compile a self-written code for the purpose.

3.2.2 Thermal Conductivity

The Green Kubo (GK) method is a ubiquitous method of calculating the thermal conductivity and multiple other transport properties of solids and liquids, the GK method uses the statistics of vibrations and correlates the vibrations' statistics to different transport properties [51, 52, 120, 121]. The statistical approach to develop the GK method was adopted to develop other thermal conductivity calculations [127]. The analysis is based on calculating the heat current J as a function of volume V , per-atom energy (kinetic plus potential) E_i , and the per-atom stress S_i , which is calculated at every time step to observe the oscillations. Then the thermal conductivity (K) is calculated by monitoring the correlation of these oscillations along each direction (α and β) at each temperature (T),

$$J = \frac{1}{V} \left[\sum_i E_i v_i - \sum_i S_i v_i \right]$$

$$K = \frac{V}{K_b T} \int_0^\infty \langle J_\alpha(0) \cdot J_\beta(t) \rangle dt. \quad (3.1)$$

The GK method has been used to calculate the thermal conductivity of materials both in liquid [128] and solid phases. However, the lack of frequency-frequency contribution analysis motivated the development of techniques such as GK Modal Analysis that was tested for alloys, interfaces, and crystalline bulk materials [82]. Although the GK method is useful for all material phases, it can suffer from the cutoff frequency limitations on capturing a complete picture of vibrations in a simulation, as a result showing some size dependence, which is yet still less than other available method [73].

The other method that has the frequency-based analysis is the Normal Mode Decomposition (NMD) method. The method has its roots in the classical mechanics and deriving the normal coordinates of vibrations [129] to capture the modes vibration, in which all the atoms oscillate with the same frequency. This makes the method incapable of measuring the contribution of Diffusons in the thermal conductivity. This method was first utilized by Kavyani and McGaughey [112] to derive the modal lifetimes. However, the method is proven to be incapable of defining the oscillations at high temperatures due to its inability

to define vibrations at the atomic spacing scale [112]. It has provided reliable results at low and medium temperatures and was successfully compared with other methods [130] within the temperature range. The method is based on capturing the normal mode coordinates ($q(k, \nu, t)$) as a function of wave vector (k), branch (ν), and time (t) and their time derivative ($\dot{q}(k, \nu, t)$).

$$\begin{aligned} q(k, \nu, t) &= \sum_{bl} \exp(ik \cdot r_0) e_b^*(k, \nu) u(l, b, t) \\ \dot{q}(k, \nu, t) &= \sum_{bl} \exp(ik \cdot r_0) e_b^*(k, \nu) \dot{u}(l, b, t), \end{aligned} \quad (3.2)$$

where the summation is over the displacement (u) or the velocity (\dot{u}) of each atom (b) in each unit cell (l), and e_b is the eigenvector of the equations of motion eigenproblem, resulting from either lattice dynamics or MD-based methods [29, 30].

Now having the normal coordinates, I can calculate the per mode per timestep kinetic (T) and potential (U) energies and the autocorrelation of the total modal energy (E) will provide the lifetime τ , through the fit of the autocorrelation with an exponential decay function,

$$\begin{aligned} U(k, \nu, t) &= \frac{1}{2} \omega^2(k, \nu) q^*(k, \nu, t) q(k, \nu, t) \\ T(k, \nu, t) &= \frac{1}{2} \dot{q}^*(k, \nu, t) \dot{q}(k, \nu, t) \\ E(k, \nu, t) &= U(k, \nu, t) + T(k, \nu, t) \\ \exp\left(\frac{-t}{\tau(k, \nu)}\right) &= \frac{\langle E(k, \nu, t) \cdot E(k, \nu, 0) \rangle}{\langle E(k, \nu, 0) \cdot E(k, \nu, 0) \rangle}. \end{aligned} \quad (3.3)$$

By performing the quantum correction at the frequency level [131] on the specific heat (C) to correctly capture the low-temperature behavior of the thermal conductivity [73], I can calculate the thermal conductivity using the equation for frequency-based thermal

conductivity [132].

$$C(\omega) = \frac{k_b x^2 \exp(x)}{[\exp(x) - 1]^2}, \quad x = \frac{\hbar\omega}{k_b T}$$

$$k = \frac{1}{3} \int_0^{\omega_{max}} \tau(\omega) v^2(\omega) C(\omega) DOS(\omega) d\omega, \quad (3.4)$$

where v and DOS are the frequency-based group velocity, which is the derivative of the dispersion relation, and Density of States, which is the result of the solution to the dynamical matrix, respectively.

These two methods are easy to apply and can capture the full anharmonicity of vibrations with less computational expense compared to other methods such as Anharmonic Lattice Dynamics [122]. It is essential to mention that these methods in their classical format are not suitable for measuring thermal conductivity in amorphous materials [67]. Other methods were developed to cover both areas [133], alongside less popular methods such as the perturbed MD method [134] but these methods are beyond the scope of this paper. Considering the easiness of application, strengths of the first two methods, and their weaknesses, I decided to simultaneously perform both methods to create a better and more comprehensive measure of the effect randomness has on the thermal conductivity.

The uncertainty analysis is an important part of any property calculation. The uncertainty analysis of the NMD Method is through the lifetime calculation and the exponential fit's covariance matrix. I performed the Monte Carlo uncertainty propagation algorithm [135] to propagate the exponential fit's uncertainty and get the uncertainty of the calculated thermal conductivity. The uncertainty analysis of the GK method is commonly calculated through a power mean formula to get the overall deviation of different ensembles from their arithmetic mean [73]. Ruan et al. offered a more statistically involved calculation [136], they found a linear relation between the correlation time (t_{corr}), integration time (t_{int}), average thermal conductivity and the its uncertainty (σ_k), $(t_{int}/t_{corr}) \propto (\sigma_k/k_{avg})$. I can not use their equation as they did not consider the Brownian Dynamics in their analysis. However, I adopted their suggestion with choosing long correlation and small integration

time ($(t_{int}/t_{corr}) = 1/80$); I also performed ten different simulations with ten different random seeds for each temperature with a specific potential condition (CR or Conventional) for ensemble averaging (Fig.3.4).

3.2.3 Vibrational Characterization

To measure the spatial disorder in vibrations, and explore the existence of local modes I use the DSF method. This method is defined as the energy per frequency per wave vector, also called Spectral Energy Density [124]. The DSF is proven analytically to be equal to the Static Structure Factor that takes advantage of the eigenvectors and requires a Lattice Dynamics Calculation beforehand [137]. The method was used to derive the dispersion relation of complex systems [124]. More importantly and related to our work, it was used to define the Ioffe-Regel limit, which is the P-D transition location [125, 138, 139], and was used to characterize complex systems as amorphous systems [140, 141].

I am using the DSF instead of the Static structure factor for two reasons. First, to capture the Brownian dynamics, and second to skip a step of calculation and finding the eigenvectors of vibrations, which is computationally very expensive for 64000 atoms. The DSF is based on taking the spatial and temporal Fourier Transform of vibrations. It results in a Lorentzian type of decay at each wave vector vs. frequency, which characterizes the lifetime of the mode [130], and another Lorentzian behavior of wave vector at each frequency that characterizes the spatial coherence [123]. The temporal Fourier transform is taken over the simulation time (t_{sim}), and the spatial is taken over the k-mesh in the reciprocal space. The equation for a system of particles containing N atoms of one kind with the mass m is as follows,

$$S(k, \omega) = \frac{m}{4\pi N t_{sim}} \sum_{\alpha} \left| \int_0^{t_{sim}} \sum_{n_x, n_y, n_z}^N \dot{u}_{\alpha}(t) \exp(ik \cdot r_0 - i\omega t) dt \right|^2.$$

3.3 Results and Discussion

Using the methods I presented in my previous work [119] I evaluated the lifetime of a frequency-band for two different conditions. One, without any other frequencies in the system, two with a close to zero kelvin thermostat (Fig.3.2). The results show no decay for the simulation with no thermostating (black plot) showing that although the oscillations are set to an interatomic distance that activates the anharmonic behavior, the vibrations do not decay. The decay value is not calculated as the autocorrelation function shows a negligible exponential decay. Comparing the results of the single frequency (red plot) system with the thermostated system show that even after 2 ns the single frequency-band system show no decay but the addition of close to zero thermostat creates a decaying behavior. The observation suggests either the no decay behavior is due to the lack of other modes and due to a random dynamics induced by the existence of temperature in the system.

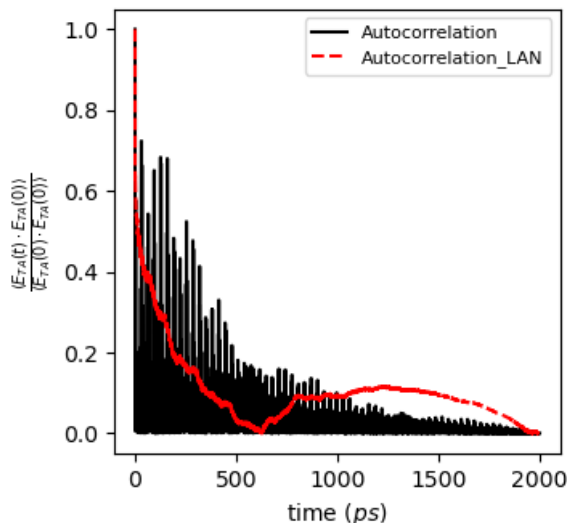


Fig. 3.2: Autocorrelation decay calculated using NMD method for a system under presence of a single frequency mode and thermostated at a temperature close to zero

The results of the thermal conductivity calculation is presented in the Fig. 3.3. The values are at four different temperatures 10 K, 30 K, 50 K, and 70 K, and at each temper-

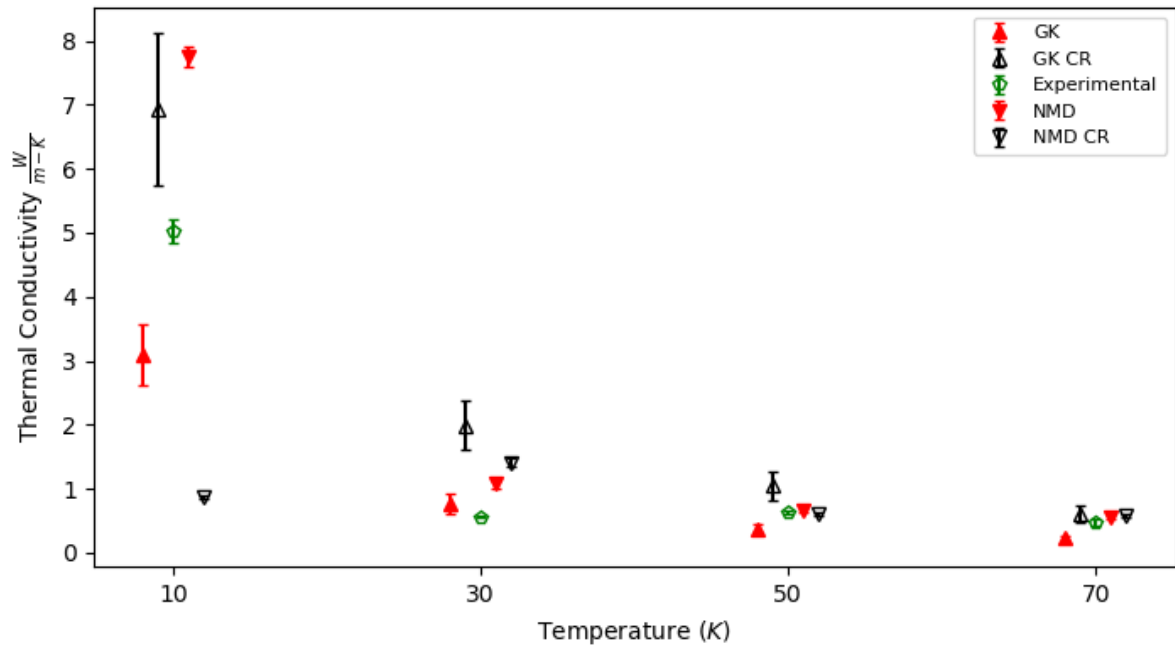


Fig. 3.3: A comparison between thermal conductivity values calculated with NMD and GK, under conventional and CR potential, and the experimental values [Thermal conductivity of solid argon] at four different temperatures 10 K, 30 K, 50 K, and 70 K. The x-axis values are shifted by 1K for every temperature for better visibility

ature I shifted the results by 1K for better readability. In general all the data points follow the trend observed in the experimental values [142] except for the NMD under CR potential (black hollow down-pointing triangles). Despite the mentioned match in trend, the non-Langevin simulations (red markers) are more comparable with the experiment, although they fall out of the uncertainty band of the experimental values (green pentagons) and the maximum deviation of the corresponding calculations is 55% of the experimental value. The mentioned deviation is expected for these types of calculations and higher values up to 80% was also reported [73]. One might argue that the uncertainty bands should cover the deviation, but that requires the knowledge of biased uncertainty due to the potential used and knowing in general how far the estimation created by MD is from reality. The reported uncertainty for every data point is based on the consideration of the random uncertainty inherited in the computational approaches used [135].

Comparison between the GK values obtained under conventional (red up-pointing triangles) and CR (black up-pointing triangles) potential revealed consistent higher values of thermal conductivity at all four temperatures for the system under CR potential, the observation is due to the nature of GK method that is calculating the material's conductivity in terms of the time correlation of oscillations. As a result, I believe the `fix-langevin` used for the application of the Brownian dynamics applies oscillations as perturbations with high temporal correlation that adds to the final calculated thermal conductivity. The temporal correlation is becomes clearer by observing higher standard deviation in the simulations using CR potential, which is due to high correlated perturbations affecting the trajectories over a certain period of simulation and changing after a period of time (Fig.3.4). In our uncertainty analysis I looked at the correlation over a long period of time and moved the correlation window, this was able to capture the high correlation in sections of the heat flux signal, but the correlation character is changing from one correlation window to another causing the high standard deviation of the GK results.

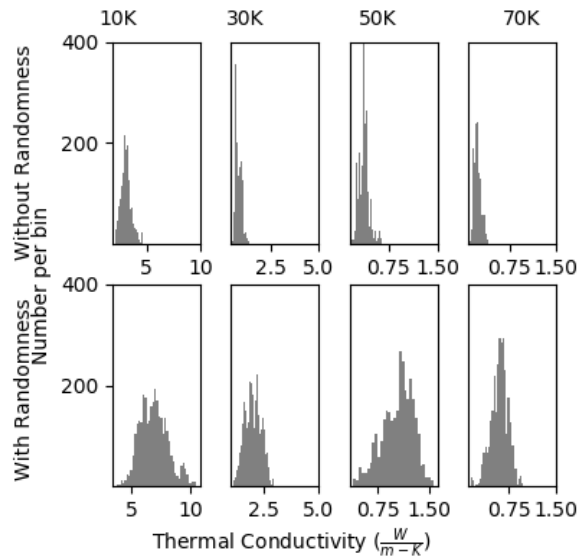


Fig. 3.4: Uncertainty analysis of the Green-Kubo method using 3000 data points derived from ten different ensembles and 100 different trajectories, k_x , k_y , and k_z are considered equal due to the isotropy of the thermal conductivity in argon[20]

The difference between the conventional and CR potential results are not as pronounced for the NMD calculations (down-pointing triangles) except for the 10 K results. At 10 K the application of the CR potential increases the scattering events as a result, the thermal conductivity is lower for the CR NMD data point (black down-pointing triangle) compared to the NMD under the conventional potential (red down-pointing triangle). I observed almost no difference at high temperatures and I attribute it to the nature of the NMD analysis. NMD is a harmonic analysis based method that analyzes the vibrations in terms of the superposition of single harmonic motions up to the maximum Debye frequency as a result, being less affected by the high frequency vibrations added by the Brownian dynamics. The addition of high frequencies is clear in the difference between GK (up-pointing triangles) and NMD results (down-pointing triangles) at high temperatures. This is due to the statistical nature of the GK analysis and its capability of capturing the dynamics of vibrations irrespective of their collective or local nature. It is also observable in the scattered frequencies in the DSF analysis and the addition of high frequencies around the mean (Fig. 3.1). Considering all the discussed results so far I have not observed an evidence suggesting the same thermal properties for both conventional and CR potential at each simulated temperature that is not explainable by the characteristics of the methods used. However, an equal thermal property for cases under the conventional and the CR potential is a piece of evidence that would suggest similarity in the physics of systems under the conventional and the CR potential.

The NMD method is based on the calculations of the modal lifetimes and the data is another measure of finding similarities between the dynamics of crystalline and amorphous materials in their frequency space (Fig.3.5). The comparison of 10 K data (Fig.3.5 a and e) shows a higher number of scattering events in the CR potential case, as I see smaller lifetimes in the frequency range in the case under CR potential compared to the conventional at 10 K. With increasing temperature, lifetimes decrease but the decrease is pronounced more at higher frequencies (a steeper lifetime vs frequency scaling). This claim is clearer comparing 30 K and 50 K data for both cases under conventional and CR potentials (Fig.3.5

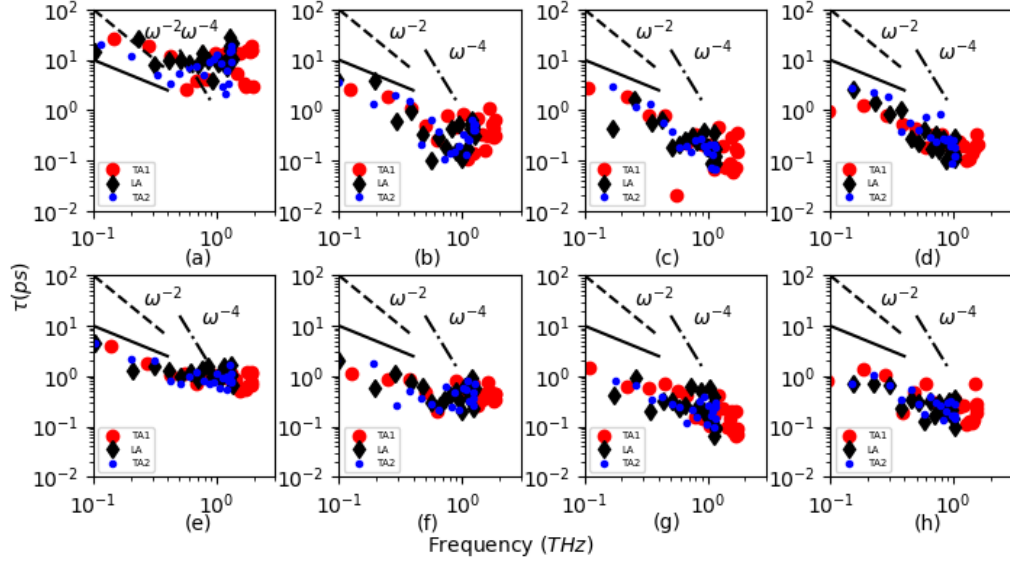


Fig. 3.5: Lifetime of modes travelling in the [100] direction. The top row is showing results under the conventional potential and at four different temperature (left to right 10k,30k,50k,70k), The bottom row is showing the results for the same temperatures but for a CR system. The solid black line is the Ioffe-Regel limit of frequency and lifetime.

b,c and f,g). In general the application of the CR potential flattens the lifetime behaviour in the low and medium frequency range for temperatures in the range of 30-70 K (Fig.3.5 f, g, and h) and in the mid/high frequency range at 10 K (Fig.3.5 h). This is the behavior that is described by Kittel scattering [65] and was observed at high frequencies in experimental works [69], this comparison with works on amorphous materials illustrates that the application of CR potential is a good choice to model random dynamics in crystalline materials. The observation of this type of scattering is due to the high frequencies added by `fix-langevin` and is affecting all modes from low to high frequencies. This affect on a wide range of frequencies is not comparable to the dynamics of amorphous materials. I also put the ω^{-2} and ω^{-4} scales observed for the propagating modes in amorphous materials [69, 73] on the lifetime graph (Fig.3.5). By visually inspecting the data the ω^{-2} scale is comparable with the low frequency behavior of 30-70 K under the conventional potential (Fig.3.5 b, c, and d), the behavior has been observed in other works on Lennard-Jones crystals [130]. One might argue that the Rayleigh scales should be more observable in the cases under the

CR potential as the potential is simulating the randomness, but the vibrational modes are scattered by events that are dominated by high frequency modes added with the Brownian Dynamics. As a result, the Kittel scattering is dominating the cases with CR potential.

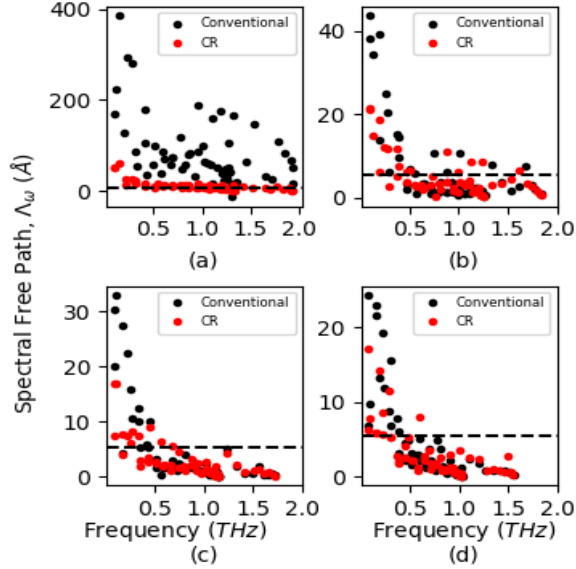


Fig. 3.6: Spectral Free Path comparison of cases under conventional and CR potential at temperature from 10 K-70 K, the dashed line is indicating the equilibrium lattice constant at the indicated temperature. The calculation is based on $\Lambda_\omega = \tau_\omega v_\omega$, in which the mode velocity (v_ω) is calculated as the derivative of the polynomial fitted to the dispersion relation curve. The graphs are (a), (b), (c), and (d) related to temperatures 10-70 K, respectively.

The main character of vibrations in amorphous materials is the existence of non-propagating modes (Diffusons and Locons) that are limited to the atomic separations distances, meaning that the vibrational mode will not travel beyond a distance larger than the smallest atomic spacing. To check this I plotted the spectral free path (Fig.3.6). As a result, I found that starting at 30 K have free paths smaller than the lattice constant and the trend is consistent for 50 K and 70 K simulations. It is also interesting to observe almost no difference between the Λ_ω values of modes simulated under conventional and the CR potential at temperatures 50 K and 70 K supporting the almost no difference observation in the NMD thermal conductivity results of conventional and CR potential. Despite the

failure in showing comparable result in the thermal conductivity of crystalline and amorphous materials, So far I have observed lifetimes below the Ioffe-Regel limit (Solid black line in Fig. 3.5) at high temperatures in the lifetime analysis, and below the atomic spacing extent of travel for modes at temperatures above half of Debye temperature of argon. These observations lead us to the next step of our analysis.

Observing the evidence for possible existence of non-propagating modes mandates the search for the known vibrational modes of amorphous structures known as Diffusons. To discover the existence of Diffusons in our systems I used the dynamical structure factor (DSF), which is proven to be equal to the structure factor analysis [137]. The Static Structure factor analysis is a two-step method and the derivation of eigenvectors is the first, and the main calculation is the second step. I used the DSF to target lower uncertainty due to less computational work involved and to capture the full picture of the dynamics. The DSF is not limited to the analysis of understanding vibrations as harmonic oscillators, involved in the structure factor analysis through the eigenvector calculation. As a result, it is able to capture the Brownian Dynamics applied to the simulations under the CR potential. In the literature the DSF is used to provide the dispersion relation of materials using a spatial and temporal Fourier Transform of the vibrations [138, 139], and the broadening of the branches in the DSF is the evidence of the existence of Diffusons in the simulation [125, 139].

As presented in Figure 3.1, DSF provides clear evidence for the existence of Diffusons with increasing temperature specifically at temperatures of 30 K, 50 K, and 70 K. This section of the results, in addition to the free paths being lower than the lattice constant (Fig.3.6 b, c, and d), and the observed low lifetimes in comparison with the Ioffe-Regel limit (Fig.3.5 b, c and d), are evidence of the fact that the frequency-space behavior of crystalline materials, at high temperatures, is comparable to the frequency space of the amorphous materials. In other words, the spatial disorder in amorphous materials is comparable to the temporal and spatial disorder of vibrations in crystalline materials at high temperatures. It is also understood from the DSF comparison of the CR cases with the corresponding

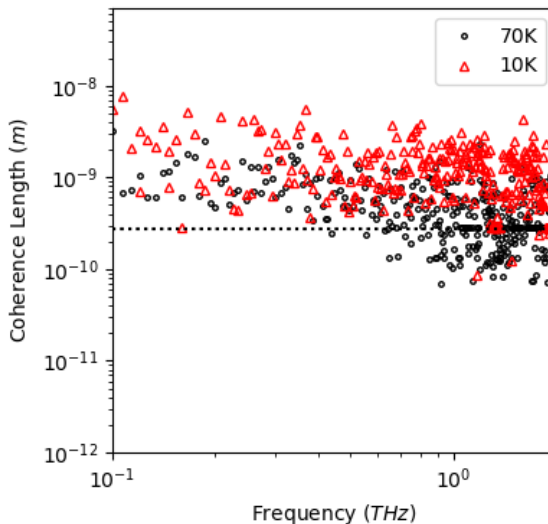


Fig. 3.7: Spatial coherence calculations for two temperatures 10 K and 70 K. The dotted line is indicating the lattice constant of the argon crystal.

cases under the conventional potential that the applied randomness to the system through Brownian dynamics is an overestimation of the amount of randomness in a system. In addition, tunable randomness [118] in a system of particles could better resemble a system under conventional potential.

I claimed the existence of the spatial disorder in other words, spatial discontinuity of waves in a time instant, in addition to the temporal broadening observed in the DSF graphs. The broadening of DSF at each frequency fitted to a Lorentzian function provides the spatial coherence of each frequency [123]. Using this approach, I calculated the spatial coherence for two temperatures 10 K and 70 K (Fig. 3.7). This data provides clear evidence for the reduction of coherence, which is intuitive considering the increase of scattering events. The most important point is the reduction of coherence length to values below the lattice constant. this is another approach to show the existence of non-propagating modes at high temperatures. As a result, a proof of and temporal disorder of vibrations in crystalline systems at high temperatures.

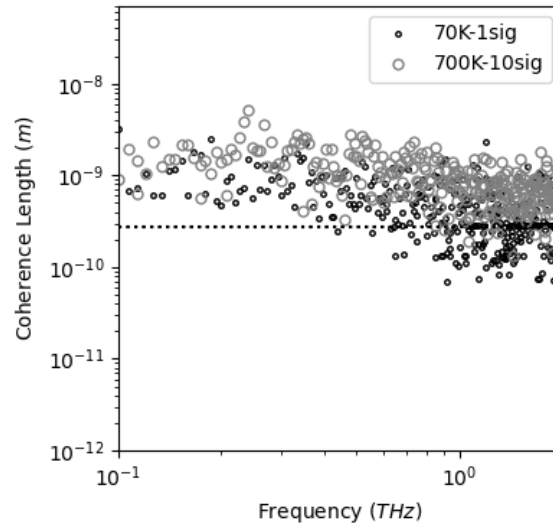


Fig. 3.8: Spatial coherence calculations for two temperatures 70 K and 700 K. The dotted line is indicating the lattice constant of the argon crystal.

In addition, I evaluated the effect of change in the depth of the interatomic potential well to explore the possibility of observation of such temperature dependent localization for a hypothetical material having a stronger potential. To make a fair comparison I increased the strength of the Lennard-Jones potential by ten times and observed the melting temperature increase from 90 K to 900 K. As a result, I compared the special coherence of modes in a system at 70 K that has the conventional potential strength with another system at 700 K, which had a potential ten times stronger than the conventional Lennard-Jones potential. The results (Fig.3.8) clearly show by in the hypothetical system with a stronger potential the localized modes disappear. As a result, the temperature induced local modes are a function of potential and might not happen in a stiff system of particles.

To clarify the outcome of the last pieces of evidence provided here I summarize them by observing the break of temporal coherence due to spectral free paths below the lattice constant and the broadening of the DSF. I have also observed the break of spatial coherence based on the observation of coherence lengths below the lattice constant. The observations are a potential-dependent phenomenon and in Fig. 3.8 I should by increasing the strength of

the potential the local incoherent modes disappear. In general the dynamics of disorder is observed in crystalline material at high temperatures, which was almost half of the Debye temperature for argon, and the local modes are absent in a hypothetical material with a strong potential. The last piece of our observation is showing that the phenomenon is a potential dependent one.

3.4 Conclusion

I evaluated the possibility of comparing the dynamics of vibrations of crystalline materials with the amorphous. The reason for our comparison is to evaluate the possibility of using methods such as random matrix theory to model crystalline materials as these methods have been used to model systems with number of particles beyond the current capabilities of Molecular Dynamics simulations. I ran two types of simulations one under a condition, in which most modes were absent and the other with extra randomness in the system and compared the cases with a conventionally thermostated system. The results should show a temperature dependent behavior and at high temperatures the dynamics of crystalline materials are comparable with the dynamics of amorphous. The presented results are potential dependent. A hypothetical material with ten times the strength of the argon system under study should show no modes having coherence length below the lattice spacing, this observation shows the potential dependence of the phenomenon. As a result, I observed evidence for the dynamics of vibrations in amorphous materials being comparable with the dynamics of crystalline material at temperatures as high as half of the Debye temperature for the argon system. This provides evidence for the application of modeling approaches such as random matrix theory to crystalline materials to extend the capability of modeling in crystalline materials beyond the time and size limit of Molecular dynamics simulations.

CHAPTER 4

ATOMISTIC MODELING OF THE MICRON-SCALE PROPAGATION LENGTHS IN AMORPHOUS SILICON

4.1 Introduction

The desire to achieve smaller junction size and have more computational power resulted in the generation larger amounts of heat in an smaller volume as a result, larger larger volumetric heat generation. The trend initiated research attempts to understand the heat transport phenomenon in the non-diffusive transport regime [143, 144]. Non-diffusive heat transport is the regime of energy transport through a thermal gradient, when the length scale of the system is below the Mean Free Path (MFP) of the phonons. This reduction of the length scale leads to the reduction of thermal conductivity as the boundary scattering of phonons become the dominant scattering mechanism in the system [145]. The reduction of thermal conductivity is of interest in some applications such as, thermoelectrics [134, 146–149], however this is not desired in most application, such as research and design in the semiconductor industries [150, 151].

The aforementioned applications mandates the analysis and measurements of the phonon MFP. As a result, multiple computational and experimental approaches have been developed and used to serve the goal of reducing (e.g Thermoelectrics) or increasing (e.g. semiconductor industry) the thermal conductivity through characterizing the materials' thermal properties. The experimental approaches range from thin film measurement techniques such as 3ω [74, 152, 153] to more precise optical techniques as, time domain thermoreflectance (TDTR) [154], transient thermal grating (TTG) [155], and broadband frequency domain thermoreflectance (BB-FDTR) [156]. The experimental approaches provide indirect access to MFP information through a property called the thermal conductivity accumulation function, which is accessible through the experimental measurement of the thermal conduc-

tivity [157]. Computational approaches can provide a clear path to the calculation of MFP, providing direct access to the modal lifetimes [158].

The importance of MFP and micron scale calculated/measured MFPs in amorphous silicon (a-Si), which makes it different from the majority of glasses [159], is the motivation of multiple computational [4] and experimental works [160]. The rapid increase of the thermal conductivity accumulation function in a-Si suggests a scattering scaling greater than ω^{-2} in MFP or lifetimes. The observation of ω^{-4} scaling in MFPs indicates elastic scattering and is coincident with the Rayleigh law of sound attenuation [161], while the observation of ω^{-2} scaling is evidence of anharmonic scattering [162]. The scaling not only provides insight into the physics of the system, which serves the goal of understanding the MFPs of materials, but also is required for thermal conductivity models such as the Debye dispersion and power law of scattering [163].

The computational approaches, as mentioned in the previous paragraph, provide a clear path to MFPs without dealing with the convolutions of mapping experimental values of thermal conductivity to the thermal conductivity accumulation function, pertinent to the experimental approaches [164]. The computational works on silicon lack a wide MFP spectrum of analysis, covering low to high frequencies [4,139]. As a result, I explore this gap and expand the computational works by employing a larger system, and a new frequency analysis approach called dynamical structure factor to understanding the dynamics of amorphous silicon system under two established potentials, Tersoff and Stillinger-Weber [165, 166]. I also examine the possibility of tiling a system along one of the axes to access lower frequencies.

I structure the paper as follows; first, I explain the simulation procedure, the procedure to perform the dynamical structure factor analysis, the fitting procedure that is used to extract the lifetimes, followed by the hybrid approach to obtain the MFPs in the methods section. I analyze the obtained computational data and compare them to the existing experimental data in the discussion section to paint the picture explaining the physics of scattering in an amorphous silicon system of particles.

4.2 Methods

Our methods are categorized in three groups, structural analysis, the procedure to perform the Molecular Dynamics (MD) and lattice dynamics simulations, and the post-processing procedure to calculate the Mean Free Paths named in this paper as spectral free paths. I will also use well established methods such as the Green-Kubo (GK) thermal conductivity calculation [51, 52, 120, 121, 167], and the Non-Equilibrium Molecular Dynamics (NEMD) calculation of thermal conductivity [168] to support our results that are not discussed in detail.

4.2.1 Structural Analysis and MD simulations procedure

I performed our simulations in a 100k atoms system of particles created by the WWW algorithm, which was developed by F. Wooten, K. Winer, and D. Weaire and named respectively [140]. This algorithm was modified further by Normand et. al. [141]. I use the Radial Distribution Function (RDF) as a measure of the structural compatibility of the WWW structure with the actual amorphous structure of silicon. To develop the RDF of our system I have defined a 15 Å off-set from the edges of our structure and put a sphere of radius 10 Å on atoms in the selected region. Then I divided the sphere into 200 shells and counted the number of each atom in each shell. I have performed the analysis on all atoms in the selected region and averaged the values to get a smooth RDF.

I performed the MD simulation using the LAMMPS [101] package and used the GULP [108] package for the lattice dynamics calculation of the Allen-Feldman (AF) diffusivity [169]. In both simulations I have used both the 1985 Stillinger-Weber potential [165] and the 1989 Tersoff potential [166] for silicon. All simulations I performed at 300 K and due to stress release requirements I have annealed all systems at 600 K. During the annealing procedure I have started the simulation under an NPT ensemble [170] at 600 K and kept it at this condition for 3 ns. This step was followed by cooling back to 300 K under an NPT ensemble for 6 ns and an equilibration under the same ensemble for 9 ns. Following the mentioned steps I have simulated the system under the microcanonical ensemble for another 3 ns

and collected the position and velocity information for 210 ps every 0.025 ps. I have also evaluated the stability of the data acquisition process through monitoring the pressure and energy trends in the microcanonical ensemble section of the simulation. I performed lattice dynamics calculations to develop the AF velocities (`thermal` keyword in `GULP`) by setting the total energy calculated by `LAMMPS` and the choice of broadening values. The choice of broadening value is a matter of trial and error to find a value that provides an acceptable resolution and results in stable diffusivity values. The calculation of the diffusivity is based on evaluating the modal heat current operator S_{ij} that measures the coupling between the modes i and j . This operator has a delta function in its definition that tunes the extent of overlap between modes using a Gaussian estimation of the delta function. The diffusion calculation is also under the effect of volume (V), reduced Planck's constant, and the mode's frequency (ω_i).

$$D(\omega_i) = \frac{\pi V^2}{\hbar^2 \omega_i^2} \sum_{i \neq j} \|S_{ij}\|^2 \delta(\omega_i - \omega_j) \quad (4.1)$$

4.2.2 Post-Processing

To calculate the lifetimes I have used the dynamical structure factor (DSF) analysis [162]. This analysis has been used in parallel with the static structure factor (SSF) notion [139] and the difference is based on the use of eigenvectors in the SSF analysis and the eigenvector calculation are not required in an DSF analysis. As a result, DSF analysis is capable of deriving the lifetimes under full anharmonic conditions. The SSF analysis is using the notion of eigenvectors, calculated using the lattice dynamics calculation, which is a calculation at 0 K and will not reflect the full anharmonic effects caused by temperatures. Other methods that are based on the statistics of vibrations [29, 30] can calculate the eigenvalues of vibration under the full effect of temperature modeled in an MD system, but they require supercell averaging through tiling of multiple supercells. Considering the fact that these types of simulations are computationally expensive, the addition of supercell averaging will make them even less computationally feasible. The DSF is based on taking the spatial and temporal Fourier Transform of vibrations. The temporal Fourier transform

is taken over the simulation time (t_{sim}), and the spatial is taken over the k -mesh in the spatial reciprocal space. The equation for a system of particles containing N atoms of one kind with the mass m is as follows,

$$S(k, \omega) = \frac{m}{4\pi N t_{\text{sim}}} \sum_{\alpha} \left| \int_0^{t_{\text{sim}}} \sum_{n_x, n_y, x_z}^N \dot{u}_{\alpha}(t) \exp(ik \cdot r_0 - i\omega t) dt \right|^2.$$

The decay behavior observed is modeled using a Lorentzian function. The choice of the Lorentzian function is based on the similarity of the decay in real space to a forced damped harmonic oscillator [171] as a result, a Lorentzian decay in the frequency space. The linewidth ($\Gamma(k)$) of a mode is the half-width at the half-height of the Lorentzian fit based on the definition of the Lorentzian function.

$$S(k, \omega) = \frac{C_0(k)}{[\omega_0(k) - \omega]^2 + \Gamma^2(k)}, \quad (4.2)$$

where $C_0(k)$ is a mode-dependent constant and $\omega_0(k)$ is the frequency at the peak of the Lorentzian peak. The lifetime of each mode is defined as the inverse of 2 times the linewidths,

$$\tau(\omega) = \frac{1}{2\Gamma(k)}. \quad (4.3)$$

I calculate the AF velocities through the diffusivity values. The calculation of AF velocities is based on the diffusion of kinetic energy and its squared dependence on the velocity of diffusion. As a result, I define the AF velocities as the square root of the diffusivities divided by the appropriate lifetimes [172]. I used these velocities instead of the group velocities defined based on the derivative of the dispersion curve for a section of the frequency interval, which exhibits spread in frequencies of a wavevector in the DSF function (Fig. 4.1). Using the group/AF velocities and the lifetimes I have calculated the spectral free paths through a linear relationship between spectral free path, lifetime, and group/AF velocities.

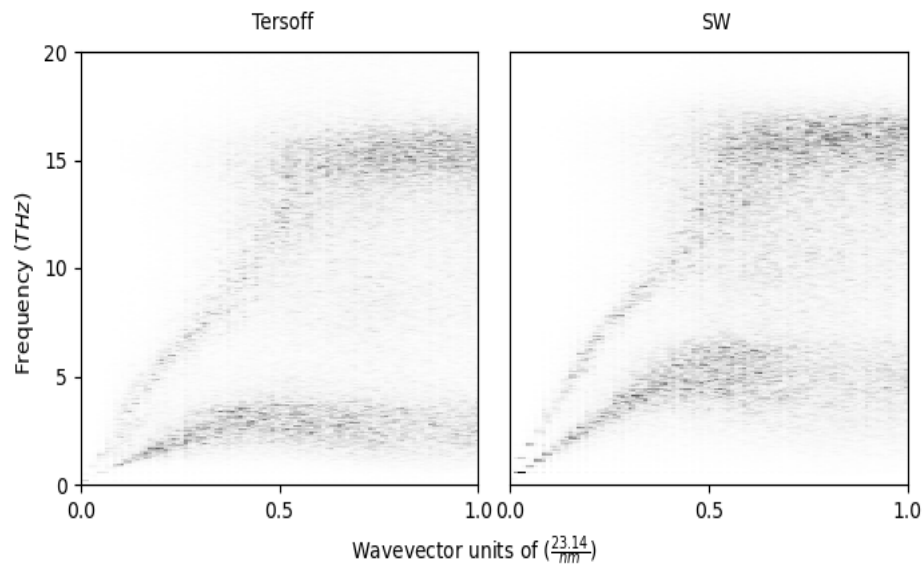


Fig. 4.1: The Dispersion resulted from the dynamical Structure factor analysis on both Tersoff (left) and the Stillinger-Weber (right) potentials

4.3 Results and Discussion

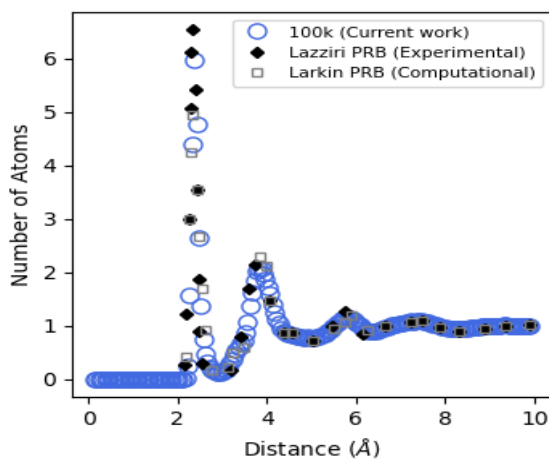


Fig. 4.2: Radial Distribution function 100k WWW system compared with two other experimental, and computational results [3, 4]. The Laaziri experimental results and the computational results of the Larkin work are extracted from the graphs.

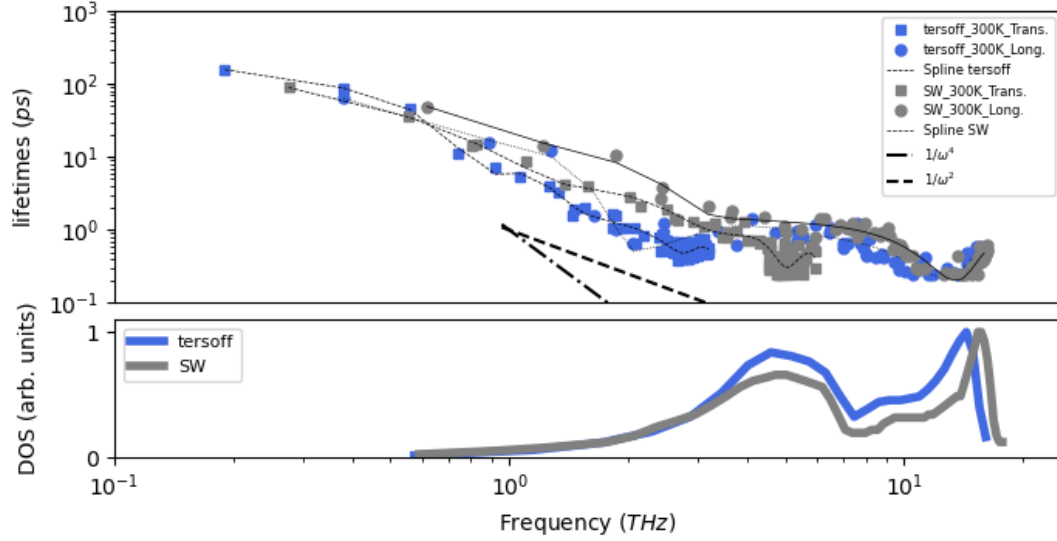


Fig. 4.3: top:lifetime of a-Si for both Stillinger-Weber and Tersoff potential. An spline fit is used to fit the data of each branch (Transverse and Longitudinal) for the purpose of eye guide. Bottom: The comparison of density of states for both SW and Tersoff potentials, obtained from lattice dynamics analysis.

Our first measure of the systems I studied, is their RDF analysis and how close the peaks are to the experimental values. The RDF provides a very close match to the experimental values and the shape of the function follows the experimental values precisely [3]. The RDF of the WWW structure is a better match to the experimental values at the first peak compared to the RDF of a melt-quench structure reported by Larkin and McGauhey (Fig.4.2). The better match is clear by comparing the black Rhombus, blue circle, and grey square at the first peak.

Fig.4.3 presents the spectral lifetimes of amorphous silicon under two different potentials. These results are drawn from the Lorentzian fit of the DSF peaks. There is a clear difference between the mid-range frequency scaling of the Tersoff and SW lifetimes. The Tersoff results show a stiffer behavior in the low frequency range (0.1-0.3 THz) and the mid-frequency scaling follows a ω^{-4} scaling in comparison with the ω^{-2} scaling of the SW lifetimes. The stiffness of the Tersoff system is also observable in density as a bulk property, the Tersoff Density is $2.34 \frac{\text{g}}{\text{cm}^3}$ and the density of the system under SW potential is

2.30 $\frac{\text{g}}{\text{cm}^3}$. The high frequency behavior as well as the lifetime values are consistent with the observation of Larkin and McGaughey [4]. It is also important to mention that Larkin and McGaughey have used the SW potential in their analysis. The overall trend of decrease in the lifetimes from low to high frequencies is consistent with the increase in the density of states (DOS), which is due to the presence of more modes as a result more scattering events will occur. The minimum of the lifetime graph is comparable to the maximum of the DOS curve. The difference in the position of accumulation of modes in the lifetime graph and the first peak in the DOS data presented in Fig.4.3 is mainly due to the different source of the information, which is DSF for the lifetimes and lattice dynamics for the DOS. The effect of temperature on the position of the peak in the DOS is studied in our previous work and evident in the lattice dynamics results with missing the temperature effects [119]. The statistical and fit uncertainties in finding the peaks of the DSF graph and Lorentzian fits of the DSF data are also affecting the position of the peak in the DOS. Other researchers have used the Tersoff potential [139] in their lifetime analysis and their results show a crossing of the Ioffe-Regel limit, which is not the case for the result of this work, and are an order of magnitude lower for the high frequency region compared to our results, although the trend matches the observed trend in our results for both SW and Tersoff potential. The broadening at high frequencies, specifically the broadening of the peaks above the Ioffe-Regel limit is the convolution of multiple peaks [173], and these types of peaks cannot be analyzed as a damped harmonic oscillator and the peaks cannot be fitted with a Lorentzian function [174, 175], which makes the obtained results above the limit unreliable. This notion will not affect our work as I am focused on the low to mid frequency spectrum of the vibrations.

The Time Domain Thermal Reluctance (TDTR), the picosecond acoustics, and transient grating spectroscopy data provide the spectral free path, which is in direct relationship with the spectral lifetimes through the linear relation between the mean free path, lifetime, and group velocity [162]. The group velocities can be drawn from the dispersion relation resulting from the DSF analysis for a crystalline material. The material under study in this

paper is amorphous and vibrations in these types of materials are not all propagating. For amorphous materials the one-to-one correspondence between wavevectors and frequencies breaks at some point on the frequency spectrum. As a result, defining the group velocity as the derivative of the dispersion relation ($\frac{\partial\omega}{\partial k}$) is correct definition [125]. The thermal conductivity of non-propagating modes are defined with the AF theorem for diffusons [67]. As a result, I draw velocities of energy propagation using the AF velocities and calculated from the AF diffusivity definition.

To have the right combination of group and AF velocities, I have distinguished the transition from dispersion relation group velocities to the AF velocities based on the distinctness of the DSF peaks and used the wavevector as our measure (Fig. 4.1). The transition wavevectors are 10.3 and 9.6 $\frac{1}{\text{nm}}$ for the longitudinal and the transverse branches, respectively. From the transition point forward I use the AF velocities. Before I explore the group and AF velocities I will review the results of the diffusivity analysis.

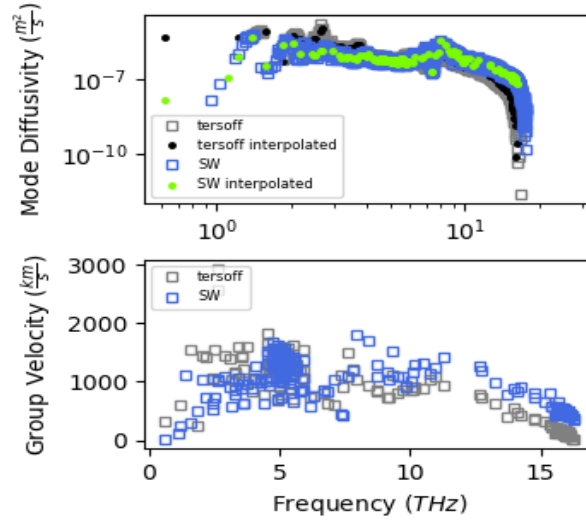
The results of both SW and Tersoff diffusivities are presented in Fig. 4.3-a. The diffusivities of both potentials behave the same at first glance but the SW potential creates lower diffusivities in the low frequency region but the trend reverses in the high frequency region and the SW results exceed the Tersoff values. The Tersoff and SW diffusivity results also have different features in the 2-3 THz and 7-8 THz frequency intervals. The feature between 2-3 THz creates higher AF velocities for the Tersoff potential and the feature between 7-8 THz creates higher AF velocities for the SW case. I am using the wavevector as the measure of the transition from group velocity to AF velocities that makes our approach to have different transition points for each branches (9.6 THz for Transverse and 10.3 THz for Longitudinal branches of both potentials). Considering the fact that the Lattice Dynamics result of diffusivities are versus frequencies, I had to map the diffusivity results versus frequencies to diffusivity versus wavevectors. For this purpose, I used the peaks of the dispersion relation, although the peaks at high frequencies are debatable. The use of high frequency peaks is not a new approach used in this paper and is a method used in the literature [139]. The remapping result of this basis-change are plotted for both

potentials in Fig.4.3-a and are labeled with green and black circles for SW and Tersoff potentials, respectively. The remapping result shows no loss of information, when mapping the diffusivity result vs. frequency to diffusivity vs. wavevector and mapping them back vs. frequency basis.

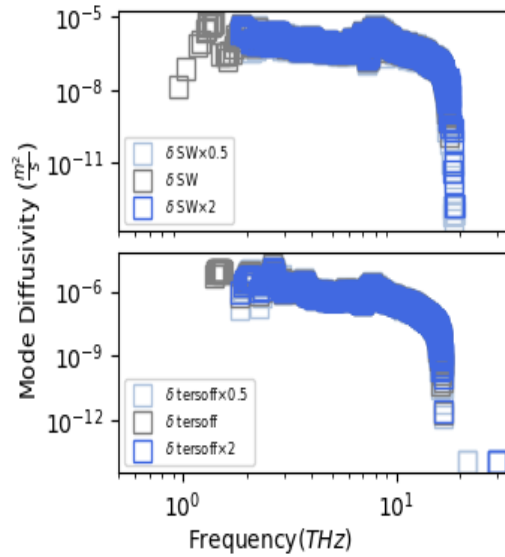
It is also important to measure the diffusivity results for different broadening factors to estimate the effect of delta function broadening on the formulation of diffusivity (Fig.4.3-b). I have checked this effect by comparing the values of diffusivity for broadening values twice and half of the main used value, which was set to 5. The result of this analysis provided almost no change for most of the frequency range but the values obtained with 5 as the broadening factor show capturing of lower frequency diffusivities for both the Tersoff, and the SW potential and predicts less oscillating result for the Tersoff potential in the low frequency region Fig.4.3-b.

The result of group velocity analysis is presented in Fig.4.5. The velocities show an abrupt change at the transition to the AF velocities. The discontinuity is justified as the velocities are attributed to two different regimes of transport. One form of transport is through coherent and collective motions of atoms to a diffusive penetration of energy and the second is the mode of transport where the notion of one-to-one correspondence to frequency is lost [70]. It is noticeable that the SW velocities are higher in the propagating region of the frequency range. Although the Tersoff potential is stiffer and the diffusion is lower for stiffer systems [176], the AF velocities are higher for the low frequency region (1-5 THz) for this potential and the fact is due to lower lifetime values in that frequency range for the Tersoff potential.

The dispersion relation is a one-to-one correspondence between the frequencies and wavevectors. I presented the dispersion relation with the given explanation for both SW and Tersoff potentials in Fig.4.5. The one-to-one correspondence is disputed for the high frequency region in the literature, which is after a transition frequency from propagons to diffusons [125]. Despite the mentioned fact, it is a great measure of comparison of the dynamics of the WWW a-Si structure under the SW and Tersoff potentials for the low and



(a)



(b)

Fig. 4.4: (a) comparison of diffusivities for both SW and Tersoff potentials (top) and the resting group velocities (bottom) the circles are the interpolations required to map the frequency based diffusivities to the wavevector based ones (b) comparison between different values of the broadening factor in the computation of the diffusion for both the SW (top), and the Tersoff potential.

mid frequency region.

The SW frequencies are higher that is comparable to the stiffer dispersion of a solid at lower temperatures [119], the stiffer frequency behavior of SW-Si has been reported previ-

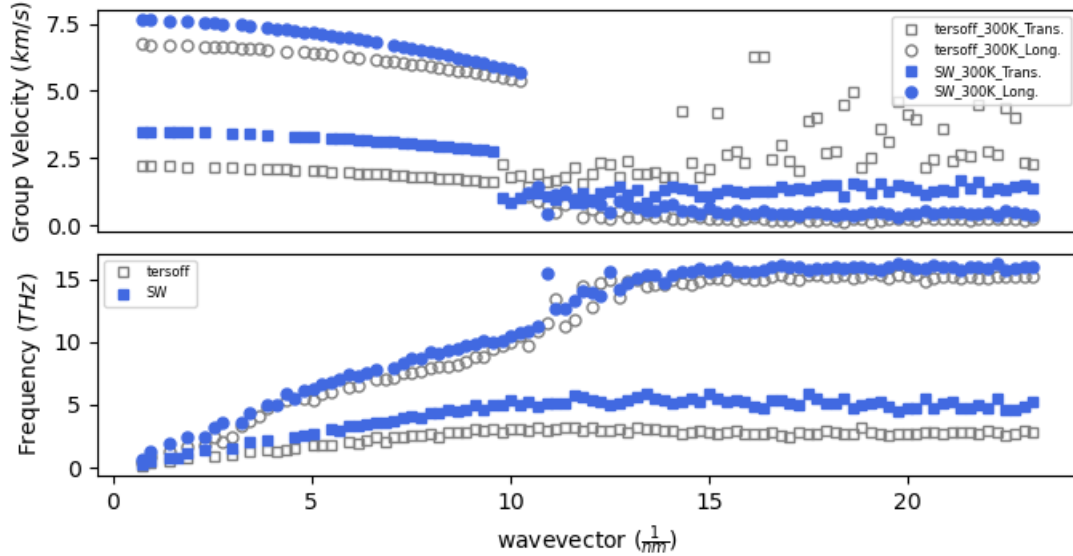


Fig. 4.5: Group Velocity as a combination of the derivative of the dispersion relation and the AF velocity (top), and the dispersion relation resulted from the peaks of the dynamical structure factor

ously in the literature [177], although it contradict our previous observations in this paper. I attribute the difference in the longitudinal branch to the uncertainty of our measurements. The difference is pronounced more for the transverse branch, which might be attributed to the directional dependence of both potentials [177].

Using the calculated group velocities for each frequency and the calculated lifetimes, I calculated the mean free paths (spectral free path) of each mode. The spectral free paths for both SW and Tersoff potentials follow the same trend in the low frequency region (0.2-0.4 THz). The behavior changes for both potentials in the mid-frequency region (0.4-6 THz). The Tersoff scaling is more compliant with a scaling between ω^{-3} and ω^{-4} for both the transverse and longitudinal branches. other researchers have also reported ω^{-3} scaling [178]. The trend starts somewhere between 1-2 THz in the longitudinal branch, but the initiation of the mentioned scaling starts from 0.4 THz for the transverse branch and softens from 0.7 THz for the rest of the frequency range. The mid-range behavior of the spectral free paths are different for the SW potential. The trend follows an ω^{-2} scaling after 0.6 THz up to 6-7 THz and the behavior is similar for both branches of vibrations.

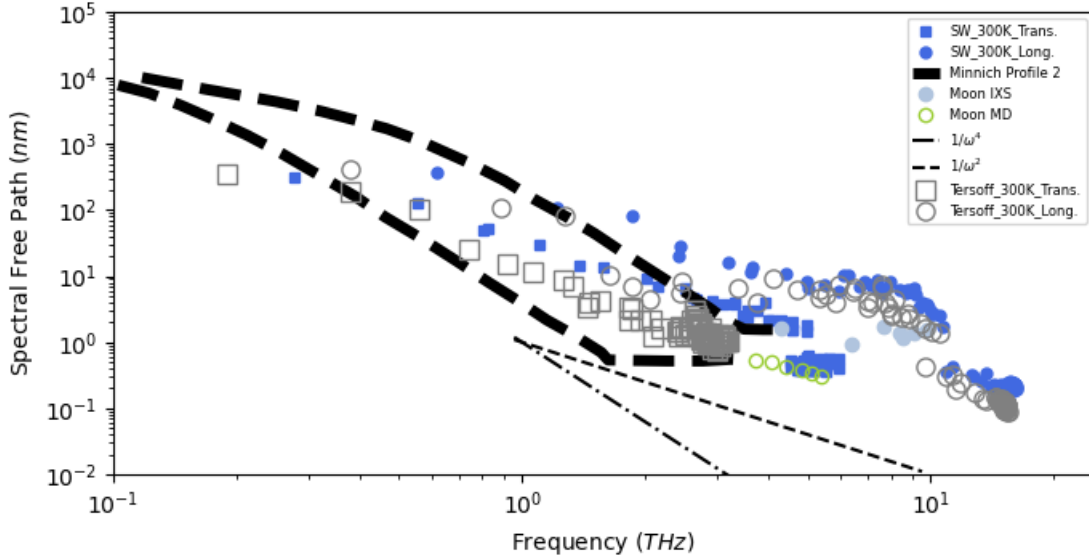


Fig. 4.6: Spectral Free path of modes calculated using both SW and Tersoff potential, in comparison with other experimental and computational data, and the predicted profile by Minnich

As mentioned earlier in the text, the importance of the scaling reveals the physics of scattering. Early attempts to understand the excess of the phonon vibrational density of states (VDOS) in comparison to the Debye estimation of the VDOS, known as the Boson Peak [179], led to the introduction of local density fluctuations, which some authors attributed to the elastic phonon scattering known as Rayleigh scattering [133]. This elastic scattering is known to scale the lifetimes as a function of frequency with an ω^{-4} scaling. As a result such scaling of lifetimes can be an indication of Rayleigh scattering and local fluctuation of density. It is also insightful to notice that the Rayleigh scattering is commonly considered as the source of plateau of the amorphous materials' thermal conductivity graph versus temperature [66], although it has been disputed in the literature [180].

I have also added the predicted profiles (two dashed lines) by Minnich et. al. [69], each line represents a branch of vibration. The low-frequency region of the profile predicts higher spectral free paths compared to our calculation but the trends both comply with the ω^{-1} scaling. This scaling for the low frequencies of amorphous materials has been reported by Walton, and in their approach they model lifetime vs. frequency of these types of

materials [181]. Our results provide additional evidence for ω^{-1} scaling at low frequencies, which was interpreted by Minnich et. al. as the absence of thermally activated relaxations and the origin of the micron-scale modes in amorphous silicon. I am not able to observe the micron scale modes due to the size limitation of our simulations but as mentioned in Minnich's work, lower scaling is the notion of weak thermally activated relaxations. Moving from high to low frequencies, our results predicted the initiation of modes scaling with ω^{-1} at higher frequencies for both branches and the mid range frequency trends in our results are different from their result. The difference between the profiles presented by Minnich et. al. and our data is dissimilar comparing the profile to the data resulting from different potentials, used in this work. The Tersoff potential in its longitudinal branch is following the longitudinal branch of the profile but this compliance deviates for the transverse branch, where the profile follows an ω^{-4} scaling and our data follows an ω^{-3} scaling. The data based on the SW potential deviates from profile for both transverse and longitudinal branches and our data for this potential follows a ω^{-2} scaling. There are some features that are present in our data (2-3 THz and 7-8 THz) for both SW and Tersoff potentials. These features have their roots in the diffusivity data at the two mentioned frequency intervals, presented in Fig.4.3-a. I have also added the experimental data by Moon et. al. [138] (light blue circles) and MD results by Moon et. al. [139] (green circles), the experimental data is closer to the SW results, but the MD results comply with the results from both potentials in the context of trend but our data are generally higher within the range of Moon's results.

The Tersoff lifetimes can produce ω^{-4} scaling but the scaling is less pronounced in the Spectral Free Path results, the fact is clear comparing the scaling of the Tersoff potential in Figs.4.3 and 4.6.

I have attempted to induce the ω^{-4} scaling through the addition of 1% and 3% of Hydrogen, Germanium, and Si-29 impurities (Fig. 4.7 and 4.8). The logic behind the addition of impurities is based on possible light to heavy mass impurities in a deposition chamber. I used the SW potential and implemented the effect of impurities through mass change. The results did not produce the scaling for the impurities under study. The unsuccessful results

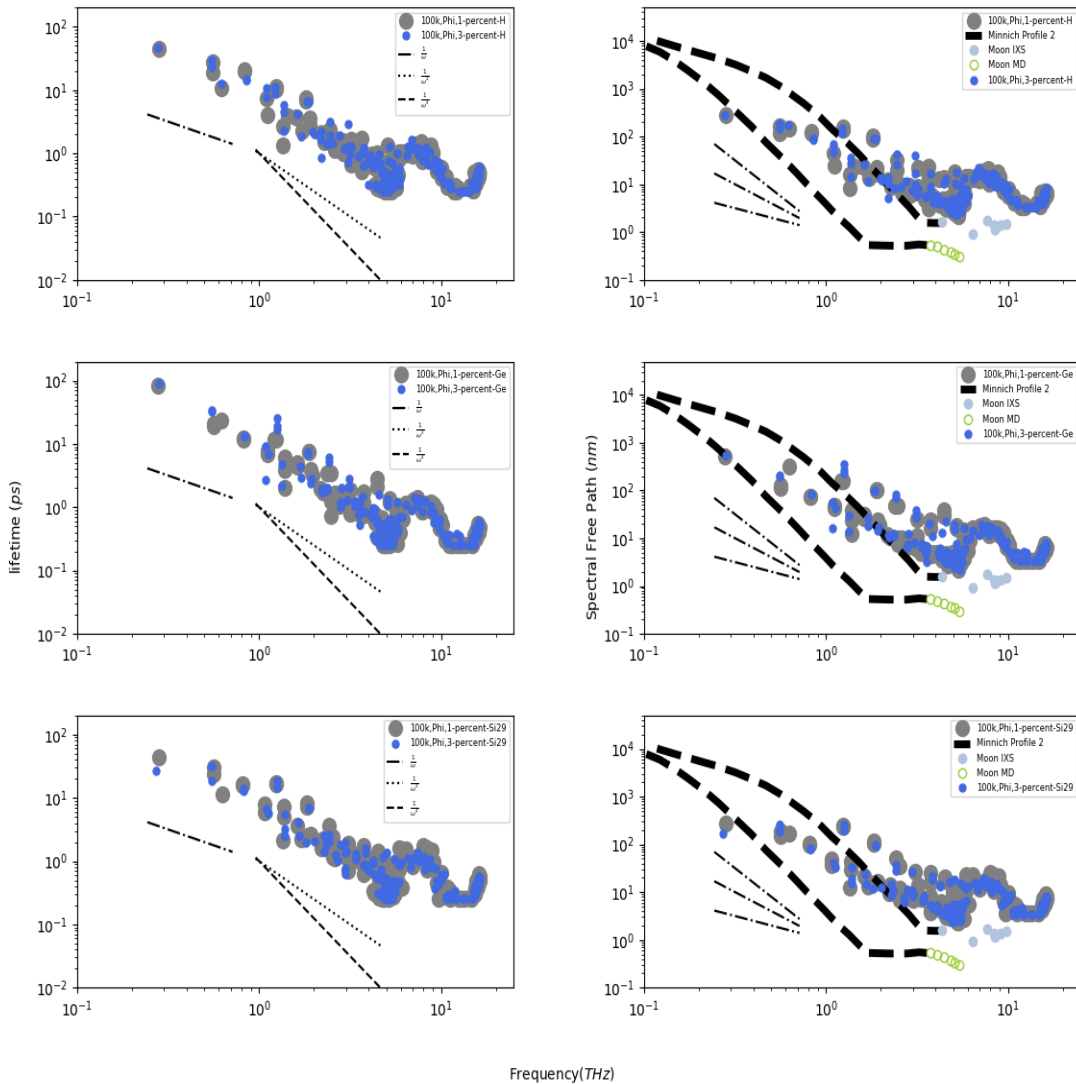


Fig. 4.7: lifetimes of doped samples with Hydrogen, Germanium, and Si-29 (right column) and the corresponding spectral free paths with a constant group velocity approximation (left column)

can be due to the bad choice of potential, and a better potential that model impurity-silicon interactions in more detail, rather than a mass difference model, might be able to reproduce the the scaling and provide evidence of the impurity related scaling. The spectral free paths are generated with two assumption about the group velocity, one as a constant value and two as the derivative of the dispersion relation, which was interpolated with a sinusoidal

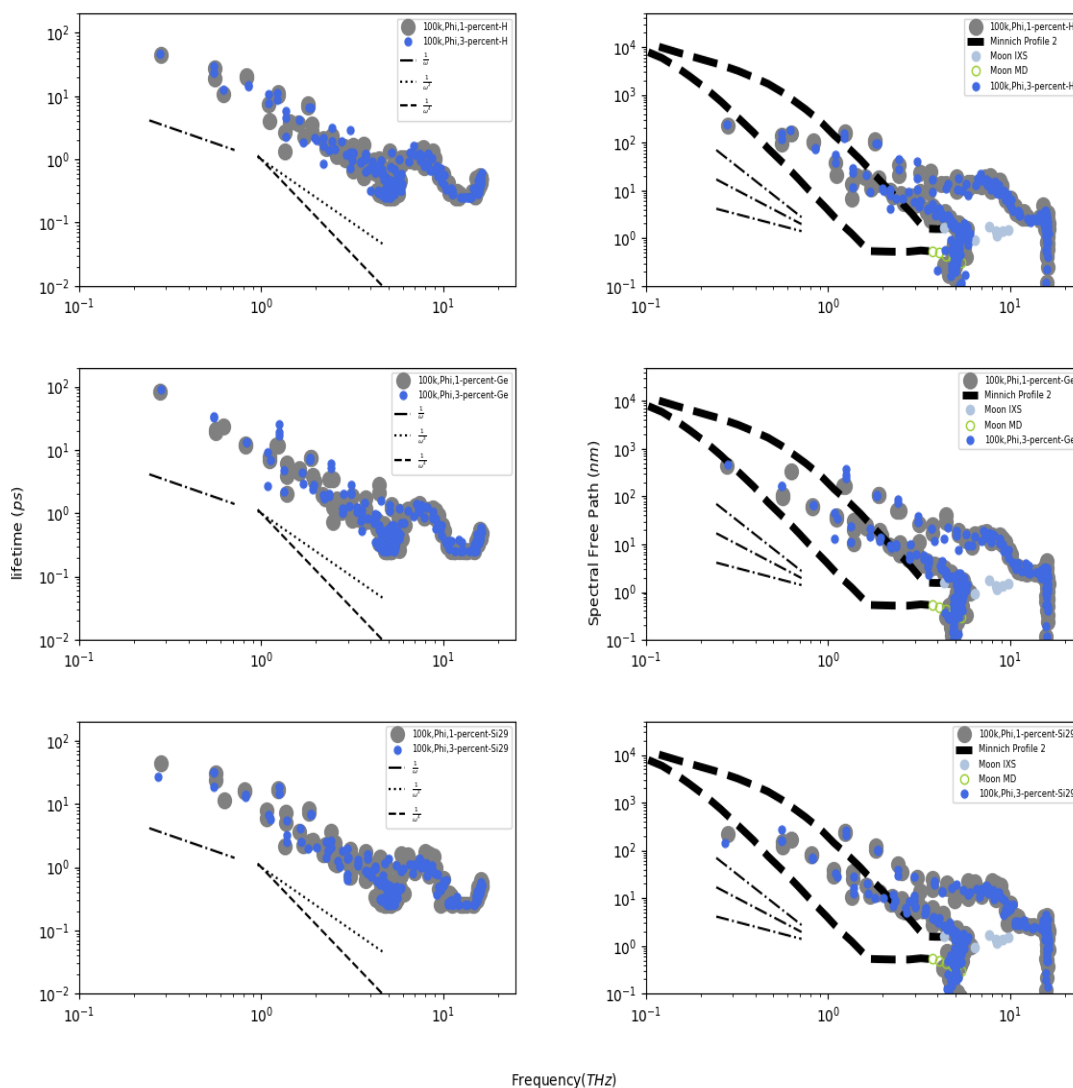


Fig. 4.8: lifetimes of doped samples with Hydrogen, Germanium, and Si-29 (right column) and the corresponding spectral free paths with a sine interpretation of the dispersion relation and defining group velocity as its derivative (left column)

function. The result are on the same order of the profile predicted by Minnich et. al. but do not match the trends in most of the frequency interval.

To support the observed scaling, I calculated the thermal conductivity of different system sizes, and under different potentials, using the GK and the Non-Equilibrium Molecular Dynamics (NEMD) approach (Fig.4.9). The GK results clearly show a divergence behavior

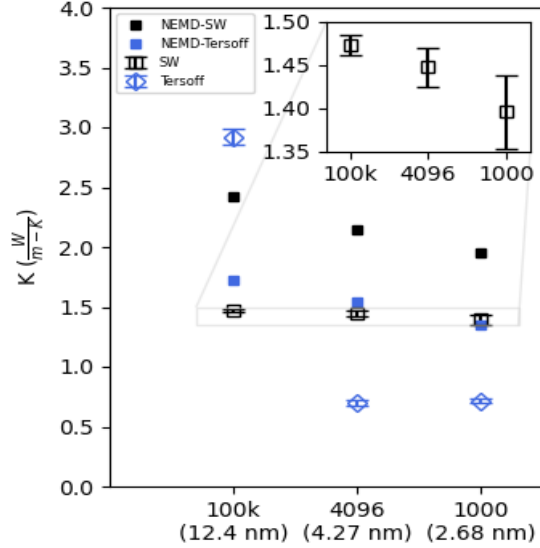


Fig. 4.9: Green-Kubo calculation of thermal conductivity of three different system sizes. 100k, 4096, and 1000 atom systems

of the thermal conductivity for the Tersoff system, which is an indication of $> \omega^{-4}$ scaling in the lifetimes. The decay is less pronounced moving from the 4096 system to the 1000 atom system as the 2-4 nm length scale is within the high frequency region of vibration. This section of the frequency band accommodates the excess in the mode number (First peak in the DOS) and the excess amount of modes create non-propagating modes that are less affected by the size effect [182]. The GK results of the SW potential show minimal size dependence for 100k and 4096, which is an indication of the plateau behavior in the thermal conductivity accumulation function of the ω^{-2} scaling and the reduction in the thermal conductivity from 4096 to 1000 atom system is due to the size effects on the excess modes. In our GK analysis I used the first-avalanche (FAV) method [183] to choose the integration extent of the calculations. To support our GK results I performed NEMD thermal conductivity calculation for all systems and the results follow the trend of the GK result III, although they are known to be III under the influence of the size effects [184]. The NEMD result for the system sizes with majority of modes being non-propagating are higher than the GK results and this trend was also observed in other works, which was attributed

to the difference in the nature of methods and the inclusion of hot and cold regions in the NEMD measurements [185]. The smaller change in the NEMD result of the Tersoff potential compared to the GK result is an evidence of the effect of long wavelength modes on the thermal conductivity of the Tersoff systems as the long wavelengths that are present in the GK systems due to periodic boundary conditions get scattered in the cold and hot region of and NEMD simulation. The scattering is due to the random added/subtracted velocities in the cold and hot region. In addition, this is another evidence for higher scaling in the Tersoff system compared to the SW system, as the faster reduction in the lifetimes will make the contribution of higher wavelengths more important.

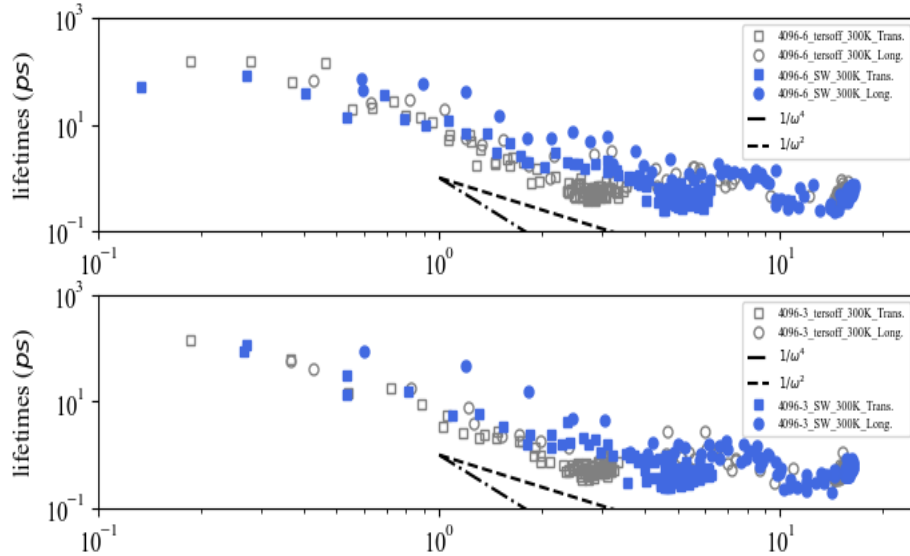


Fig. 4.10: Lifetimes of a 4096 atom sample tiled three (down) and six (up) times.

Our Tersoff results are different compared to the He and Gali's results [71] as they observed a plateau in the thermal conductivity of large samples that I didn't. The difference is due to their approach of creating systems with high number of particles, using a tiling approach these types of systems create flawed lifetimes for low-frequency modes. To demonstrate this claim I modeled larger systems by tiling the 4096 atom system three and six times in one direction and performed the lifetime analysis on these systems (Fig. 4.10).

The result of our analysis shows different lifetimes in the low-frequency region compared to the lifetimes of the 100k system. The tiled systems illustrate a less steep lifetime scaling compared to the 100k system, which is the result of the absence of scattering events emerging from the non-extended direction.

4.4 Conclusion

In this paper I presented a computational proof of lower lifetime scaling of low frequency region for amorphous silicon. In our analysis I used two commonly used potentials for amorphous silicon. In our methodology I utilized a hybrid approach to define the velocity of energy penetration that is known as group velocity for the vibrations with known wavevector- frequency correspondence and AF velocity for the type of vibrations missing the aforementioned correspondence. The result of this approach in parallel with using $12 \times 12 \times 12$ nm system is the observation of up to micron-scale spectral free paths. The observation of such spectral free paths is not a violation of size effect as the lifetime is the source of such analysis and the periodic boundaries provide the possibility of such values for the spectral free paths. The scaling of spectral free paths follow ω^{-2} for the SW potential, which is an indication of inelastic scattering. However, I didn't observe a clear ω^{-4} scaling in the mid-region of the frequency for any of the potentials and the scaling was between ω^{-3} and ω^{-4} for the Tersoff potential, this scaling is known as the elastic scattering and is known to create a plateau in the thermal conductivity accumulation function for modes having large spectral free paths. I also evaluated the possibility of the lifetime/spectral free path scaling modification in the SW potential by the impurities in the deposition chamber and observe negligible change stemming just from the change of masses in the SW potentials implementation. This might result in a different outcome if I had access to SW potentials modified for atom-atom interactions other than silicon-silicon interactions. I have also evaluated the effect of extending a system along one side to access lower frequencies but the implementation results in less scattering due to the missing phonons along the non-extended directions. I used the last piece our work to explain our results in comparison with other scholarly works.

CHAPTER 5

Summary and Conclusion

In this dissertation I characterized the dynamics of disorder in crystalline and amorphous materials. To make the evaluation first, I developed a methodology to capture the energy of a frequency band in a wavepacket. The energy was based on the Quantum Mechanical definition of phonon energy. I have used a frequency detection approach to check for the frequencies present in the system to evaluate the performance of the method. The evaluation provided excellent match with the target frequencies. I have also used the method to evaluate the validity of Molecular Dynamics simulations at the frequency level and found that these simulations are still valid, even at low temperatures (10 K for argon), up to frequencies as high as 1 THz. The method was eventually used for the main purpose of this study as it provided negligible decay after a long simulation time of 2 ns, although the atom displacements were well within the anharmonic region of the potential. As a result, I hypothesised that random dynamics, resulting from the existence of temperature (kinetic energy), is the cause of the decay of phonons. To evaluate the hypothesis, I evaluated the dynamics of a crystalline argon system with and without the addition of random perturbations to the interatomic forces. The result of this analysis with the calculation of phonon lifetime, spectral free paths, and coherence length provided the evidence for the resemblance between the dynamics of crystalline materials at high temperature (above half of the Debye temperature for argon) to the dynamics of amorphous materials. The result is the evidence for random motions of atoms at high temperatures in crystalline materials creating scattering events more often. In addition, the result of this section of my work can lead to future research efforts that use methods such as random matrix theory to model crystalline materials that will enable researchers to reach longer simulation times and larger

simulations cells, which is a current limitation of molecular dynamics.

Additionally, I have used a methodology seldom used in the literature to evaluate the reason for high thermal conductivity of amorphous silicon. The method doesn't require an eigenvalue evaluation of the dynamics of the system and, as a result, is a faster approach to capture temperature dependent lifetimes of any system of particles. By applying the DSF analysis in addition to the calculation of diffusive energy transport velocity using the Allen-Feldmann definition of diffusion, I was able to define the spectral free paths in amorphous silicon and provide computational-based evidence for sub-micron modes in amorphous silicon for the first time. The reason for this is mentioned in the literature and based on experimental works as the absence of thermally activated relaxations not affecting the low-frequency modes.

In conclusion, the research presented in this dissertation will have a lasting impact of the nanoscale thermal transport and the broader atomistic simulation communities. The methods that I have developed provide (1) an improved physical representation of phonon modes in crystalline materials that captures temperature dependent behavior, (2) a new physical understanding of phonon scattering mechanisms at high temperatures in crystalline and amorphous materials, and (3) a modeling method that captures this improved understanding and provides a path to increasing the scale for which molecular based simulations can be applied.

REFERENCES

- [1] D. G. Cahill and R. O. Pohl, "Heat flow and lattice vibrations in glasses," *Solid State Communication*, vol. 70, no. 10, pp. 927–930, 1989.
- [2] Y. Fuji, N. A. Lurie, R. Pynn, and G. Shirane, "Inelastic neutron scattering from solid ar," *Physical Review B*, vol. 10, no. 8, pp. 3647–3659, 1974.
- [3] K. Laaziri, S. Kycia, S. Roorda, M. Chicoine, J. Robertson, J. Wang, and S. Moss, "High-energy x-ray diffraction study of pure amorphous silicon," *Physical Review B*, vol. 60, no. 19, p. 13520, 1999.
- [4] J. M. Larkin and A. J. H. McGaughey, "Thermal conductivity accumulation in amorphous silica and amorphous silicon," *Physical Review B*, vol. 89, no. 14, p. 144303, 2014.
- [5] L. E. Bell, "Cooling heating generating power and recovering waste heat with thermoelectric systems," *Science*, vol. 321, no. 5895, pp. 1457–1461, 2008.
- [6] G. J. Snyder and E. S. Toberer, "Complex thermoelectric materials," *Nature Materials*, vol. 7, no. 2, pp. 105–114, 2008.
- [7] R. Venkatasubramanian, E. C. T. Siivola, and B. O'Quinn, "Thin-film thermoelectric devices with high-room temperature figures of merit," *Nature*, vol. 413, no. 6856, pp. 597–602, 2001.
- [8] K. F. Hsu, "Cubic $\text{Ag}_3\text{SbSbTe}_2$: Bulk thermoelectric materials with high figure of merit," *Science*, vol. 303, no. 5659, pp. 818–821, 2004.
- [9] A. I. Hochbaum, R. Chen, R. D. Delgado, W. Liang, E. C. Garnett, and M. Najarian, "Enhanced thermoelectric performance of rough silicon nanowires," *Nature*, vol. 451, no. 7175, pp. 163–167, 2008.
- [10] B. Poudel, Q. Hao, Y. Ma, Y. Lan, A. Minnich, and B. Yu, "High-thermoelectric performance of nanostructured bismuth antimony telluride bulk alloys," *Science*, vol. 320, no. 5876, pp. 634–638, 2008.
- [11] K. Biswas, J. He, I. D. Blum, C. Wu, T. P. Hogan, and D. Seidman, "High-thermoelectric performance of nanostructured bismuth antimony telluride bulk alloys," *Nature*, vol. 489, no. 7416, pp. 414–418, 2012.
- [12] K. Zhang, Y. Chai, M. M. F. Yuen, D. G. W. Xiao, and P. C. H. Chan, "Carbon nanotube thermal interface material for high-brightness light-emitting-diode cooling," *Nanotechnology*, vol. 19, no. 21, p. 215706, 2008.
- [13] R. Prasher, "Thermal boundary resistance and thermal conductivity of multiwalled carbon nanotubes," *Physical Review B*, vol. 77, no. 7, 2008.

- [14] P. E. Hopkins, M. Baraket, E. V. Barnat, T. E. Beechem, S. P. Kearney, J. C. Duda, J. T. Robinson, and S. G. Walton, “Manipulating thermal conductance at metal-graphene contacts via chemical functionalization,” *Nano Letters*, vol. 12, no. 2, pp. 590–595, 2012.
- [15] D. M. Leitner, “Thermal boundary conductance and thermal rectification in molecules,” *The Journal of Physical Chemistry B*, vol. 117, no. 42, pp. 12 820–12 828, 2013.
- [16] E. Kim, S. Kwun, S. Lee, H. Seo, and J. Yoon, “Thermal boundary resistance at $Ge_2Sb_2Te_5/ZnS:SiO_2$ interface,” *Applied Physics Letters*, vol. 76, no. 26, pp. 3864–3866, 2000.
- [17] D. Rugar, R. Budakian, H. Mamin, and B. Chui, “Single spin detection by magnetic resonance force microscopy,” *Nature*, vol. 430, no. 6997, p. 329–332, 2004.
- [18] M. Li, H. Tang, and M. Roukes, “Ultra-sensitive nems-based cantilevers for sensing, scanned probe and very high-frequency applications.” *Nature Nanotechnology*, vol. 2, no. 2, p. 329–332, 2007.
- [19] E. Gil-Santos, D. Ramos, A. Jana, M. Calleja, A. Raman, and J. Tamayo, “Mass sensing based on deterministic and stochastic responses of elastically coupled nanocantilevers,” *Nano Letters*, vol. 9, no. 12, pp. 4122–4127, 2009.
- [20] M. Spletzer, A. Raman, A. Q. Wu, and X. Xu, “Ultrasensitive mass sensing using mode localization in coupled microcantilevers,” *Applied Physical Letters*, vol. 88, no. 25, p. 254102, 2006.
- [21] H. Okamoto¹, A. Gourgout¹, C.-Y. Chang, K. Onomitsu¹, I. M. abd Edward Yi Chang, and H. Yamaguchi, “Coherent phonon manipulation in coupled mechanical resonators,” *Nano Letters*, vol. 9, no. 8, pp. 480–480, 2013.
- [22] C. Kittel, *Solid State Physics*. John Wiley and Sons, 2005.
- [23] A. Fetter and J. D. Walecka, *Theoretical Mechanics of particles and Countinua*. McGraw-Hill Book Company, 1980.
- [24] A. Henry and G. Chen, “Spectral phonon transport properties of silicon based on molecular dynamics simulations and lattice dynamics,” *Journal of Computational and Theoretical Nanoscience*, vol. 5, no. 2, pp. 141–152, 2004.
- [25] S. Wei and M. Y. Chou, “Ab initio calculation of force constants and full phonon dispersions,” *Physical Review Letters*, vol. 69, no. 19, pp. 2799–2802, 1992.
- [26] K. K and D. PG., “Real-space convergence of the force series in the lattice dynamics of germanium,” *Phys Rev B Condens Matter*, vol. 32, no. 4, pp. 2010–2021, 1985.
- [27] D. M. Riffel, J. D. Christensen, and R. B. Wilson, “Vibrational dynamics within the embedded-atom-method formalism and the relationship to born–von-kármán force constants,” *Journal of Physics: Condensed Matter*, vol. 30, no. 45, p. 455702, 2018.

- [28] P. Heino, “Dispersion and thermal resistivity in silicon nanofilms by molecular dynamics,” *The European Physical Journal B*, vol. 60, no. 2, p. 171–179, 2007.
- [29] L. T. Kong, “Phonon dispersion measured directly from molecular dynamics simulations,” *Computer Physics Communications*, vol. 182, no. 10, pp. 2201–2207, 2011.
- [30] L. TiKong, G. Bartels, C. Campaña, C. Denniston, and M. H. Müser, “Implementation of Green’s function molecular dynamics: An extension to LAMMPS,” *Computer Physics Communications*, vol. 180, no. 6, pp. 1004–1010, 2009.
- [31] M. I. Ralphs, B. L. Smith, and N. A. Roberts, “Technique for direct measurement of thermal conductivity of elastomers and a detailed uncertainty analysis,” *Measurement Science and Technology*, vol. 27, no. 11, p. 115014, 1985.
- [32] D. G. Cahill¹, P. V. Braun, G. Chen, D. R. Clarke, S. Fan, K. E. Goodson, P. Keblinski, W. P. King, G. D. Mahan, A. Majumdar, H. J. Maris¹, S. R. Phillpot, E. Pop¹, and L. Shi¹, “Nanoscale thermal transport. ii. 2003–2012,” *Applied Physics Reviews*, vol. 1, no. 1, p. 011305, 2014.
- [33] D. G. Cahill, “Analysis of heat flow in layered structures for time-domain thermoreflectance,” *Review of scientific instruments*, vol. 75, no. 12, pp. 5119–5122, 2004.
- [34] S. P. Gurrum, W. P. King, Y. K. Joshi, and K. Ramakrishna, “Size effect on the thermal conductivity of thin metallic films investigated by scanning joule expansion microscopy,” *Journal of Heat Transfer*, vol. 130, no. 8, p. 082403, 2008.
- [35] P.-O. Chapuis, , J.-J. Greffet, K. Joulain, and S. Volz, “Heat transfer between a nano-tip and a surface,” *Nanotechnology*, vol. 17, no. 12, pp. 2978–2981, 2006.
- [36] S. Chung¹, J. R. Felts, D. Wang, W. P. King, and J. J. D. Yoreo, “Temperature-dependence of ink transport during thermal dip-pen nanolithography,” *Applied Physical Letters*, vol. 99, no. 19, p. 193101, 2011.
- [37] D. G. Cahill and R. O. Pohl, “Thermal conductivity of amorphous solids above the plateau,” *Physical Review B*, vol. 35, no. 8, pp. 4067–4073, 1987.
- [38] —, “Thermal transport measurements of individual multiwalled nanotubes,” *Physical Review Letters*, vol. 87, no. 21, p. 215502, 2001.
- [39] M. Alaghemandi, E. Algaer, M. C. Bohm, and F. Müller-Plathe, “The thermal conductivity and thermalrectification of carbon nanotubes studied using reverse non-equilibrium molecular dynamics simulations,” *Nanotechnology*, vol. 20, no. 11, p. 115704, 2008.
- [40] W. T. Yorgason, A. N. Barnes, and N. Roberts, “Improvement of thermoelectric properties through reduction of thermal conductivity by nanoparticle addition and stoichiometric change to Mg_2Si ,” *MRS Advances*, vol. 2, no. 59, pp. 3637–3643, 2017.
- [41] J. Callaway, “Model for lattice thermal conductivity at low temperatures,” *Physical Review*, vol. 113, no. 4, pp. 1046–1051, 1959.

- [42] J. Callaway and H. C. V. Bakker, “Effect of point imperfections on lattice thermal conductivity,” *Physical Review*, vol. 120, no. 4, pp. 1149–1154, 1930.
- [43] M. G. Holland, “Analysis of lattice thermal conductivity,” *Physical Review*, vol. 132, no. 6, pp. 2461–2471, 1963.
- [44] ———, “Phonon scattering in semiconductors from thermal conductivity studies,” *Physical Review*, vol. 134, no. 2, pp. A471–A480, 1963.
- [45] D. G. Cahill, W. K. Ford, K. E. Goodson, G. D. Mahan, A. Majumdar, H. J. Maris, R. Merlin, and S. R. Phillpot, “Nanoscale thermal transport,” *Journal of Applied Physics*, vol. 93, no. 2, pp. 793–818, 2003.
- [46] S. Mazumder and A. Majumdar, “Monte carlo study of phonon transport in solid thin films including dispersion and polarization,” *Nano Letters*, vol. 123, no. 4, pp. 749–759, 2001.
- [47] A. Mittal and S. Mazumder, “Monte carlo study of phonon heat conduction in silicon thin films including contributions of optical phonons,” *Journal of Heat Transfer*, vol. 132, no. 5, p. 052402, 2010.
- [48] Y.-J. Han and P. G. Klemens, “Anharmonic thermal resistivity of dielectric crystals at low temperature,” *Physical Review B*, vol. 48, no. 9, pp. 6033–6042, 2005.
- [49] S. V. J. Narumanchi, J. Y. Murthy, and C. H. Amon, “Submicron heat transport model in silicon accounting for phonon dispersion and polarization,” *Journal of Heat Transfer*, vol. 126, no. 6, pp. 946–955, 2005.
- [50] A. J. Minnich, S. M. G. Chen, and B. S. Yilbas, “Quasiballistic heat transfer studied using the frequency-dependent boltzmann transport equation,” *Physical Review B*, vol. 84, no. 23, p. 235207, 2011.
- [51] R. Kubo, “Statistical-mechanical theory of irreversible processes. i. general theory and simple applications to magnetic and conduction problems,” *Journal of the Physical Society of Japan*, vol. 12, no. 6, pp. 570–586, 1957.
- [52] R. Kubo, M. Yokota, and S. Nakajima, “Statistical-mechanical theory of irreversible processes. ii. response to thermal disturbance,” *Journal of the Physical Society of Japan*, vol. 12, no. 11, pp. 1203–1211, 1957.
- [53] V. S. G. and G. Chen, “Molecular-dynamics simulation of thermal conductivity of silicon crystals,” *Physical Review B*, vol. 61, no. 4, pp. 2651–2656, 1999.
- [54] ———, “Molecular dynamics simulation of thermal conductivity of silicon nanowires,” *Physical Review B*, vol. 75, no. 14, pp. 2056–5058, 1999.
- [55] A. McGaughey and M. Kaviani, “Thermal conductivity decomposition and analysis using molecular dynamics simulations. part i. Lennard-Jones argon,” *International Journal of Heat and Mass Transfer*, vol. 47, no. 9, pp. 1783–1798, 2004.

- [56] —, “Thermal conductivity decomposition and analysis using molecular dynamics simulations: Part ii. complex silica structures,” *International Journal of Heat and Mass Transfer*, vol. 47, pp. 1799–1816, 2004.
- [57] —, “Quantitative validation of the boltzmann transport equation phonon thermal conductivity model under the single-mode relaxation time approximation,” *Physical Review B*, vol. 69, no. 9, 2004.
- [58] I. Khalatnikov, “Theory of diffusion and thermal conductivity for dilute solutions of he3 in helium ii,” *JETP*, vol. 22, no. 6, pp. 687–704, 1952.
- [59] E. T. Swartz and R. O. Pohl, “Thermal boundary resistance,” *Reviews of Modern Physics*, vol. 61, no. 3, pp. 605–668, 1989.
- [60] P. K. Schelling, S. R. Phillpot, and P. Keblinski, “Phonon wave-packet dynamics at semiconductor interfaces by molecular-dynamics simulation,” *Applied Physical Letters*, vol. 80, no. 14, pp. 2484–2486, 2002.
- [61] W. Zhang, T. S. Fisher, and N. Mingo, “The atomistic Green’s function method: An efficient simulation approach for nanoscale phonon transport,” *Numerical Heat Transfer*, vol. 51, no. 4, p. 333–349, 2007.
- [62] N. Mingo and L. Yang, “Phonon transport in nanowires coated with an amorphous material: An atomistic green’s function approach,” *Physical Review B*, vol. 68, no. 24, p. 245406, 2003.
- [63] J.-L. Barrat and F. Chiaruttini, “Kapitza resistance at the liquid—solid interface,” *Molecular Physics*, vol. 101, no. 11, pp. 1605–1610, 2002.
- [64] H. R. Seyf, K. Gordiz, F. DeAngelis, and A. Henry, “Using Green-Kubo modal analysis (gkma) and interface conductance modal analysis (icma) to study phonon transport with molecular dynamics,” *Journal of Applied Physics*, vol. 125, no. 8, p. 081101, 2019.
- [65] C. Kittel, “Interpretation of the thermal conductivity of glasses,” *Physical Review*, vol. 75, no. 6, pp. 972–974, 1949.
- [66] R. C. Zeller and R. O. Pohl, “Thermal conductivity and specific heat of noncrystalline solids,” *Physical Review B*, vol. 4, no. 6, pp. 2029–2041, 1971.
- [67] P. B. Allen, J. L. Feldman, J. Fabian, and F. Wooten, “Diffusons, locons and propagons: Character of atomic vibrations in amorphous si,” *Philosophical Magazine B*, vol. 79, no. 11-12, pp. 1715–1731, 1999.
- [68] J. T. EDWARDS and D. J. THOULESS, “Numerical studies of localization in disordered systems,” *Journal of Physics C: Solid State Physics*, vol. 5, pp. 807–820, 1972.
- [69] T. Kim, J. Moon, and A. J. Minnich, “Origin of micron-scale propagation lengths of heat-carrying acoustic excitations in amorphous silicon,” *arXiv*, pp. 1–12, 2020.

- [70] J. L. Feldman, P. B. Allen, and S. R. Bickham, “Numerical study of low-frequency vibrations in amorphous silicon,” *Physical Review B*, vol. 59, no. 5, pp. 3551–3559, 1999.
- [71] Y. He, D. Donadio, and G. Galli, “Heat transport in amorphous silicon: Interplay between morphology and disorder,” *Applied Physics Letters*, vol. 98, no. 14, p. 14101, 2011.
- [72] P.G.Klemens, “Thermal conductivity and lattice vibrational modes,” *Solid State Physics*, vol. 7, pp. 1–98, 1958.
- [73] K. Esfarjani, G. Chen, and H. T. Stokes, “Heat transport in silicon from first-principles calculations,” *Physical Review B*, vol. 84, no. 8, p. 085204, 2011.
- [74] X. Liu, J. L. Feldman, D. G. Cahill, R. S. Crandall, N. Bernstein, and D. M. Photiadis, “High thermal conductivity of a hydrogenated amorphous silicon film,” *Physical Review Letters*, vol. 102, no. 3, p. 035901, 2009.
- [75] S. Neogi and D. Donadio, “Anisotropic in-plane phonon transport in silicon membranes guided by nanoscale surface resonators,” *Physical Review Applied*, vol. 14, no. 2, p. 024004, 2020.
- [76] V. Chiloyan, S. Huberman, A. A. Maznev, K. A. Nelson, and G. Chen, “Thermal transport exceeding bulk heat conduction due to nonthermal micro/nanoscale phonon populations,” *Applied Physics Letters*, vol. 116, no. 16, p. 163102, 2020.
- [77] R. Chen, I. Sharony, and A. Nitzan, “Local atomic heat currents and classical interference in single-molecule heat conduction,” *The Journal Of Physical Chemistry Letters*, vol. 11, no. 11, pp. 4261–4268, 2020.
- [78] T. Sun and P. B. Allen, “Lattice thermal conductivity: Computations and theory of the high-temperature breakdown of the phonon-gas model,” *Physical Review B*, vol. 82, no. 22, p. 224305, 2010.
- [79] A. Jain, S. P. Ong, G. Hautier, W. Chen, W. D. Richards, S. Dacek, S. Cholia, D. Gunter, D. Skinner, G. Ceder, and K. A. Persson, “Commentary: The materials project: A materials genome approach to accelerating materials innovation,” *APL Materials*, vol. 1, no. 1, p. 011002, 2013.
- [80] M. Maldovan, “Phonon wave interference and thermal bandgap materials,” *Nature Materials*, vol. 14, no. 7, pp. 667–674, 2015.
- [81] D. Singh, J. Y. Murthy, and T. S. Fisher, “Effect of phonon dispersion on thermal conduction across si/ge interfaces,” *Journal of Heat Transfer*, vol. 133, no. 12, 2011.
- [82] W. Lv and A. Henry, “Direct calculation of modal contributions to thermal conductivity via Green–Kubo modal analysis,” *New Journal of Physics*, vol. 18, no. 1, p. 013028, 2016.
- [83] N. Mingo, “Anharmonic phonon flow through molecular-sized junctions,” *Physical Review B*, vol. 74, no. 12, p. 125402, 2006.

- [84] P. E. Hopkins, "Multiple phonon processes contributing to inelastic scattering during thermal boundary conductance at solid interfaces," *Journal Of Applied Physics*, vol. 106, no. 1, p. 013528, 2009.
- [85] Y. Chalopin and S. Volz, "A microscopic formulation of the phonon transmission at the nanoscale," *Applied Physics Letters*, vol. 103, no. 5, p. 01602, 2013.
- [86] M. Shen, P. K. Schelling, and P. Keblinski, "Heat transfer mechanism across few-layer graphene by molecular dynamics," *Physical Review B*, vol. 88, no. 4, p. 045444, 2013.
- [87] Z. Wei, Y. Chen, and C. Dames, "Wave packet simulations of phonon boundary scattering at graphene edges," *Journal Of Applied Physics*, vol. 112, no. 2, p. 024328, 2012.
- [88] P. K. Schelling, S. R. Phillpot, and P. Keblinski, "Kapitza conductance and phonon scattering at grain boundaries by simulation," *Journal Of Applied Physics*, vol. 95, no. 11, pp. 6082–6091, 2004.
- [89] C. H. Baker, D. A. Jordan, and P. M. Norris, "Application of the wavelet transform to nanoscale thermal transport," *Physical Review B*, vol. 86, no. 10, p. 104306, 2012.
- [90] T. Hori, "Verification of the phonon relaxation time approximation by probing the relaxation process of a single excited mode," *Physical Review B*, vol. 100, no. 21, 2019.
- [91] E. S. Landry and A. J. H. McGaughey, "Effect of interfacial species mixing on phonon transport in semiconductor superlattices," *Physical Review B*, vol. 79, no. 7, p. 075316, 2009.
- [92] G. Chen, M. Neagu, and T. Borca-Tasciuc, "Thermal conductivity and heat transfer in superlattices," *MRS Proceedings*, vol. 478, 1997.
- [93] C. Jeong, S. Datta, and M. Lundstrom, "Full dispersion versus Debye model evaluation of lattice thermal conductivity with a Landauer approach," *Journal of Applied Physics*, vol. 109, no. 7, p. 073718, 2011.
- [94] Y. Wang, "Temperature-dependent phonon dispersion relation in magnetic crystals," *Solid State Communications*, vol. 54, no. 3, pp. 279–282, 1985.
- [95] J. M. Hastings, S. P. Pouget, and G. Shirane, "One-dimensional phonons and "phase-ordering" phase transition in HgTe ," *Physical Review Letters*, vol. 39, no. 23, pp. 1484–1487, 1977.
- [96] J. D. Axe, J. Harada, and G. Shirane, "Anomalous acoustic dispersion in centrosymmetric crystals with soft optic phonons," *Physical Review B*, vol. 1, no. 3, pp. 1227–1234, 1970.
- [97] K. Tajima, Y. Endoh, and Y. Ishikawa, "Acoustic-phonon softening in the invar alloy Fe_3Pt ," *Physical Review Letters*, vol. 37, no. 9, pp. 519–522, 1976.
- [98] J. Hone, *Phonons and Thermal Properties of Carbon Nanotubes*. Berlin, Heidelberg: Springer Berlin Heidelberg, 2001, pp. 273–286.

- [99] A. Savin, B. Hu, and Y. Kivshar, “Thermal conductivity of single-walled carbon nanotubes,” *Physical Review B*, vol. 80, no. 19, 2009.
- [100] M. D. Gerboth and D. G. Walker, “Effects of acoustic softening on thermal conductivity beyond group velocity,” *Journal of Applied Physics*, vol. 127, no. 20, p. 204302, 2020.
- [101] S. Plimpton, “Fast parallel algorithms for short-range molecular dynamics,” *Journal of Computational Physics*, vol. 117, no. 1, pp. 1–19, 1995.
- [102] P. Tan, Y. Deng, and Q. Zhao, “Temperature-dependent Raman spectra and anomalous Raman phenomenon of highly oriented pyrolytic graphite,” *Physical Review B*, vol. 58, no. 9, pp. 5435–5439, 1998.
- [103] Y. Yun, D. Legut, and P. M. Oppeneer, “Phonon spectrum, thermal expansion and heat capacity of UO₂ from first principles,” *Journal of Nuclear Materials*, vol. 426, no. 3, pp. 109–114, 2012.
- [104] S. Popov, J. J. Carbajo, and G. Yoder, “Thermophysical properties of MOX and UO₂ fuels including the effects of irradiation,” *ORNL*, vol. 27, pp. 4–00, 2000.
- [105] N. W. Ashcroft and N. D. Mermin, *Solid State Physics*. Saunders College Publishing, 1967.
- [106] W. J. P., *Imaging Phonons: acoustic wave propagation in solids*. Cambridge University Press, 2005.
- [107] K. C. Sood and M. K. Roy, “Longitudinal phonons and high-temperature heat conduction in germanium,” *Journal of Physics: Condensed Matter*, vol. 5, no. 3, pp. 301–312, 1993.
- [108] J. Gale and A. L. Rohl, “The general utility lattice program (GULP),” *Molecular Simulation*, vol. 29, no. 5, pp. 291–341, 2003.
- [109] F. Occelli, M. Krisch, P. Loubeyre, F. Sette, R. L. Toullec, C. Masciovecchio, and J.-P. Rueff, “Phonon dispersion curves in an argon single crystal at high pressure by inelastic x-ray scattering,” *Physical Review B*, vol. 63, no. 22, p. 224306, 2001.
- [110] J. D. Launay, “Measurements of x-ray lattice constant, thermal expansivity, and isothermal compressibility of argon crystals,” *The Journal of Chemical Physics*, vol. 22, no. 10, pp. 1676–1677, 1954.
- [111] A. J. H. McGaughey and M. Kaviani, “Phonon transport in molecular dynamics simulations: Formulation and thermal conductivity prediction,” *Advances in Heat Transfer*, vol. 39, pp. 169–255, 2006.
- [112] A. McGaughey and M. Kaviani, “Observation and description of phonon interactions in molecular dynamics simulations,” *Physical Review B*, vol. 71, no. 18, p. 184305, 2005.

- [113] N. Roberts, D. Walker, and D. Li, “Molecular dynamics simulation of thermal conductivity of nanocrystalline composite films,” *International Journal of Heat and Mass Transfer*, vol. 52, no. 7-8, pp. 2002–2008, 2008.
- [114] R. H. Beaumont, H. Chihara, and J. A. Morrison, “Thermodynamic properties of krypton. vibrational and other properties of solid argon and solid krypton,” *Proceedings of the Physical Society*, vol. 78, pp. 1462–1481, 1961.
- [115] P. B. Allen, J. L. Feldman, J. Fabian, and F. Wooten, “Diffusons, locons and propagons: character of atomic vibrations in amorphous si,” *Philosophical Magazine B*, vol. 79, no. 11, pp. 1715–1731, 1999.
- [116] H. R. Seyf, L. Yates, T. L. Bougher, S. Graham, B. A. Cola, T. Detchprohm, M.-H. Ji, J. Kim, R. Dupuis, W. Lv, and A. Henry, “Rethinking phonons: The issue of disorder,” *npj Computational Materials*, vol. 426, no. 3, 2012.
- [117] P. Klemens, “The thermal conductivity of dielectric solids at low temperatures (theoretical),” *Proceedings of the Royal Society of London. Series A. Mathematical and Physical Sciences*, vol. 208, no. 1092, pp. 108–133, 1951.
- [118] D. Conyuh, Y. Beltukov, and D. Parshin, “Application of the random matrix theory to the boson peak in glasses,” in *Journal of Physics: Conference Series*, vol. 1400, no. 4. IOP Publishing, 2019, p. 044026.
- [119] A. Behbahanian and N. A. Roberts, “Phonon wave-packet simulations using the quantized definition of energy and a temperature-dependent phonon dispersion relation and phonon density of states,” *Physical Review E*, vol. 103, no. 4, p. 043311, 2021.
- [120] M. S. Green, “Markoff random processes and the statistical mechanics of time-dependent phenomena,” *The Journal of Chemical Physics*, vol. 20, no. 8, pp. 1281–1295, 1952.
- [121] —, “Markoff random processes and the statistical mechanics of time-dependent phenomena. ii. irreversible processes in fluids,” *The Journal of Chemical Physics*, vol. 22, no. 3, pp. 398–413, 1954.
- [122] J. Turney, E. Landry, A. McGaughey, and C. Amon, “Predicting phonon properties and thermal conductivity from anharmonic lattice dynamics calculations and molecular dynamics simulations,” *Physical Review B*, vol. 79, no. 6, p. 064301, 2009.
- [123] B. Latour and Y. Chalopin, “Distinguishing between spatial coherence and temporal coherence of phonons,” *Physical Review B*, vol. 95, no. 21, p. 214310, 2017.
- [124] J. A. Thomas, J. E. Turney, R. M. Iutzi, C. H. Amon, and A. J. McGaughey, “Predicting phonon dispersion relations and lifetimes from the spectral energy density,” *Physical Review B*, vol. 81, no. 8, p. 081411, 2010.
- [125] F. DeAngelis, M. G. Muraleedharan, J. Moon, H. R. Seyf, A. J. Minnich, A. J. McGaughey, and A. Henry, “Thermal transport in disordered materials,” *Nanoscale and Microscale Thermophysical Engineering*, vol. 23, no. 2, pp. 81–116, 2019.

- [126] T. Schneider and E. Stoll, “Molecular-dynamics study of a three-dimensional one-component model for distortive phase transitions,” *Physical Review B*, vol. 17, no. 3, p. 1302, 1978.
- [127] B. Cheng and D. Frenkel, “Computing the heat conductivity of fluids from density fluctuations,” *Physical Review Letters*, vol. 125, p. 130602, 2020.
- [128] S.-H. Lee, “Molecular dynamics simulation study of the transport properties of liquid argon: The green-kubo formula revisited,” *Bulletin of the Korean Chemical Society*, vol. 28, no. 8, pp. 1371–1374, 2007.
- [129] M. Dove, “Introduction to the theory of lattice dynamics,” *École thématique de la Société Française de la Neutronique*, vol. 12, pp. 123–159, 2011.
- [130] A. J. McGaughey and J. M. Larkin, “Predicting phonon properties from equilibrium molecular dynamics simulations,” *Annual review of heat transfer*, vol. 17, 2014.
- [131] J. Turney, A. McGaughey, and C. Amon, “Assessing the applicability of quantum corrections to classical thermal conductivity predictions,” *Physical Review B*, vol. 79, no. 22, p. 224305, 2009.
- [132] R. E. Peierls, *Quantum theory of solids*. Clarendon Press, 1996.
- [133] S. Elliott, “A unified model for the low-energy vibrational behaviour of amorphous solids,” *EPL (Europhysics Letters)*, vol. 19, no. 3, p. 201, 1992.
- [134] N. Takahashi, Y. Liu, and C. Kaneta, “Materials informatics approach for design of si/ge layered nanostructures with low thermal conductivity,” *Japanese Journal of Applied Physics*, vol. 59, no. 5, p. 051005, 2020.
- [135] H. W. Coleman, W. G. Steele Jr, and W. G. Steele, *Experimentation and uncertainty analysis for engineers*. John Wiley & Sons, 1999.
- [136] Z. Wang, S. Safarkhani, G. Lin, and X. Ruan, “Uncertainty quantification of thermal conductivities from equilibrium molecular dynamics simulations,” *International Journal of Heat and Mass Transfer*, vol. 112, pp. 267–278, 2017.
- [137] T. Feng, B. Qiu, and X. Ruan, “Anharmonicity and necessity of phonon eigenvectors in the phonon normal mode analysis,” *Journal of Applied Physics*, vol. 117, no. 19, p. 195102, 2015.
- [138] J. Moon, R. P. Hermann, M. E. Manley, A. Alatas, A. H. Said, and A. J. Minnich, “Thermal acoustic excitations with atomic-scale wavelengths in amorphous silicon,” *Physical Review Materials*, vol. 3, no. 6, p. 065601, 2019.
- [139] J. Moon, B. Latour, and A. J. Minnich, “Propagating elastic vibrations dominate thermal conduction in amorphous silicon,” *Physical Review B*, vol. 97, no. 2, p. 024201, 2018.
- [140] F. Wooten, K. Winer, and D. Weaire, “Computer generation of structural models of amorphous Si and Ge,” *Physical review letters*, vol. 54, no. 13, p. 1392, 1985.

- [141] G. T. Barkema and N. Mousseau, “High-quality continuous random networks,” *Physical Review B*, vol. 62, no. 8, p. 4985, 2000.
- [142] D. K. Christen and G. L. Pollack, “Thermal conductivity of solid argon,” *Physical Review B*, vol. 12, no. 8, p. 3380, 1975.
- [143] A. J. Minnich, J. A. Johnson, A. J. Schmidt, K. Esfarjani, M. S. Dresselhaus, K. A. Nelson, and G. Chen, “Thermal conductivity spectroscopy technique to measure phonon mean free paths,” *Physical review letters*, vol. 107, no. 9, p. 095901, 2011.
- [144] P. Sverdrup, S. Sinha, M. Asheghi, S. Uma, and K. Goodson, “Measurement of ballistic phonon conduction near hotspots in silicon,” *Applied Physics Letters*, vol. 78, no. 21, pp. 3331–3333, 2001.
- [145] K. T. Regner, J. P. Freedman, and J. A. Malen, “Advances in studying phonon mean free path dependent contributions to thermal conductivity,” *Nanoscale and Microscale Thermophysical Engineering*, vol. 19, no. 3, pp. 183–205, 2015.
- [146] S. Perumal, M. Samanta, T. Ghosh, U. S. Shenoy, A. K. Bohra, S. Bhattacharya, A. Singh, U. V. Waghmare, and K. Biswas, “Realization of high thermoelectric figure of merit in GeTe by complementary co-doping of Bi and In,” *Joule*, vol. 3, no. 10, pp. 2565–2580, 2019.
- [147] B. Cai, L.-D. Zhao, J.-F. Li *et al.*, “High thermoelectric figure of merit $z_t > 1$ in SnS polycrystals,” *Journal of Materiomics*, vol. 6, no. 1, pp. 77–85, 2020.
- [148] G. Yang, L. Sang, F. F. Yun, D. R. Mitchell, G. Casillas, N. Ye, K. See, J. Pei, X. Wang, J.-F. Li *et al.*, “Significant enhancement of thermoelectric figure of merit in BiSbTe-based composites by incorporating carbon microfiber,” *Advanced Functional Materials*, vol. 31, no. 15, p. 2008851, 2021.
- [149] Y. Liao, S. Iwamoto, M. Sasaki, M. Goto, and J. Shiomi, “Heat conduction below diffusive limit in amorphous superlattice structures,” *Nano Energy*, vol. 84, p. 105903, 2021.
- [150] Y. Hong, J. Zhang, and X. C. Zeng, “Monolayer and bilayer polyaniline c 3 n: two-dimensional semiconductors with high thermal conductivity,” *Nanoscale*, vol. 10, no. 9, pp. 4301–4310, 2018.
- [151] J. S. Kang, M. Li, H. Wu, H. Nguyen, and Y. Hu, “Experimental observation of high thermal conductivity in boron arsenide,” *Science*, vol. 361, no. 6402, pp. 575–578, 2018.
- [152] S. Moon, M. Hatano, M. Lee, and C. P. Grigoropoulos, “Thermal conductivity of amorphous silicon thin films,” *International Journal of Heat and Mass Transfer*, vol. 45, no. 12, pp. 2439–2447, 2002.
- [153] D. G. Cahill, M. Katiyar, and J. Abelson, “Thermal conductivity of a-Si: H thin films,” *Physical review B*, vol. 50, no. 9, p. 6077, 1994.

- [154] D. G. Cahill, “Analysis of heat flow in layered structures for time-domain thermoreflectance,” *Review of scientific instruments*, vol. 75, no. 12, pp. 5119–5122, 2004.
- [155] K. C. Collins, A. A. Maznev, Z. Tian, K. Esfarjani, K. A. Nelson, and G. Chen, “Non-diffusive relaxation of a transient thermal grating analyzed with the Boltzmann transport equation,” *Journal of Applied Physics*, vol. 114, no. 10, p. 104302, 2013.
- [156] K. Regner, S. Majumdar, and J. A. Malen, “Instrumentation of broadband frequency domain thermoreflectance for measuring thermal conductivity accumulation functions,” *Review of Scientific Instruments*, vol. 84, no. 6, p. 064901, 2013.
- [157] Y. K. Koh and D. G. Cahill, “Frequency dependence of the thermal conductivity of semiconductor alloys,” *Physical Review B*, vol. 76, no. 7, p. 075207, 2007.
- [158] Y. Beltukov, V. Kozub, and D. Parshin, “Ioffe-Regel criterion and diffusion of vibrations in random lattices,” *Physical Review B*, vol. 87, no. 13, p. 134203, 2013.
- [159] S. Kwon, J. Zheng, M. C. Wingert, S. Cui, and R. Chen, “Unusually high and anisotropic thermal conductivity in amorphous silicon nanostructures,” *ACS nano*, vol. 11, no. 3, pp. 2470–2476, 2017.
- [160] K. T. Regner, D. P. Sellan, Z. Su, C. H. Amon, A. J. McGaughey, and J. A. Malen, “Broadband phonon mean free path contributions to thermal conductivity measured using frequency domain thermoreflectance,” *Nature communications*, vol. 4, no. 1, pp. 1–7, 2013.
- [161] J. W. S. B. Rayleigh, *The theory of sound*. Macmillan, 1896, vol. 2.
- [162] Z. Liang and P. Keblinski, “Sound attenuation in amorphous silica at frequencies near the boson peak,” *Physical Review B*, vol. 93, no. 5, p. 054205, 2016.
- [163] F. Yang and C. Dames, “Mean free path spectra as a tool to understand thermal conductivity in bulk and nanostructures,” *Physical Review B*, vol. 87, no. 3, p. 035437, 2013.
- [164] A. A. Maznev, J. A. Johnson, and K. A. Nelson, “Onset of nondiffusive phonon transport in transient thermal grating decay,” *Physical Review B*, vol. 84, no. 19, p. 195206, 2011.
- [165] F. H. Stillinger and T. A. Weber, “Computer simulation of local order in condensed phases of silicon,” *Physical review B*, vol. 31, no. 8, p. 5262, 1985.
- [166] J. Tersoff, “Empirical interatomic potential for silicon with improved elastic properties,” *Physical Review B*, vol. 38, no. 14, p. 9902, 1988.
- [167] R. Kubo, M. Toda, and N. Hashitsume, *Statistical physics II: nonequilibrium statistical mechanics*. Springer, 1998.
- [168] P. Wirnsberger, D. Frenkel, and C. Dellago, “An enhanced version of the heat exchange algorithm with excellent energy conservation properties,” *The Journal of chemical physics*, vol. 143, no. 12, p. 124104, 2015.

- [169] P. B. Allen and J. L. Feldman, “Thermal conductivity of disordered harmonic solids,” *Physical Review B*, vol. 48, no. 17, p. 12581, 1993.
- [170] M. E. Tuckerman, J. Alejandre, R. López-Rendón, A. L. Jochim, and G. J. Martyna, “A Liouville-operator derived measure-preserving integrator for molecular dynamics simulations in the isothermal–isobaric ensemble,” *Journal of Physics A: Mathematical and General*, vol. 39, no. 19, p. 5629, 2006.
- [171] H. Shintani and H. Tanaka, “Universal link between the boson peak and transverse phonons in glass,” *Nature materials*, vol. 7, no. 11, pp. 870–877, 2008.
- [172] R. Rengel and M. Martín, “Diffusion coefficient, correlation function, and power spectral density of velocity fluctuations in monolayer graphene,” *Journal of Applied Physics*, vol. 114, no. 14, p. 143702, 2013.
- [173] T. Damart, A. Tanguy, and D. Rodney, “Theory of harmonic dissipation in disordered solids,” *Physical Review B*, vol. 95, no. 5, p. 054203, 2017.
- [174] G. Baldi, V. M. Giordano, B. Ruta, and G. Monaco, “On the nontrivial wave-vector dependence of the elastic modulus of glasses,” *Physical Review B*, vol. 93, no. 14, p. 144204, 2016.
- [175] U. Buchenau, “Evaluation of x-ray Brillouin scattering data,” *Physical Review E*, vol. 90, no. 6, p. 062319, 2014.
- [176] S. Plimpton and E. Wolf, “Effect of interatomic potential on simulated grain-boundary and bulk diffusion: a molecular-dynamics study,” *Physical Review B*, vol. 41, no. 5, p. 2712, 1990.
- [177] C. S. Moura and L. Amaral, “Molecular dynamics simulation of silicon nanostructures,” *Nuclear Instruments and Methods in Physics Research Section B: Beam Interactions with Materials and Atoms*, vol. 228, no. 1-4, pp. 37–40, 2005.
- [178] M. P. Zaitlin and A. Anderson, “Phonon thermal transport in noncrystalline materials,” *Physical Review B*, vol. 12, no. 10, p. 4475, 1975.
- [179] N. Ahmad, K. Hutt, and W. Phillips, “Low-frequency vibrational states in As₂S₃ glasses,” *Journal of Physics C: Solid State Physics*, vol. 19, no. 20, p. 3765, 1986.
- [180] W. Dietsche and H. Kinder, “Spectroscopy of phonon scattering in glass,” *Physical Review Letters*, vol. 43, no. 19, p. 1413, 1979.
- [181] D. Walton, “Random-network model, density fluctuation, and thermal conductivity of glasses,” *Solid State Communications*, vol. 14, no. 4, pp. 335–339, 1974.
- [182] J. L. Braun, C. H. Baker, A. Giri, M. Elahi, K. Artyushkova, T. E. Beechem, P. M. Norris, Z. C. Leseman, J. T. Gaskins, and P. E. Hopkins, “Size effects on the thermal conductivity of amorphous silicon thin films,” *Physical Review B*, vol. 93, no. 14, p. 140201, 2016.

- [183] J. Chen, G. Zhang, and B. Li, “How to improve the accuracy of equilibrium molecular dynamics for computation of thermal conductivity?” *Physics Letters A*, vol. 374, no. 23, pp. 2392–2396, 2010.
- [184] Z. Wang and X. Ruan, “On the domain size effect of thermal conductivities from equilibrium and nonequilibrium molecular dynamics simulations,” *Journal of Applied Physics*, vol. 121, no. 4, p. 044301, 2017.
- [185] K. Termentzidis, S. Merabia, P. Chantrenne, and P. Keblinski, “Cross-plane thermal conductivity of superlattices with rough interfaces using equilibrium and non-equilibrium molecular dynamics,” *International Journal of Heat and Mass Transfer*, vol. 54, no. 9-10, pp. 2014–2020, 2011.

CURRICULUM VITAE

Amir Behbahanian

Email: amir.behbahanian@gmail.com

Phone: 801-425-5252

Linkedin: [Amir Behbahanian](#)

Github: [Amir Behbahanian](#)

Education

- Utah State University
Ph.D. Mechanical Engineering 2016-2021
- Sharif University of Technology
B.Sc. Mechanical Engineering 2008-2012

Professional Experience

- Texas A&M
Postdoctoral Researcher 2021-2021
- Tokyo Electron U.S.
Chemistry Modeling Scientist 2021-2021
- Utah State University
Research/Teaching Assistant 2016-2021

Selected Journal Articles

- Phonon wave-packet simulations using the quantized definition of energy and a temperature-dependent phonon dispersion relation and phonon density of states, Behbahanian, A., Roberts, N. A., *Physical Review E* , vol. 4, pp. 043311, 2021.
- Large Area Substrate-Based Nanofabrication of Controllable and Customizable Gold Nanoparticles Via Capped Dewetting, Behbahanian, A., Roberts, N. A., *Journal of Visualized Experiments*, vol. 144, pp. e58827, 2019.
- The effect of different thickness alumina capping layers on the final morphology of dewet thin Ni films, Behbahanian, A., Roberts, N. A., *Applied Physics A* , vol. 124, pp. 1-7, 2018.
- Characterization of Randomness effect on interatomic potentials: A Temperature Dependent Analysis, Behbahanian, A., Larkin, J.M., Roberts, N. A., *Physical Review E* , *Manuscript in Preparation*
- Atomistic Modeling of the Micron-Scale Propagation lengths in Amorphous Silicon, Behbahanian, A., Larkin, J.M., Roberts, N. A., *Physical Review B* , *Manuscript in Preparation*

Conference Presentations

- Characterization of Randomness effect on interatomic potentials: A Temperature Dependent Analysis, Behbahanian, A., Larkin, J.M., Roberts, N. A., in *APS March Meeting*, 2022.
- Thermal Conductivity Measurement of Thermal Interface Materials., Behbahanian, A., in *ASPIRE internal meeting*, 2020.
- Thermal Characterization of Carbon Nanofiber Structures based on their Aspect Ratio, Behbahanian, A, Roberts, N. A. in *IMECE Annual Congress and Exposition*, 2018.

- Open Educational Resources in the Undergraduate Engineering Curriculum: A Materials Science Case Study, Behbahanian, A., Davis, E. L., Wendel, S., Roberts, N. A. in *ASEE Annual Conference and Exposition*, 2018.
- Thermal management of electrical circuits, Behbahanian, A., Roberts, N. A. in *usu student research symposium*, 2017

Certificates and Awards

- Computational Materials Physics (2020), The Center for Molecular Modeling at Ghent University (Online)
- Stochastic processes (2020), National Research University-School of Economics (Online-Coursera)
- Introduction to Molecular Modeling Concepts in Polymers(2021), Schrödinger, Inc. (Online)
- Outstanding Doctoral Student Researcher (2019), Utah State University